Uncovering Pathways Regulating ILC Metastasis Through miRNA Expression Analysis and Generation of Novel Invasive ILC Models

Victoria Allen

Supervisor: Dr. Christina Addison

A thesis submitted in partial fulfillment of the requirements for the
Master's degree in Biochemistry with Specialization in Human and Molecular Genetics

Department of Biochemistry, Microbiology and Immunology
Faculty of Medicine
University of Ottawa

Abstract

Invasive lobular carcinoma (ILC) is the second most common form of breast cancer. ILC presents at later stages with many challenges, therefore improved diagnostic and therapeutic targets are needed. A microRNA (miRNA) genome analysis identified miR-23c and miR-23b-3p as possible regulators of ILC invasion due to their significantly increased expression in invasive compared to minimally invasive ILC cell lines. By decreasing the levels of miR-23c and miR-23b-3p using hairpin inhibitors, the invasive MDA-MB-330 cell line had significantly reduced invasion, while overexpressing these miRNAs using mimics in the minimally invasive MDA-MB-134VI cell line increased invasion. During the course of this study, it became apparent that limited tools exist for studying invasive ILC. Therefore, two more invasive ILC cell line models were created by isolating and expanding MDA-MB-134VI cells that had invaded through Matrigel® coated invasion chambers. This thesis has thus created new models of invasive ILC as well as identified miR-23c and miR-23b-3p as regulators of MDA-MB-330 and MDA-MB-134VI cell line invasion.

Contribution of Collaborators

The Génome Québec Innovation Center at McGill University for checking RNA quality, preforming the Clariom™ Assays and returning the data to our lab for analysis.

Dr. Christina Addison, for analyzing the Clariom™ Assay data using the TAC software and returning the output and volcano plots to myself for further investigation.

Dr. Christina Addison, Dr. Grant Howe and HuiJun Zhao, who together isolated RNA from nine archival surgical specimens, made cDNA, preformed the preamplification and conducted the miRNome analysis of the 9 preliminary samples patient ILC formalin-fixed paraffin-embedded (FFPE) tumour samples. The cDNA made for Figure 17, was then used in Figure 16 & 18 to analyze the expression of the select miRNA by qPCR in the 9 preliminary samples.

HuiJun Zhao, who found blocks to use for the archival surgical specimens' investigations, and who isolated the RNA from the FFPE tissues to be used for further experiments.

Dr. Angel Arnaout and Dr. Susan Robertson for obtaining and identifying relevant samples for the investigation of ILC FFPE tissues.

Histology Core Facility at the University of Ottawa for cutting and mounting the FFPE tissues onto slides for our use in downstream experiments.

Dr. Grant Howe, who during his time in the Addison Lab devised the idea to isolate more invasive cells from the bottom of an invasion chamber to devise a more invasive sub-population. His initial idea led to the creation of the VIVA sub-populations.

Funding for this project was awarded to the Addison Laboratory by the Canadian Breast Cancer Foundation-Ontario Chapter, who are now the Canadian Cancer Society Research Institute.

Acknowledgments

First, I would like to acknowledge my supervisor, Dr. Christina Addison. She gave me the opportunity to pursue my master's and a project that I was truly passionate about. She gave me guidance and many opportunities to learn, and for that I am very grateful.

I would like to thank my thesis advisory committee Dr. Douglas Gray and Dr. Jocelyn Côté, for their assistance and guidance with my project. I appreciate your help in keeping me on the right track and giving advice whenever we faced a challenging problem.

I would like to acknowledge Huijun Zhao as well as past and present members of the Addison laboratory. I want to thank you all for your help and support over the course of my master's.

I want to thank my friends; you have been amazing sounding boards and are always there when I need you. Your ability to listen to me for hours on end is uncanny. I appreciate all the advice, support and encouragement you have given me over the years . Thank you for being such amazing people.

Finally, to my family, you are truly incredible people who have never given up on me. Your constant love and support have brought me to this point, and I cannot ever thank you enough. Thank you so much for your dedication to my education, it is such an amazing gift.

Table of Contents

List of Abbreviations

AEBSF 4-(2-Aminoethyl)benzenesulfonyl Fluoride Hydrochloride

APS Ammonium Persulfate

BSA Bovine Serum Albumin

cDNA Complementary DNA

CHRM1 Cholinergic Receptor Muscarinic 1

Control Hairpin Inhibitor miScript® Inhibitor Negative Control

Control Mimic AllStars Neg. siRNA tagged with Alexa Flour 488 (AF488)

C_t Threshold Cycle

DMEM Dulbecco's Modification of Eagle's Medium 1X with 4.5g/L glucose, L-glutamine and sodium pyruvate

DNA Deoxyribonucleic Acid

dNTP 2'-deoxynucleoside 5'-trihosphate

DPBS Dulbecco's phosphate-buffered saline 1X

DTT Dithiothreitol

E-64 N-(trans-Epoxysuccinyl)-L-leucine 4-guanidinobutylamide

EDTA Ethylenediaminetetraacetic Acid

EGTA Egtazic Acid

EMT Epithelial to Mesenchymal Transition

ER Estrogen Receptor

Erbin ERBB2IP

FFPE Formalin-Fixed Paraffin-Embedded

GPCR G Protein-Coupled Receptors

HEPES N-2-hydroxyethylpiperazine-N-2ethane Sulfonic Acid

hr Hours

IDC Invasive Ductal Carcinoma

ILC Invasive Lobular Carcinoma

Invasion Chamber Growth Factor Reduced Corning® Matrigel® Invasion Chamber 24-well plate 8.0 micron

Leibovitz's Leibovitz's 1X L-15 medium with L-glutamine

LCM Laser Capture Microdissection

MDA-MB-134VI MDA-MB-134-VI

M-MLV Moloney Murine Leukemia Virus

min Minutes

miRNA microRNA

miRNome miRNA genome

MRI Magnetic Resonance Imaging

mRNA Messenger RNA

nt Nucleotides

Opti-MEM™ Opti-MEM™ I (1X) reduced serum medium with HEPES, 2.4g/L sodium bicarbonate and L-glutamine

p120 p120-Catenin

PAGE Polyacrylamide Gel Electrophoresis

PBS Phosphate-Buffered Saline

PR Progesterone Receptor

qPCR Quantitative Real-Time Polymerase Chain Reaction

RISC RNA Induced Silencing Complex

RNA Ribonucleic Acid

RPMI-1640 Roswell Park Memorial Institute 1X with 2.05mM L-glutamine

s Seconds

SDS Sodium Dodecyl Sulfate

SEM Standard Error of the Mean

shRNA Short Hairpin RNA

SNORD95 Small Nucleolar RNA, C/D box 95

SPINK13 Serine Peptidase Inhibitor, Kazal Type 13

TAC Transcriptome Analysis Console

TBS Tris-Buffered Saline

TBST Tris-Buffered Saline with Tween

TCGA The Cancer Genome Atlas

TEMED Tetramethylethylenediamine

Transwell® Transwell® Permeable supports 6.5mm insert 24 well plate 8.0μm polycarbonate membrane

UTR Untranslated Region

List of Figures

List of Tables

Chapter 1: Introduction

1.1 Breast Cancer

Forms of breast cancer are determined by the cell type and histology of the tumour (Yoder et al., 2007). Breast cancer can be separated into the following six subtypes: luminal A, luminal B, luminal C, basal-like, HER2 and normal breast-like (Sørlie et al., 2001). The breast is comprised of a collection of ducts that finish with a terminal duct lobular unit (Yoder et al., 2007). The lobule making up the terminal duct lobular unit is formed by a collection of acini, each derived from a ductule (Yoder et al., 2007). It is within these structures that different forms of breast cancer originate (Yoder et al., 2007). The two most common forms of breast cancer are invasive ductal carcinoma (IDC) (Sinn and Kreipe, 2013) and invasive lobular carcinoma (ILC) (Hwang and Sahoo, 2016), with both amounting to >95% of breast cancers (Yoder et al., 2007). ILC accounts for ~15% of invasive breast cancer cases (Martinez and Azzopardi, 1979) therefore making it the second most common subtype of breast cancer (Ciriello et al., 2015). In Canada, breast cancer accounts for 25% of diagnosed cases of cancer in women (Canadian Cancer Society, 2019a; Canadian Cancer Statistics Advisory Committee, 2018), in 2017 this amounted to 26,300 breast cancer diagnoses (Canadian Cancer Society, 2019a; Canadian Cancer Statistics Advisory Committee, 2018). Therefore, breast cancer is the most common cancer diagnosis among Canadian women (Canadian Cancer Statistics Advisory Committee, 2018). Commonly presenting with a fatal prognosis is metastatic breast cancer, which is the dissemination of the tumour to other locations of the body (Hanahan and Weinberg, 2000; McGuire et al., 2015). Between the two most common forms of breast cancer (Hwang and Sahoo, 2016; Sinn and Kreipe, 2013), ILC has a slightly higher rate of metastatic recurrence among patients (Pestalozzi et al., 2008).

1.2 Metastasis

Metastatic lesions consists of cancer cells that were able to leave the primary tumour and establish growth in other locations within the body (Hanahan and Weinberg, 2000). Metastasis is achieved through the cells invading the local tissue, followed by the cells intravasating into blood and lymphatic vessels (Hanahan and Weinberg, 2011). Cells must then survive in circulation and travel throughout the body until they then extravasate into various tissues, and may form a new metastatic lesion (Hanahan and Weinberg, 2011). Cancer cells that are able to metastasize have acquired the ability to invade, survive in circulation and establish in their new tissue site through adjustments to their cellular phenotypes (Hanahan and Weinberg, 2011).

One cellular phenotypic change that is associated with increased metastatic potential is the ability to undergo epithelial to mesenchymal transition (EMT) (Hanahan and Weinberg, 2011). Cells with an EMT phenotype are more readily able to disseminate from the primary tumour and invade to alternative metastatic sites (Reed et al., 2015). To achieve this ability, cells undergo characteristic changes whereby they are less adhesive and polar, giving them a more invasive/metastatic phenotype (Reed et al., 2015). This ability may be derived in part due to changes in cell adhesion molecules such as E-cadherin (Christgen and Derksen, 2015), or microRNA (miRNA) expression within the cell (Reed et al., 2015).

Other mechanisms which contribute to cancer cell metastasis and their ability to thrive in their new environment can be dependent on their acquisition of the hallmarks of cancer (Hanahan and Weinberg, 2000). Established by Hanahan and Robert A. Weinberg (2000), the hallmarks of cancer to achieve malignant growth also contribute to progression of metastases and are as follows: cancer cells must provide growth signals, perform angiogenesis, have immortalized replication, avoid apoptosis, and disregard anti-growth signals (Hanahan and Weinberg, 2000). Many

biological and genetic processes are modified for a cell to become cancerous and obtain these malignant characteristics (Hanahan and Weinberg, 2000). Current research is underway to identify the mechanisms by which specific cancer cells become metastatic with the desire to identify putative therapeutic targets and develop tailored effective treatment regimens for patients with metastatic cancer (Hanahan and Weinberg, 2000, 2011).

Breast cancer patients in Canada have a 5 year net survival rate of 87%, this drops in patients with stage 4 breast cancer to a 22% 5 year net survival rate (Canadian Cancer Society, 2019b; Canadian Cancer Statistics Advisory Committee, 2018). Stage 4 breast cancer is categorized by metastatic lesions at diagnosis, which presents with treatment challenges (Canadian Cancer Society, 2019c; National Comprehensive Cancer Network, 2018a). At present, current treatments of metastatic breast cancer are palliative as presently there is no cure (Canadian Cancer Society, 2019c; National Comprehensive Cancer Network, 2018a). Therefore, further investigation is needed to uncover more direct and targeted effective therapies for patients diagnosed with metastatic breast cancer.

1.3 Invasive Lobular Carcinoma

1.3.1 Invasive Lobular Carcinoma is a Distinct Breast Cancer

ILC is a distinct form of breast cancer (Jacobs et al., 2015) that accounts for ~15% of invasive breast cancers (Martinez and Azzopardi, 1979). It is more likely to be found in older patients and present with larger tumours than IDC (Pestalozzi et al., 2008). Due to the nature of ILC, it often presents with a better prognosis than IDC (Arpino et al., 2004); however, this does

not result in increased survival (Arpino et al., 2004) as ILC has worse disease-free survival than IDC following 6 years of the primary tumour (Pestalozzi et al., 2008).

ILC can be characterized by its distinct growth pattern in which the cells invade the stroma in a single file fashion (Christgen and Derksen, 2015; Jacobs et al., 2015; Martinez and Azzopardi, 1979; Reed et al., 2015), which may be seen around the ducts as well (Yoder et al., 2007). ILC cells are commonly small, with limited cytoplasm and lack cohesion (Christgen and Derksen, 2015; Reed et al., 2015), giving rise to the characteristic single file growth pattern which is speculated to be a result of E-cadherin loss (Reed et al., 2015), a transmembrane protein whose function regulates cell-cell adhesion and polarization (Reed et al., 2015; Yoder et al., 2007). Inside the cell, E-cadherin binds the cytoskeleton through catenins, one in particular is p120-catenin (p120) which is often found accumulated in the cytoplasm of ILC cells (Reed et al., 2015; Sarrió et al., 2004) due to the signature loss of E-cadherin in ILC (Moll et al., 1993; Sarrió et al., 2004). The loss of E-cadherin which results in relocation and accumulation of p120 (Sarrió et al., 2004), attains anoikis resistance allowing for ILC tumour growth and possibly its metastasis (Schackmann et al., 2011).

ILC is most often luminal A or luminal B subtypes (Iorfida et al., 2012), on account of its commonly increased levels of steroid hormone receptors (Iorfida et al., 2012). As such, ILC is more likely to be estrogen receptor (ER) positive, progesterone receptor positive (PR) (Arpino et al., 2004) and HER2 negative in comparison to IDC (Hwang and Sahoo, 2016). Accordingly, positive HER2 cases are scarce in ILC; if this is the case, it poses an increased risk of worse outcome for the patient (Iorfida et al., 2012). The expression of ER, PR and HER2 was observed in 981 primary lobular breast cancers by Iorfida et al., (2012). They found that of the investigated ILC cases: 96.5% were estrogen receptor positive, 79.6% were both estrogen and progesterone

receptor positive and 68.5% were HER2 negative (Iorfida et al., 2012). In ILC, *TP53* mutations are rare (Christgen and Derksen, 2015), however the two most prominent mutations in ILC are *CDH1* and *PIK3CA* (Reed et al., 2015). Another distinctive characteristic of classic ILC is its low mitotic rate which is reflective of its slow growing nature (Ciriello et al., 2015; Hwang and Sahoo, 2016; Yoder et al., 2007). Though these characteristics of ILC may indicate a better prognosis, this does not culminate with increased survival (Arpino et al., 2004) as there are challenges in the detection and treatment of the cancer (Jacobs et al., 2015).

1.3.2 Subtypes of Invasive Lobular Carcinoma

ILC has six distinct subtypes each with their own diagnosis, while maintaining unique variant characteristics of ILC (Sinn and Kreipe, 2013). These discrete subtypes are classic, alveolar, solid, mixed, tubulolobular and pleomorphic ILC (Sinn and Kreipe, 2013). Of the subtypes, classic is the most common (Hwang and Sahoo, 2016) with pleomorphic following at 15% of all ILC cases (Rosa-Rosa et al., 2019). These subtypes refer to the varying forms of ILC growth, leading to solid, alveolar nests and tubule formation (Hwang and Sahoo, 2016). Solid and alveolar subtypes of ILC have similar cellular structure; however, their growth pattern differs, as they grow in sheets and as an area of 20+ cells, respectively (Reed et al., 2015). Tubulolobular ILC has infiltrating properties that reflect the lobular nature of the subtype; however, growing in more tubular and cord formations (Kuroda et al., 2006). The more aggressive subtype of ILC is the pleomorphic subtype (Jacobs et al., 2015). Though there are a limited number of pleomorphic ILC cases, when detected the cancer is often found at a later stage (Jacobs et al., 2015), therefore patient survival of pleomorphic ILC is worse than the classical variant (Bentz et al., 1998).

Pleomorphic ILC can be luminal A and B, triple negative and HER2-enriched according to the characterization in the study by Rosa-Rosa et al., (2019). A study by Rakha et al., (2013) found that ~90% of pleomorphic cases were ER positive. HER2 expression is rare in ILC (Iorfida et al., 2012), but in pleomorphic ILC it is more commonly overexpressed and identified in 30% of incidences (Jacobs et al., 2015). Pleomorphic ILC still maintains the mutations in E-cadherin (Rosa-Rosa et al., 2019) that are common nature to ILC (Moll et al., 1993). Pleomorphic ILC has a more aggressive nature (Jacobs et al., 2015), due to its regular mutations in *TP53* (Rosa-Rosa et al., 2019) as well as its increased mitotic rate (Reed et al., 2015). Growth of pleomorphic ILC maintains similar characteristics of ILC, apart from the larger amount of cytoplasm, pale/eosinophilic, and granular/foamy appearance of the cells (Bentz et al., 1998). Although there are various subtypes of ILC (Sinn and Kreipe, 2013), the classical form still maintains the role as the most common variant (Hwang and Sahoo, 2016) and at present warrants focused research into its detection and treatments.

The Cancer Genome Atlas (TCGA) investigation of ILC by Ciriello et al., (2015) yielded three types of genetically characterized ILC that they distinguished as: reactive-like, immune-related and proliferative. In relation to these findings however, the paper by Michaut et al., (2016) only found two genetically characterized subtypes of ILC, immune related and hormone related. Through the investigation of genes expressed in both subtypes, Michaut et al., (2016) discussed that immune related ILC possesses an increase in chemokine and cytokine gene expression; whereas, hormone related was found to have increased ER, PR, hormone targeting and cell cycling gene alterations. The reactive-like identified by Ciriello et al., (2015) pertains to microenvironment signaling, while proliferative ILC has higher proliferation due to increased cell-cycle regulators.

These new subtypes distinguish various forms of ILC suggesting that further investigation is warranted into their identification, drivers and possible regulators.

1.3.3 Metastatic Invasive Lobular Carcinoma

Many of the investigations assessing metastatic ILC are in comparison to IDC (Arpino et al., 2004; Ciriello et al., 2015; Pestalozzi et al., 2008; Tasdemir et al., 2018). As such, in comparison to IDC, ILC has greater disease-free survival and overall survival until 6 and 10 years post primary tumour respectively; however, beyond these times there is a reversal of prognosis and IDC has greater disease free and overall survival compared to ILC (Pestalozzi et al., 2008). This drop in disease-free and overall survival may be attributed to the fact that ILC's incidence of local, contralateral and distant recurrence is higher than that of IDC (Pestalozzi et al., 2008). The rate of recurrence after the primary tumour, was found to be 31% for ILC, and 27.4% in IDC in the study be Pestalozzi et al., (2008). Sites of metastasis for ILC differentiate from those of IDC, wherein ILC will metastasize to the peritoneum, gastrointestinal tract (Arpino et al., 2004; Ciriello et al., 2015) and ovaries (Arpino et al., 2004). In comparison to IDC, ILC is less likely to metastasize to the lung (Arpino et al., 2004), and more likely to metastasize to the bone (Pestalozzi et al., 2008). As metastatic ILC is quite different from metastatic IDC the two should be treated as distinct metastatic breast cancers in future investigations (Jacobs et al., 2015).

1.4 Detection and Treatment of Invasive Lobular Carcinoma Presents with Challenges

1.4.1 Invasive Lobular Carcinoma is Not Readily Detectable

There are challenges in identifying ILC (Jacobs et al., 2015), as it does not form a palpable mass (Hwang and Sahoo, 2016) or induce an inflammatory response (Jacobs et al., 2015).

Accordingly, ILC is not readily detected early (Arpino et al., 2004) and is commonly diagnosed at later stages (Cristofanilli et al., 2005). The preferred method to detect breast cancer is through mammography (Jacobs et al., 2015); however, it is the least capable method of identifying ILC in comparison with ultrasound and MRI (Hwang and Sahoo, 2016). Of these imaging techniques, the most proficient is MRI (Hwang and Sahoo, 2016; Jacobs et al., 2015), although it is not the conventional method for detecting breast cancer (Jacobs et al., 2015). When ILC is imageable, new challenges present when trying to define margins of the tumour (Pestalozzi et al., 2008), which may be contributed of the cancer's linear growth pattern (Reed et al., 2015). Issues in defining margins of the tumour commonly results in mastectomy (Pestalozzi et al., 2008), which is a severe treatment strategy. Therefore, it is imperative that more effective diagnostic tools are derived for ILC as it is essential in defining appropriate treatment strategies for the cancer.

1.4.2 Limited Treatment Options are Available for Invasive Lobular Carcinoma

Standard of care treatment for invasive breast cancer is dependent on a number of factors including the type of breast cancer; however, the regimen usually includes possible neoadjuvant therapy, followed by surgery and often adjuvant therapy (National Comprehensive Cancer Network, 2018b). If neoadjuvant therapy is undergone, it will consist of either: chemotherapy, targeted therapy or endocrine therapy (National Comprehensive Cancer Network, 2018b). This would be followed by surgery, and then adjuvant therapy options which may consist of: chemotherapy, targeted, radiation, or endocrine therapy (National Comprehensive Cancer Network, 2018b). Classical ILC has been shown to have a reduced response to chemotherapy (Cristofanilli et al., 2005) which may be attributed to the cancer's low mitotic index (Reed et al., 2015) and the cancer's increased levels of hormone receptors (Iorfida et al., 2012). Consequently,

selected treatment for ILC is mastectomy (Cristofanilli et al., 2005; Pestalozzi et al., 2008) followed by adjuvant endocrine therapy (Reis-Filho et al., 2006). This is in line with minimal common practice for treating hormone positive breast cancers, which is 5 years adjuvant hormone therapy after surgical resection of the tumour (Jacobs et al., 2015). If the tumour were to return, metastatic breast cancer treatment options would be: surgery if locally recurrent or recurrent to a resectable organ, chemotherapy, radiation, endocrine or targeted therapy (National Comprehensive Cancer Network, 2018a). Many of these common treatment options for metastatic breast cancer are not effective for metastatic ILC, as again, ILC does not respond well to primary chemotherapy (Cristofanilli et al., 2005). Therefore new treatment regimens and effective prognostic indicators of ILC are needed, more specifically for patients that may relapse (Jacobs et al., 2015). This thesis aims to identify biomarkers and potential therapeutic targets of ILC, that may assist in the detection and treatment of metastatic ILC.

1.5 Invasive Lobular Carcinoma has a Limited Number of Resources for its Investigation

1.5.1 Invasive Lobular Carcinoma is Commonly Compared to Invasive Ductal Carcinoma

Due to the increased prevalence of IDC compared to ILC, most breast cancer investigations and subsequent verdicts with respect to biology and treatment recommendations are predominantly based on IDC (Pestalozzi et al., 2008). ILC and IDC are distinct breast cancers and investigations should treat them as such (Jacobs et al., 2015). This is not limited to clinical or laboratory investigations of ILC, where it is often compared to IDC (Arpino et al., 2004; Ciriello et al., 2015; Pestalozzi et al., 2008; Tasdemir et al., 2018). An ongoing challenge that has been faced throughout this investigation has been the lack of datasets pertaining to ILC. The TCGA Program investigated ILC genomics, and although valuable research, the caveat to the TCGA dataset is that ILC is

evaluated in comparison to IDC and normal breast tissue, and not within subgroups of ILC itself (Ciriello et al., 2015). Furthermore, this data does not consider the comparison between metastatic and non-metastatic ILC which could have identified potential regulators of ILC metastasis (Ciriello et al., 2015). The limited number of studies focusing on ILC itself does pose a challenge, but there are other pressing challenges of investigating ILC.

1.5.2 Resources for Studying Invasive Lobular Carcinoma are Minimal

Although ILC is the second most common subtype of breast cancer (An et al., 2018), resources for studying ILC are minimal (Jacobs et al., 2015). These challenges include but are not limited to a lack of availability of cell lines, mouse models (An et al., 2018) and tissue samples. The limited number of ILC cell lines (Jambal et al., 2013) available globally culminates to approximately seven confirmed lines (Brinkley et al., 1980; Cailleau et al., 1978; Christgen and Derksen, 2015; Christgen et al., 2009; Domann et al., 2000; Ethier et al., 1993; Jambal et al., 2013). Regrettably, only a few of these seven cell lines are available commercially (Brinkley et al., 1980; Cailleau et al., 1978; Christgen and Derksen, 2015; Christgen et al., 2009; Domann et al., 2000; Ethier et al., 1993; Jambal et al., 2013). In addition to limited availability, the confirmed ILC cell lines have a limited number of publications (Christgen and Derksen, 2015; Christgen et al., 2009; Sikora et al., 2014; Tasdemir et al., 2018), of which there appears to be only one identifying their invasive capabilities which were found to be minimal (Tasdemir et al., 2018).

1.5.3 Invasive Lobular Carcinoma Cell Lines are Rare

In research conducted by Tasdemir et al., (2018), they characterized four ILC cell lines: MDA-MB-134VI, SUM44PE, MDA-MB-330 and BCK4. In this paper it was found that all four

ILC cell lines had restricted migratory, and invasive capabilities; however, when the four ILC cell lines were tested for haptotaxis to Collagen I they found only the MDA-MB-330 and SUM44PE cell lines were responsive (Tasdemir et al., 2018). Another ILC cell line, IPH-926, was created by Christgen et al., (2009) who gives no indication of this cell line having invasive or migratory properties in their published study. UACC-3133, the newest available cell line has limited publications describing its characteristics, but these again do not describe its invasive capabilities (Domann et al., 2000). This evident lack of invasive ILC cell lines available for use as models of metastatic behavior indicates the drastic need for additional ILC models in a laboratory setting in order to effectively investigate ILC metastasis.

1.5.4 Mouse Models of Invasive Lobular Carcinoma

There is a lack of description using ILC cell lines in xenograft models *in vivo*. Whether it is due to their inability to grow *in vivo*, or that no one has tried these experiments is unclear. Of the available ILC cell lines, only the IPH-926 cell line has been shown to grow following subcutaneous injection in xenografts (Christgen et al., 2009). This lack of ILC growth within mice is perhaps not surprising as the study by Cottu et al., (2012) documented that patient derived xenografts of ER positive tumours in nude mice fat pads, with a large portion of the tumours being of lobular origin, do not readily take and grow as only 2.5% were able to form tumours. Since this study, Sflomos et al., (2016) having known that ER positive ILC are not readily able to grow *in vivo*, attempted to establish a mouse model of ER positive breast cancer. Through intraductal injection, they were able to establish a xenograft model of MDA-MB-134VI cell line growth in milk ducts (Sflomos et al., 2016). We concur with Sflomos et al., (2016) findings that this instance, to our knowledge, is the only successful model of the MDA-MB-134VI cell line *in vivo.* Based on

these findings, our lab is attempting intraductal injections to create xenograft models of some of the ILC cell lines used in this thesis (Sflomos et al., 2016). Our lab has found ILC to have slow growth *in vivo*, which is not unexpected as classic ILC is known to have a low mitotic rate (Ciriello et al., 2015; Hwang and Sahoo, 2016; Yoder et al., 2007). Though there is limited use of ILC cell lines in conjunction with mice, mouse models do present advantages to investigating ILC.

At present there seems to be a limited number of mouse models that may accurately reflect classical ILC metastasis *in vivo.* Efforts have been made to create a model of ILC through intraductal CRISPR/Cas-9 mediated-targeting of E-cadherin and *Pten* (Annunziato et al., 2016). Although this method has created a viable replicate of ILC in mice, it is not suitable for metastatic investigations as only 30% of injections resulted in ILC tumours (Annunziato et al., 2016). An additional model was created by Kas et al., (2017), where they performed a *Sleeping Beauty* insertional mutagenesis screen on *Cdh1* null mice. During the investigation it was found that 34% of tumours metastasized; however, these mice develop tumours of variable genetic composition and therefore is not conducive for use as a model of metastatic ILC (Kas et al., 2017).

A well-founded mouse model derived by An et al., (2018) was created to mimic immune-related ILC. To do so, they created a mouse model with a gain-of-function and a loss-of-function of *PIK3CA* and *CDH1* respectively, as both of these genes have been found to be the most prevalently mutated in ILC (An et al., 2018; Ciriello et al., 2015). This mouse model found a number of possible regulators of invasion to be expressed in their model compared to the human counterpart which they speculated is indicative of significant invasive capabilities; however, they do not elude to having identified metastatic lesions in their mouse model (An et al., 2018). Through personal communication with Dr. Sean Egan (Personal communication, May 22, 2019)(Supplementary Figure 5) we confirmed that they did not see any metastatic lesions in their

mice (An et al., 2018). Though the model developed by Dr. Sean Egan and his lab may be the best representation of ILC in mice, it cannot at present be used as a model of metastatic ILC (An et al., 2018).

Derksen et al., (2006) created *Cdh1* and *Trp53* null mice with a cytokeratin 14 promoted Cre recombinase (Derksen et al., 2006, 2011) located within the mammary and skin epithelium, which resulted in spontaneous ILC and skin tumours (Derksen et al., 2006). Though their model was found to metastasize in just under 50% of mice, to primarily the lymph nodes and in some instances to organs similar to ILC, this model represents a small proportion of ILC tumours since the model resembles the pleomorphic ILC subtype (Derksen et al., 2006). Additionally, though the metastatic lesions were believed to originate from the ILC tumours as they possessed similar traits to ILC tumours, the study did not confirm that the metastatic lesions originated from the breast tumours rather than the skin tumours (Derksen et al., 2006). Since publishing these findings, Derksen et al., (2011) has published a paper recanting the efficacy of their mouse model as a model of metastatic ILC due to the generation of skin tumours. Therefore Derksen et al., (2011) created another *Cdh1* and *Trp53* null mouse model; however, this time they used a whey acidic protein promoter with a Cre recombinase in an attempt to abolish the skin tumours. This model was found to be more invasive than the last, as 74% of mice developed tumour metastasis (Derksen et al., 2011). Though this model seems more promising, it is again more reflective of a pleomorphic ILC mouse model (Derksen et al., 2011).

Branching on the findings of Derksen et al., (2006), Doornebal et al., (2012) used the same mouse model however, they isolated tumours from transgenic animals and transplanted this into the mammary fat pad of syngeneic murine hosts, then surgically removed the implanted tumour upon sufficient growth. This resulted in growth of spontaneous metastatic ILC in 32/44 mice with

metastatic lesions in locations similar to that of human ILC (Doornebal et al., 2012). Unfortunately, Doornebal et al., (2012) could not confirm that this metastasis was not a consequence of surgery on the primary tumour. This model is most likely a representation of pleomorphic ILC, like the model created by Derksen et al., (Derksen et al., 2011; Derksen et al., 2006; Doornebal et al., 2012). Pleomorphic ILC only accounts for 15% of ILC cases (Rosa-Rosa et al., 2019) whereas classical ILC is the most common subtype (Hwang and Sahoo, 2016).

The mouse model created by Boelens et al., (2016) was generated through the inactivation of *Cdh1* and *Pten.* Their model was found to possess characteristics of classical ILC, the most common subtype of the cancer (Boelens et al., 2016; Hwang and Sahoo, 2016). With metastatic sites similar to ILC, the study discovered that metastasises was seen in only 5% of *Cdh1* and *Pten* null mice (Boelens et al., 2016). This may be the best representation of classical metastatic ILC, despite its low yield of metastatic sites (Boelens et al., 2016). While improved mouse models of ILC are being generated, at the beginning of this thesis project, none of these mouse models were available or suitable for our investigative needs.

1.6 Selected Investigation Materials of Invasive Lobular Carcinoma for this Thesis

1.6.1 Invasive Lobular Carcinoma Cell Lines Elected for the Study

To investigate metastatic ILC, we opted to use formalin-fixed paraffin-embedded (FFPE) archival ILC tumour tissues and cell lines for *in vitro* examinations. The four selected ILC cell lines were the MDA-MB-330 (ATCC® HTB-127™), MDA-MB-134-VI (MDA-MB-134VI) (ATCC® HTB-23™), UACC-3133 (ATCC® CRL-2988™) and IPH-926 (Christgen et al., 2009). The MDA-MB-330 cell line was derived from a pleural effusion of a metastatic tumour (Brinkley

et al., 1980; Cailleau et al., 1978). Although there are controversial reports that the MDA-MB-330 cell line is ER negative (Christgen and Derksen, 2015; Tasdemir et al., 2018) recent discovery by Tasdemir et al., (2018) proves that the cell line does express ERα. The MDA-MB-330 cell line is HER2 overexpressing (Hollestelle et al., 2010), PR negative, and E-cadherin positive; however, E-cadherin was found to be non-functional as it and p120 re-localized to the cytoplasm (Tasdemir et al., 2018). The MDA-MB-134VI cell line was isolated from a pleural effusion of a metastatic tumour (Cailleau et al., 1974, 1978). Since then, it has been re-evaluated to be considered an ILC cell line (Reis-Filho et al., 2006). MDA-MB-134VI cells have been reported to be positive for ER and PR (Cailleau et al., 1978; Tasdemir et al., 2018), and negative for E-cadherin (Tasdemir et al., 2018) and HER2 (Christgen et al., 2009; Reis-Filho et al., 2006). The UACC-3133 cell line was isolated from a case of poorly differentiated (Domann et al., 2000) ILC like (American Type Culture Collection, 2019a) adenocarcinoma that was metastatic to the pleural fluid (American Type Culture Collection, 2019a; Domann et al., 2000). According to ATCC® (American Type Culture Collection), the UACC-3133 cell line has the following characteristics; HER2 expression, low ER expression, and PR is not expressed (American Type Culture Collection, 2019a). Isolated from malignant ascites, the IPH-926 cell line has a loss of heterozygosity at *CDH1* resulting in cytoplasmic re-localization of p120 (Christgen et al., 2009). IPH-926 cells were additionally, found to be HER2 and ER negative, with a doubling time of about 14 days (Christgen et al., 2009).

1.6.2 Formalin-Fixed Paraffin Embedded Tissues Were Chosen for Investigation of Invasive Lobular Carcinoma

Our lab has found it difficult to obtain fresh frozen ILC tumour samples for gene expression analysis on account of limited availability of samples with associated sufficient long-term clinical follow-up to identify the tumour's fate. The Ontario Tumour Bank has approximately 32 fresh

frozen lobular tissue samples (Personal communication with Dr. Christina Addison, 2018), of which we could speculate that a limited number metastasized based on a recurrence rate of 31% in ILC (Pestalozzi et al., 2008). This limited number of metastatic samples does not generate sufficient statistical power to investigate the properties of metastatic ILC. On another note, the Ontario Tumour Bank started collecting samples in 2004 (Ontario Tumour Bank and Ontario Institute for Cancer Research, 2019), therefore their oldest sample is approximately 12 years old. As previously discussed the likelihood of ILC metastasizing occurs 5-10 years post primary tumour (Pestalozzi et al., 2008), and as such many of these samples would therefore not have the sufficient long-term follow-up needed to determine the tumour's fate with respect to metastases. Since this long-term follow-up of ILC is required, our lab has had great interest in the potential of FFPE tissues to support biomarker analysis (Bovell et al., 2013). FFPE tissues are archival (Bovell et al., 2013) and therefore tumours can be dated, ensuring long term follow-up of the tumour (Li et al., 2007). Furthermore, FFPE tissues were more accessible thus allowing sufficient sample numbers to provide the statistical power needed for identifying markers associated with metastatic ILC. A caveat to performing an investigation using FFPE tissues is that ribonucleic acid (RNA) and protein are susceptible to cross-linking during the fixation process (Bovell et al., 2013; Li et al., 2007). Therefore FFPE tissues are often inadequate for messenger RNA (mRNA) analysis due to the deletions and modifications that may occur during the fixation process and long term storage (Li et al., 2007). Smaller RNA, such as miRNA, are not as likely to be affected in this way as due to their small size they may not form cross-links with protein during the fixation process and have been found to be stable and efficiently recovered from FFPE tissues (Bovell et al., 2013; Li et al., 2007) up to 28 years old (Bovell et al., 2013). In addition to being stable in archival FFPE tissues, miRNA have been found to be stable in plasma and serum (Chen et al., 2008), due in part to their

nuclease resistance (Chen et al., 2008). As such, due to their stability in plasma, serum (Chen et al., 2008) and FFPE tissues (Bovell et al., 2013; Li et al., 2007), miRNA are an ideal choice to pursue as a candidate biomarker (Chen et al., 2008) of metastatic ILC.

1.7 miRNA

1.7.1 miRNA are Post-Transcriptional Regulators of mRNA

miRNA are small RNA molecules of 20-22 nucleotides (nt) in length (Li et al., 2007) that are involved in numerous biological pathways (Thomson et al., 2013). These pathways include but are not limited to; development (Calin et al., 2004), apoptosis (Liu et al., 2011) and differentiation (Schoolmeesters et al., 2009). Due to their role as post-transcriptional regulators (Lin and Gregory, 2015), miRNA bind to mRNA, resulting in their subsequent repression or degradation (Iorio et al., 2005) concluding in a lack of protein production (McGuire et al., 2015). miRNA genes were found to be distinctly allocated throughout specific chromosomes, and within close proximity to fragile sites, therefore increasing the risk that miRNA genes will be a casualty of mutations to these cancer prone genes (Calin et al., 2004). As such, miRNA have been found to have differential expression in cancer, including breast cancer (Riaz et al., 2013).

1.7.2 miRNA Synthesis and Their Role as Post-Transcriptional Regulators

miRNA synthesis begins in the nucleus where the hairpin primary miRNA is translated by polymerase II (Lin and Gregory, 2015; Wang and Luo, 2015). From this point the primary miRNA is then cleaved by Drosha within the nucleus to form the hairpin precursor miRNA (Jeong et al., 2017; Lin and Gregory, 2015). The precursor miRNA is then exported from the nucleus to the cytoplasm through the assistance of Exportin 5 (Jeong et al., 2017; Lin and Gregory, 2015). Once

in the cytoplasm, the precursor miRNA is cleaved by DICER (Iorio et al., 2005; Jeong et al., 2017). Of the two resulting strands of the mature miRNA, the passenger strand is disposed of (Jeong et al., 2017), and the guide strand is integrated into Argonaute (Jeong et al., 2017; Lin and Gregory, 2015) to form the RNA induced silencing complex (RISC) (Lin and Gregory, 2015; Thomson et al., 2013). miRNA that have been integrated into the RISC are thus functional, and are responsible for bringing the RISC to their target mRNA (Thomson et al., 2013). Through their 2-8nt seed sequence located at the 5' end of the mature miRNA, miRNA are able to bind to complementary sequences in target mRNA (Jeong et al., 2017). Although the presence of the seed sequence itself may be enough to target the mRNA, greater results are seen when it binds with the 3' untranslated region (UTR) as well (Brennecke et al., 2005). When seed pairing itself is not sufficient, due to partial homology, additional 3' UTR binding is needed to initiate (Brennecke et al., 2005) post-transcriptional regulation of the mRNA (Lin and Gregory, 2015). This post-transcriptional regulation of the mRNA by the miRNA may be conducted within processing bodies (P-bodies) located within the cytoplasm (Lin and Gregory, 2015), thus resulting in repression or degradation of the mRNA target (Iorio et al., 2005).

1.7.3 miRNA Nomenclature

There is specific nomenclature involved with miRNA for their identification. The beginning portion of their designated names represents the species of origin, examples are: hsa for human, and mmu for mouse (Griffiths-Jones et al., 2006). miR indicates a mature miRNA (Griffiths-Jones et al., 2006), whereas precursor miRNA (Jeong et al., 2017; Lin and Gregory, 2015) are referred to as pre-mir, and primary miRNA transcripts are indicated by pri-mir terminology (Griffiths-Jones et al., 2006). miRNA with the same numerical portion of the name,

but originating from different species are orthologous (Griffiths-Jones et al., 2006). This similarity in numerical portion of the name may indicate miRNA that are from the same family, sharing alike sequences and thus may have similar and differing targets, though they may originate from different chromosomes (Granados-López et al., 2017). After the numerical portion of the name may be letters which indicate mature miRNA with similar sequences except for 1-2nt differences resulting in paralogous miRNA (Griffiths-Jones et al., 2006) derived from a common ancestor (Jeong et al., 2017). Paralogous miRNA have identical seed sequences but different 3' regions (Jeong et al., 2017), which may indicate that they are able to have both differing and common targets (Brennecke et al., 2005; Jeong et al., 2017). Finally, at the end of the miRNA's name may be a -3p or -5p designation (Griffiths-Jones et al., 2006). This portion of the name pertains to the arm of the hairpin precursor, whether that be the 5' or 3' arm, that the mature miRNA originated from (Griffiths-Jones et al., 2006).

1.7.4 The Role of miRNA in Cancer

miRNA regulate numerous cellular processes (Thomson et al., 2013), some examples of these processes are: development (Calin et al., 2004), apoptosis (Liu et al., 2011), angiogenesis (Howe et al., 2017) and cellular differentiation (Schoolmeesters et al., 2009). An example is in the context of angiogenesis where miR-30b and its downstream targets were discovered to regulate endothelial cell capillary morphogenesis via alteration of the TGFβ pathway (Howe et al., 2017). Schoolmeesters et al., (2009) found miR-148b, miR-27a and miR-489 were able to modulate osteogenic cell differentiation. miR-148b was found to increase, while miR-489 and miR-27a decreased osteogenic differentiation (Schoolmeesters et al., 2009). While miRNA modulate these

normal processes in the body, abnormal changes to their expression may contribute to disease (Wang and Luo, 2015), particularly cancer (Schrijver et al., 2017).

miRNA expression may vary depending on the type of cancer (Wang and Luo, 2015), as miRNA have been known to have tissue specific expression (Lagos-Quintana et al., 2002). miRNA have contextual function, as they have been found to operate as tumour suppressors and/or oncogenes (Calin et al., 2004; Iorio et al., 2005). miRNAs play a variety of roles in cancer, and tumour progression may be reflected in aberrant expression of miRNA (Iorio et al., 2005). For example, miRNA may induce cancer progression through modulation of tumour cell apoptosis (Liu et al., 2011). It was found that miR-26b had significantly lower expression in breast cancer tumours and cell lines compared to normal breast tissue and cells (Liu et al., 2011). From this discovery, the study found that elevated miR-26b resulted in decreased expression of its direct target, SLC7A11 which mediated apoptosis (Liu et al., 2011). Another manner in which miRNA may contribute to cancer progression is through mediating chemoresistance (Jiang et al., 2014). An example of this is described in the study by Jiang et al., (2014), where they found decreased miR-489 expression correlated with chemoresistance of breast cancer cells to adriamycin. It was additionally found that increased miR-489 decreased migration and possibly regulates both chemoresistance and EMT through its direct targeting of Smad3 (Jiang et al., 2014). Taken together, these studies highlight the multiple roles miRNA may play in promoting cancer progression.

Given their previously identified roles in cancer, miRNA expression levels may be associated with tumour progression, and thus could indicate poor prognosis of patients due to their regulatory roles in metastasis and proliferation in cancer (Iorio et al., 2005). In fact, miR-301 expression was found to be associated with disease free survival in ductal breast cancer patients;

wherein increased expression was associated with worse prognosis (Shi et al., 2011). Through further investigation, this was found to be in part due to the ability of miR-301 to regulate cell proliferation, migration, invasion, and angiogenesis in breast cancer cell lines (Shi et al., 2011). In addition, miRNA expression may indicate particular hormone receptor statuses within the tumour (Iorio et al., 2005). In the context of breast cancer, miRNA differential expression could lead to a signature indicating: ERBB2 overexpression, ER and E-cadherin status in breast cancer (Riaz et al., 2013). miRNA are also known to be regulated in a tissue specific manner (Lagos-Quintana et al., 2002), and thus may have differential expression and roles in various subtypes of breast cancer (Riaz et al., 2013) arising from different cellular compartments (Lagos-Quintana et al., 2002).

miRNA expression has additionally been found to vary between the primary tumour and its metastatic counterpart (Schrijver et al., 2017). Through the analysis of miRNA with known oncogenic and tumour suppressive capabilities, Schrijver et al., (2017) found that they were up- and down-regulated in metastatic compared to the primary breast tumour, respectively. At the end of their investigation however, Schrijver et al., (2017) found that the metastatic and primary tumours generally maintained similar miRNA profiles, apart from those that were metastatic site specific, suggesting that miRNA analysis from biopsies of the primary tumour will allow for identification of those tumours which may go on to metastasize.

The role miRNA play in breast cancer is not limited to diagnostic and prognostic features; miRNA can also modulate metastasis (Iorio et al., 2005; Ma et al., 2007; Schrijver et al., 2017). For example, the investigation by Ma, Teruya-Feldstein and Weinberg (2007) found that miR-10b had increased expression in metastatic breast cancer cells, compared to non-metastatic cell lines. Their investigation found that reduction of miR-10b levels resulted in decreased invasive capabilities of the cell line; however, this did not affect cell viability or motility (Ma et al., 2007).

On the other hand, when Ma, Teruya-Feldstein and Weinberg (2007) increased expression of miR-10b in non-metastatic breast cancer cell lines, an increase in motility and invasion was observed in conjunction with no change to proliferation. Thus given their established role in regulating invasion (Ma et al., 2007) and metastasis (Iorio et al., 2005; Ma et al., 2007; Schrijver et al., 2017) miRNA may be ideal candidate biomarkers (Chen et al., 2008) of metastatic ILC.

1.8 miRNAs are Ideal Candidate Biomarkers and Therapeutic Targets of Metastatic Invasive Lobular Carcinoma

As discussed above, numerous features of miRNA, including their cancer specific or differential expression (Wang and Luo, 2015) and their role in tumour progression (Iorio et al., 2005) and metastatic ability (Iorio et al., 2005; Ma et al., 2007; Schrijver et al., 2017), suggest they may be ideal candidate biomarkers (Chen et al., 2008) of metastatic ILC. Moreover, previous work indicated that similar miRNA profiles were found in primary and metastatic tumours apart from metastatic site specific miRNAs (Schrijver et al., 2017), suggesting that analysis of primary tumours may identify miRNA associated with metastatic risk. Thus, analysis of tumour cells or tissues with known metastatic capabilities or outcomes could identify specific miRNAs associated with modulation of the metastatic phenotype, therefore creating a signature of metastatic potential in ILC. Furthermore, the identification of their targets that modulate metastatic phenotypes, may be utilized as therapeutic targets to inhibit metastatic ILC.

1.9 Hypothesis and Aims

Hypothesis 1: It is hypothesized that differential miRNA expression will be observed in invasive compared to minimally invasive ILC. It is further speculated that these differentially expressed

miRNAs participate in the regulation of pathways that modulate tumour cell invasion and metastasis.

Aims:

1. Characterize and identify the invasive capabilities of four ILC cell lines.
2. miRNA genome profile invasive and minimally invasive ILC cell lines. Validate the differential expression of specific miRNAs.
3. Modulate levels of differentially expressed miRNAs and investigate their role in ILC cell line invasion.
4. Identify putative targets of validated miRNAs that may contribute to changes in invasive capabilities.
5. Evaluate miRNA expression in metastatic and non-metastatic patient ILC FFPE tissues.

Hypothesis 2: It is hypothesized that comparison of MDA-MB-134VI sub-populations with more invasive capabilities will have distinct miRNA and mRNA expression profiles.

Aims:

1. Compare the invasive capabilities of the generated sub-populations, VIVA-1 and VIVA-2, to the parental MDA-MB-134VI cell line.
2. Characterize the VIVA sub-populations and confirm ILC cellular properties relative to the parental MDA-MB-134VI cell line.
3. Analyze the miRNA and mRNA expression profile of the VIVAs.

Chapter 2: Materials and Methods

2.1 Cell Lines and Cell Culture

Throughout this investigation four ILC cell lines were primarily used. MDA-MB-330 (ATCC® HTB-127™), MDA-MB-134VI (ATCC® HTB-23™) and UACC-3133 (ATCC® CRL-2988™) were purchased from ATCC® (American Type Culture Collection, Manassas, VA), while IPH-926 was received from Dr. Matthias Christgen (Christgen et al., 2009). MDA-MB-330 and MDA-MB-134VI were adapted from air culture to CO_2 and grown along with IPH-926 in culture conditions of 37ºC and 5% CO_2 in their respective medias as described below. UACC-3133 were grown in atmospheric conditions at 37ºC using a modular incubator chamber (Billups-Rothenburg, Del Mar, CA) in media as described below.

All cell lines obtained from ATCC® were grown as recommended by ATCC®. The MDA-MB-330 cell line was grown in media containing a 1:1 ratio of Dulbecco's Modification of Eagle's Medium 1X with 4.5g/L glucose, L-glutamine and sodium pyruvate (DMEM) (Corning, Corning, NY) and Leibovitz's 1X L-15 medium with L-glutamine (Leibovitz's) (Gibco, ThermoFisher Scientific, ON) supplemented with 20% fetal bovine serum (FBS) (Sigma-Aldrich, Oakville, ON), 30ng/mL Recombinant Human epidermal growth factor (EGF) (Invitrogen, Gibco, ThermoFisher Scientific, ON), 0.016mg/mL insulin solution from bovine pancreas (Sigma-Aldrich, Oakville, ON) and 2mM L-glutathione reduced (Sigma-Aldrich, Oakville, ON). The MDA-MB-134VI cell line was grown in a 1:1 ratio media of DMEM and Leibovitz's with 20% FBS. The UACC-3133 cell line was grown in Leibovitz's with 5% FBS, 5μg/mL catalase from bovine liver (Sigma-Aldrich, Oakville, ON), 0.01mg/mL transferrin human (Sigma-Aldrich, Oakville, ON), 0.01mg/mL insulin solution from bovine pancreas, 3.6 μg/mL hydrocortisone (Sigma-Aldrich, Oakville, ON) and 2mM GlutaMAX™-1(100X) (Gibco, ThermoFisher Scientific, ON). The IPH-

926 cell line was grown following culture methods provided by Dr. Matthias Christgen (Christgen et al., 2009), with growth in Roswell Park Memorial Institute 1X medium with 2.05mM L-glutamine (RPMI-1640) (GE Healthcare Life Sciences, Mississauga, ON) supplemented with 10μg/mL insulin solution from bovine pancreas, 2.5g/L D-(+)-glucose (Sigma-Aldrich, Oakville, ON), 10mM N-2-hydroxyethylpiperazine-N-2ethane sulfonic acid (HEPES) (1M) (Gibco, ThermoFisher Scientific, ON) and 1mM sodium pyruvate (100mM) (Gibco, ThermoFisher Scientific, ON) (Christgen et al., 2009).

Three ductal breast cancer cell lines were used during this investigation for comparison to ILC. All three cell lines were purchased from ATCC® and cultured at 37ºC and 5% CO_2 in their respective medias containing 10% FBS. MDA-MB-231 (ATCC® HTB-26™) were grown in Dulbecco's Modified Eagle Medium with 1g/L D-glucose, L-glutamine and 110mg/L sodium pyruvate (Gibco, ThermoFisher Scientific, ON), T-47D (ATCC® HTB-133™) were grown in RPMI-1640, and MCF7 (ATCC® HTB-22™) were grown in DMEM.

All cells were grown and passaged under sterile conditions and were regularly checked for mycoplasma contamination by bisBenzimide stain (B-2883, Sigma-Aldrich, Oakville, ON) (Section 2.2). When passaging cells, they were first washed with Dulbecco's phosphate-buffered saline 1X (DPBS) (Corning, Corning, NY), then treated with 0.05% trypsin-0.53mM EDTA (Corning, Corning, NY) in 37ºC and 5% CO_2 conditions for approximately 5 minutes (min). Detached cells were recovered and enumerated for viable cells using Trypan blue solution (Sigma-Aldrich, Oakville, ON) and counted with a Vi-Cell™ XR (Beckman Coulter, Mississauga, ON), Countess™ II (Life Technologies, ThermoFisher Scientific, ON) or Hemocytometer (Reichert Technologies, Depew, NY). ILC cell lines were commonly split at ratios of 1:2, or 1:3 in the context of the MDA-MB-134VIs.

2.2 Mycoplasma Staining

The cell lines used in this study were regularly examined for mycoplasma contamination following staining using bisBenzimide. Cells were plated on a sterile glass coverslip in duplicate to approximately 60% confluency and incubated overnight to allow cell adherence. Next day, the media was aspirated, and the cells were washed with DPBS prior to fixing the cells for 10min in 100% methanol at room temperature. Once fixed, the coverslip was washed again once with DPBS and stained in the dark for 20min at room temperature with 0.6-0.8μL of 1:700 bisBenzimide in 200μL DPBS. After staining, the coverslip was washed up to five times for 5-10min with DPBS. The stained coverslip was then mounted onto a slide using Dako Fluorescence Mounting Medium (Agilent, Mississauga, ON) and the cells were examined using an Axioskop 2 MOT with Axiocam Carl Zeiss microscope (Carl Zeiss, Toronto, ON). All cell lines were found to be free of mycoplasma throughout the course of this thesis.

2.3 Invasive Lobular Carcinoma Archival Surgical Specimens

FFPE archival ILC tumour tissues were obtained in collaboration with Dr. Angel Arnaout under approval from Ottawa Health Science Network Research Ethics Board. Relevant samples with appropriate clinical follow up information were identified in collaboration with Dr. Arnaout and Dr. Susan Robertson, a collaborating breast pathologist. All samples used in this study were archival surgical specimens, from patients with a minimum of 5 years clinical follow-up information collected post-surgery to identify their metastatic or recurrent outcomes within this time frame.

2.4 RNA Collection and Quantification

Cells were plated in their respective media and washed once with DPBS prior to lysis using QIAzol™ (QIAGEN, Toronto, ON). After the addition of QIAzol™, cells were scraped from the dish. RNA was collected following the manufacturer's protocol using the miRNeasy® Mini Kit (QIAGEN, Toronto, ON). The spin columns provided in the miRNeasy® Mini Kit or EconoSpin® Spin Column for DNA (Epoch Life Science, Sugar Land, TX) were used for RNA isolation. The miRNeasy® protocol outlined various optional steps, of which all were followed to obtain the greatest RNA yield. RNA was eluted with 30-50µL of RNase-free water depending on the sample (QIAGEN, Toronto, ON). Due to the unique nature of lobular breast cancer cells, the DNase digestion treatment (QIAGEN, Toronto, ON) was skipped during RNA isolation as RNA yields were found to be insufficient when DNase treated. The exception was for collection of RNA used in downstream Clariom™ Assays, and mRNA analysis where the DNase digestion step was conducted. In these cases, the RNase-Free DNase kit (QIAGEN, Toronto, ON) was used for DNase digestion which was conducted following the manufacturer's protocol as outlined in the miRNeasy® Mini Kit Handbook (QIAGEN, Toronto, ON).

RNA was quantified by measuring absorbance using a ND-1000 Nanodrop™ Spectrophotometer (ThermoFisher Scientific, ON), and normalized to RNase-free water. The quantification of RNA was provided in ng/µL and the 260/280 as well as the 260/230 were recorded as a measure of RNA quality (ThermoFisher Scientific, ON). Due to the difficulties of obtaining sufficient RNA from the ILC cell lines, RNA quality and quantity varied; however, RNA was preferentially selected for that yielding a 260/280 of about 2 and a 260/230 of just greater than 2 (Matlock and ThermoFisher Scientific, 2015).

2.5 RNA Collection from FFPE Tissues

Collection of RNA from the ILC FFPE tissues was conducted using the miRNeasy® FFPE Kit (QIAGEN, Toronto, ON). FFPE tissues had already been cut using a RNase free microtome and mounted on slides by the Histology Core Facility (University of Ottawa) then stored at -80°C until use. To isolate RNA, tissues were scraped from the slide, with special attention being paid to scraping only regions of ILC tumour tissue identified in adjacent hematoxylin and eosin stained sections. Each RNA sample was generated from approximately 1-4 slides depending on the size of the FFPE tumour (adjacent sections cut from the same FFPE tissue block). Using the suggested deparaffinization solution (QIAGEN, Toronto, ON), RNA was collected from the FFPE scrapes following the manufacturer's protocol using the miRNeasy® FFPE Kit. Once isolated, the RNA was quantified using a ND-1000 Nanodrop™ Spectrophotometer and normalized to RNase-free water.

Prior to commencing the above isolation techniques as part of the investigation, nine patient RNA samples had been previously isolated. In these cases, the RNA was isolated from tissue that had been cut using laser capture microdissection (LCM) using the Arcturus® LCM system (ThermoFisher Scientific, ON). Prior to cutting, the samples were stained using the Arcturus® Paradise® Plus FFPE LCM Staining Kit (ThermoFisher Scientific, ON) according to manufacturer's instructions. Once cut, RNA was then isolated from recovered tissue following the manufacturer's protocol using the miRNeasy® FFPE Kit.

2.6 cDNA Synthesis for miRNA Analysis

Once isolated and quantified, RNA was diluted to achieve a final amount of 1µg of RNA in up to 12µL of RNase-free water for complementary DNA (cDNA) synthesis following the protocol outlined in the miScript® II RT Kit (QIAGEN, Toronto, ON). Two separate buffers are

included in the kit, the 5x miScript® HiSpec Buffer which was used for the miRNA genome (miRNome) analyses as the buffer is optimized for profiling miRNA using the miRNome arrays as described in section 2.10 or the 5x miScript® HiFlex Buffer which was used for the quantification of mature miRNAs (QIAGEN, 2011)(QIAGEN, Toronto, ON). A GeneAmp® PCR system 9700 (Applied Biosystems, ThermoFisher Scientific, ON) or T100™ Thermal Cycler (Bio-Rad, Mississauga, ON) was used to achieve the incubation temperatures of 37°C for 60min, 95°C for 5min and left at 4°C. Samples with no reverse transcriptase and no template RNA were made to be used as controls in downstream applications. Once generated, the cDNA was then stored at -20°C.

2.7 cDNA Synthesis for mRNA Analysis

RNA treated with DNase was used to make cDNA for mRNA analysis. RNA was diluted to achieve a final amount of 1µg of RNA in up to 10µL of RNase-free water for cDNA synthesis. Added to the diluted RNA was 1µL of 50µM random hexamers (Invitrogen, ThermoFisher Scientific, ON) and 1 µL 10mM 2'-deoxynucleoside 5'-triphosphate (dNTP) mix from the 100mM dNTP Set (Invitrogen, ThermoFisher Scientific, ON). The samples were then heated to 65°C for 5min using a GeneAmp® PCR system 9700 or T100™ Thermal Cycler. The samples were then placed on ice and quickly centrifuged with a microcentrifuge. To the samples an additional 4µL of 5X First Strand Buffer (Invitrogen, ThermoFisher Scientific, ON), 2µL of 0.1M dithiothreitol (DTT) (Invitrogen, ThermoFisher Scientific, ON), and 1µL RNase OUT™ recombinant ribonuclease inhibitor (Invitrogen, ThermoFisher Scientific, ON) were added. Using again a GeneAmp® PCR system 9700 or T100™ Thermal Cycler, the samples were heated to 37°C for 2min. Finally, 1µL of Moloney Murine Leukemia Virus (M-MLV) reverse transcriptase

(Invitrogen, ThermoFisher Scientific, ON) was added to each sample. Subsequently, the samples were placed in a GeneAmp® PCR system 9700 or T100™ Thermal Cycler and heated as follows: 25°C for 10min, 37°C for 50min, 70°C 15min and left at 4°C. Samples with no reverse transcriptase and no template RNA were also generated to be used as controls in downstream analyses. Once completed, the cDNA was stored at -20°C.

2.8 Preamplification of RNA Isolated from FFPE Tissues

Due to low RNA yield obtained when extracting from FFPE tissues, the samples were preamplified to increase the amount of available cDNA for miRNome profiling (QIAGEN, 2012)(QIAGEN, Toronto, ON). A 1000-4000-fold amplification of the cDNA is a result of preamplification using the miScript® PreAMP PCR kit (QIAGEN, 2012)(QIAGEN, Toronto, ON). RNA was first diluted to a final amount ranging between 10-100ng in 6µL of RNase-free water (QIAGEN, Toronto, ON). Subsequently, the protocol for miRNA cDNA synthesis for preamplification was followed as outlined by the manufacturer's protocol. The 5x miScript® HiSpec buffer was selected for cDNA synthesis due to its preferential use with miRNome profiling (QIAGEN, 2012). Once mixed, the reaction was incubated using a GeneAmp® PCR system 9700 for: 37°C for 60min and 95°C for 5min and left at 4°C. The cDNA samples were then diluted with 40µL of RNase-free water according to the manufacturer's protocol. The preamplification was conducted following the protocol outlined in the miScript® PreAMP Handbook (QIAGEN, Toronto, ON). The MBHS-3216Z miScript® PreAMP miRNome Primer Mix (QIAGEN, Toronto, ON) was selected as it ensures preamplification of miRNA targets found in the specific miRNome analysis (QIAGEN, 2012)(QIAGEN, Toronto, ON). This part of the protocol was split into the three tubes corresponding to the three specific primer mixes included in the miScript® PreAMP

miRNome Primer Mix. The samples were then preamplified using again a GeneAmp® PCR system 9700 with the following cycling conditions: 95°C for 15min, 3-step cycling of 94°C for 30 seconds (s), 55°C for 60s and 70°C for 60s for 2 cycles, then 2-step cycling of 94°C for 30s and 60°C for 3min for 10 cycles and then left for 4°C. After cycling the three tubes were combined and the resulting preamplification was diluted with 300µL of RNase-Free water.

Once preamplification was completed, a quality control Quantitative Real-Time Polymerase Chain Reaction (qPCR) was run to ensure that the preamplification was successful (QIAGEN, Toronto, ON). The qPCR was conducted using 4µL of the final diluted preamplification reaction, then diluted further with 92µL of RNase-Free water. The qPCR was executed following the protocol and using the primers included in the miScript® PreAMP PCR kit. The qPCR was run on a 96-well plate in duplicate on a 7500 Real Time PCR System (Applied Biosystems, ThermoFisher Scientific, ON) with the following conditions: 15min at 95°C, and 40 cycles of 3-step cycling of 15s at 94°C, 30s at 55°C and 34s at 70°C. Before running the qPCR plate, it was checked for bubbles and centrifuged at 1000 revolutions per minute (RPM) using a Beckman Coulter Allegra™ 6R centrifuge (Beckman Coulter, Mississauga, ON). The two primers run on the quality control qPCR were small nucleolar RNA, C/D box 95 (SNORD95), and miRTC (QIAGEN, Toronto, ON). After the qPCR was complete the threshold was set to 0.01 and the baseline was set to begin at cycle 2 and end at cycle 10. In order to pass quality control, the sample's threshold cycle (C_t) of SNORD95 should be no lower than 25 and miRTC should be within a C_t of 17 +/- 3 (QIAGEN, 2012)(QIAGEN, Toronto, ON). The samples resulting C_t values were analyzed to confirm the samples capacity to be used for further experiments, and those that did not pass the quality control thresholds were discarded.

2.9 Quantitative Real Time Polymerase Chain Reaction of mRNA and miRNA

mRNA expression was evaluated using qPCR reactions set-up using 2μL of a 1:10 dilution of cDNA (section 2.7) in RNase-Free water, 5 μL RT^2 SYBR® Green ROX qPCR MasterMix (QIAGEN, Toronto, ON), 1μL 10μM 1:1 ratio of forward and reverse custom DNA oligo primer mix (Invitrogen, ThermoFisher Scientific, ON), and 2 μL of RNase-Free water. Primers were designed using two available online software programs: Roche LifeScience's Universal Probe Library Assay Design Center (Roche Molecular Systems Inc, Indianapolis, IN) and NCBI's Primer-BLAST (National Center for Biotechnology Information, U.S. National Library of Medicine, Bethesda, MD). Primers were received as 25nmole, desalted and were reconstituted to 100μM with RNase-Free water. All samples and specific primers were run in triplicate on a 96-well plate, with no reverse transcriptase and no template samples included as controls on each plate. The selected endogenous control for the qPCR plate was a custom DNA oligo of β-Actin (Invitrogen, ThermoFisher Scientific, ON) and the reference sample was dependent on the experiment.

qPCR analysis of miRNA was conducted using the miScript® SYBR® Green PCR kit according to manufacturer's directions (QIAGEN, Toronto ON). cDNA was made as described above in section 2.6 and diluted 1:2 with RNase-Free water. All miRNA primers used were predesigned and available from the miScript® Primer Assays GeneGlobe (QIAGEN, Toronto, ON). SNORD95 was selected as an endogenous control based on its lower degree of inter-sample variance observed in the miRNome analyses and across the four ILC cell lines when tested by qPCR. The reference sample was selected depending on the type of experiment.

The use of SNORD95 which was selected from a list of controls offered by QIAGEN for the miRNA qPCR protocol was used as an endogenous control during this thesis (QIAGEN,

2011)(QIAGEN, Toronto ON). Its use is supported by previous literature attesting to their utility as an endogenous control as small nucleolar RNA (snoRNA) (Bignotti et al., 2016) are found to be evenly expressed across numerous cell types (QIAGEN, 2011)(QIAGEN, Toronto ON). They are useful for miRNA investigations as an endogenous control gene as they belong to the same type of RNA family as miRNA, that being small non-coding RNA (Bignotti et al., 2016). While snoRNA may not be miRNA, they are; however, believed to undergo similar or even shared processing as miRNA (Scott and Ono, 2011), therefore strengthening their use as normalizers for miRNA investigations. It is common practice in the investigation of miRNA to use snoRNAs as endogenous controls. Many papers, including those cited in this thesis, engage in this common practice (Shi and Teng, 2015; Zaman et al., 2012). Due to its stable expression within the FFPE tissues, and the four ILC cell lines, SNORD95 was selected as the endogenous control for all miRNA experiments of this thesis to allow datasets to be compared.

qPCR analysis was conducted in a 96-well plate, and each sample with specific primer was run in triplicate with a no reverse transcriptase and no template control included on the plate. Prior to running qPCR plates, they were checked for bubbles and centrifuged at 1000 RPM for one minute using a Beckman Coulter Allegra™ 6R centrifuge (Beckman Coulter, Mississauga, ON). qPCRs were preformed using the standard settings for SYBR® green with melt curve on a 7500 Fast Real-Time PCR System (Applied Biosystems, ThermoFisher Scientific, ON). The selected run method was as follows: holding temperatures of 50°C for 20s then 95°C for 10min, followed by 40 cycles of 95°C for 15s and 60°C for 1min, and melt curve analysis of 95°C for 15s, 60°C 1min, 95°C 30s and 60°C 15s. Calculations for relative quantification were done by the 7500 Fast Real-Time PCR System software system, 7500 Software v2.3 (Applied Biosystems, ThermoFisher Scientific, ON). Each sample was normalized to its endogenous control SNORD95 (ΔC_t), and then

normalized to its relative experimental sample control ($\Delta\Delta C_t$), which varied between experiments. The formula 2^(-ΔΔCt) was used to produce a relative quantification value, which was then plotted.

qPCR on the remaining cDNA (section 2.8) of the patient FFPE tissue samples was conducted following a similar protocol to the miRNA qPCR. First the remaining cDNA was diluted with 35µL of RNase-Free water resulting in a 1:2 dilution. The qPCR was run on a 96-well plate in duplicate and run on a 7500 Fast Real-Time PCR System following the same run method as outlined above. C_t values generated through the 7500 Fast Real-Time PCR System were taken and the mean $2^{\Delta C_t}$ was calculated and plotted.

Table 1: mRNA Primer Sequences

mRNA Primers (Invitrogen, ThermoFisher Scientific, ON)		
Target	**Forward Primer**	**Reverse Primer**
β-Actin	CCAACCGCGAGAAGATGA	CCAGAGGCGTACAGGGATA
ARHGEF1	TCTCTCTGCACCCTCTGTCC	GGACTCCAGGCTCATTGG
SV2A	CCTGGGAATATCGTGTCTGC	GCAGGAGACACAGGACATCA
CA11	TGTTCCCTGAATCCTTCGGC	CAGGGAGTGCATCTGAAGGG
SULF1	CCAATGCTTCCCAACACATA	GCAGCATTGGTCCTGTGTACT
CHPT1	GCATGTTGAGATTTGGAAAAGTGG	CCAACACCACCATGGAGGATAA
CHRD	TCTCTCTGCACCCTCTGTCC	GGACTCCAGGCTCATTGG

Table 2: miRNA Primers

miRNA Primers (QIAGEN, Toronto, ON)			
Hs_miR-28_1	MS00003255	Hs_miR-23c_1	MS00022897
Hs_miR-23b_2	MS00031647	Hs_SNORD95_11	MS00033726
Hs_miR-199b-3p_1	MS00008981	Hs_miR-3607-3p_1	MS00022953
Hs_miR-3647-3p_1	MS00031794	Hs_miR-642a_1	MS00023828
Hs_miR-199b_1	MS00003731		

2.10 miRNA Genome Analysis

miRNome analyses were conducted using the MIHS-3216Z-12 miRNome miScript® miRNA PCR Array Human miRbase V16 (QIAGEN, Toronto, ON) while following the protocol outlined in the miRNome miScript® miRNA PCR Array Handbook (QIAGEN, Toronto, ON). This array is a SYBR® based qPCR array that analyzes the expression of 1066 human miRNAs (QIAGEN, 2013)(QIAGEN, Toronto, ON), with primers for each miRNA preloaded into wells of a 384-well plate. RNA isolated from FFPE samples was preamplified following the methods outlined in section 2.8, and RNA isolated from cell lines was prepared following section 2.6 (with no preamplification) which were then used in the miRNome analyses. The preamplified cDNA from FFPE samples was already diluted as a result of the miScript® PreAMP PCR kit protocol; however, the cDNA generated from RNA isolated from cell lines was diluted with an additional 310µL of RNase-Free water prior to analysis. A master mix comprised of the miScript® SYBR® Green PCR kit and 300µL of cDNA was mixed, and 10µL was added to each well of the 384-well plate. The array plates were run on a C1000 Touch™ Thermal Cycler with a CFX384™ Real-Time System (Bio-Rad, Mississauga, ON). The cycling conditions were those outlined in the miScript® miRNA PCR Array Handbook (QIAGEN, Toronto, ON): initial activation step of

15min at 95°C, followed by 40 cycles of denaturation for 15s at 94°C, annealing for 30s at 55°C and extension of 30s at 70°C, with a final melt curve analysis conducted. Prior to analyzing the data, the baseline threshold was established across all of the sample's plates for each replicate, with each miRNome replicate consisting of 3 plates. Resulting qPCR data was analyzed using the online GeneGlobe Data Analysis Center software (https://www.qiagen.com/ca/shop/genes-and-pathways/data-analysis-center-overview-page/?akamai-feo=off) (QIAGEN, Toronto, ON). For each miRNA the data analysis software calculates fold change and fold regulation values (QIAGEN, Toronto, ON) as well as their statistical significance based on C_t values normalized using an arithmetic mean from a selection of six different internal controls included in the plate array (QIAGEN, Toronto, ON). The following are the controls found on the plate array that may be selected for normalization: SNORD61, SNORD68, SNORD72, SNORD95, SNORD96A, RUN6-6P (QIAGEN, 2018)(QIAGEN, Toronto, ON). For the comparison of the miRNome analyses, each one was controlled to SNORD95 to ensure the same control across all analyses and the following validation experiments.

2.11 miRNA Hairpin Inhibitor and Mimic Transfection

Pre-designed hairpin inhibitors and mimics were selected based on targeting miRNA of interest and purchased from QIAGEN. Each hairpin inhibitor and mimic experiment was conducted with the suggested controls according to QIAGEN's Guidelines for miRNA mimic and miRNA inhibitor experiments (QIAGEN, 2015). The selected hairpin inhibitor control was the suggested miScript® Inhibitor Negative Control (QIAGEN, 2015)(QIAGEN, Toronto, ON) and will be referred to as the control hairpin inhibitor. The selected mimic control was the recommended AllStars Neg. siRNA tagged with Alexa Flour 488 (AF488), which will be referred

to as the control mimic (QIAGEN, 2015)(QIAGEN, Toronto, ON). Though the control mimic is an siRNA, it does not target any human genes and is a recognized system for the appropriate controlling of miRNA mimic effects (QIAGEN, 2015; Qian et al., 2017). Both the hairpin inhibitor and mimic controls are negative non-gene targeting controls (QIAGEN, 2015)(QIAGEN, Toronto, ON). Each tested hairpin inhibitor and mimic dose was conducted with its corresponding control hairpin inhibitor or mimic at the same dose.

For transfection of cells with miRNA mimics or hairpin inhibitors, the day before transfection, cells were plated to 50-60% confluency, which was approximately 7.5 x 10^5 cells/6cm dish. The day after plating, mixtures of 350μL of Opti-MEM™ I (1X) reduced serum medium with HEPES, 2.4g/L sodium bicarbonate and L-glutamine (Opti-MEM™) (Gibco, ThermoFisher Scientific, ON), and doses of mimic (1-20nM)/hairpin inhibitor (20-100nM) (QIAGEN, Toronto, ON) were created. Another mixture of 8μL Oligofectamine™ Reagent (Invitrogen, ThermoFisher Scientific, ON) and 42μL Opti-MEM™ (Gibco, ThermoFisher Scientific, ON) was mixed and incubated at room temperature for 5min, following which, 50μL of the mixture was added to the combination containing either the mimic or hairpin inhibitor. The mimic or hairpin inhibitor Oligofectamine™ mixtures were incubated for an additional 15min at room temperature, during which time cells were washed once with Opti-MEM™, and 1.6mL of Opti-MEM™ was added to each dish. After the incubation, 400μL of the mimic or hairpin inhibitor Oligofectamine™ mixture was added to the cells which were returned to the incubator at culture conditions for 4 hours (hr). Following this incubation, 1mL of 3X FBS containing culture media was added to the dish, and cells were returned to culture conditions for various lengths of time, until used to isolate RNA or used in other downstream biological assays. In the context of invasion, migration or cell growth

assays, transfected cells were incubated for 24hr before being plated for these assays. RNA for analysis of transfected samples by qPCR, was isolated 48hr post-transfection.

MDA-MB-134VI cells transfected with mimic for subsequent Clariom™ Assays were transfected following the methods described above; however, due to lower RNA yields the MDA-MB-330 cells were transfected with hairpin inhibitor in 10cm dishes prior to being used for Clariom™ Assays. The MDA-MB-330 cell line was plated with approximately 21 x 10^5 cells/10cm dish and were transfected with specific miRNA or control hairpin inhibitors as described above, with the following modifications for larger dish sizes. The first mixture containing Opti-MEM™ and doses of hairpin inhibitor were made to a total of 1050µL. The second mixture consisted of 24µL Oligofectamine™ Reagent and 126µL Opti-MEM™. The cells were washed with 3mL of Opti-MEM™, then 4.8mL of Opti-MEM™ was added to each dish with the additional 1.2mL of the hairpin inhibitor containing mix. Once the 4hr incubation step was complete, 3mL of 3X FBS containing culture media was added, and 48hr later RNA was isolated for Clariom™ Assays.

Table 3: Hairpin Inhibitors and Mimics

Hairpin Inhibitors and Mimics (QIAGEN, Toronto, ON)				
Target	**Hairpin Inhibitor**		**Mimic**	
miR-23c	Anti-hsa-miR-23c	MIN0018000	Syn-hsa-miR-23c	MSY0018000
miR-23b-3p	Anti-hsa-miR-23b-3p	MIN000418	Syn-hsa-miR-23b-3p	MSY0000418
Control	miScript® Inhibitor Negative Control	1027271	AllStars Neg. siRNA tagged with Alexa Flour 488 (AF488)	1027284

2.12 Immunofluorescence of Control Mimic

To ensure effective transfection efficiency, the MDA-MB-134VI cell line was plated on a sterile glass coverslip in a 6cm dish at approximately 7.5 x 10^5 cells/dish. The cells were then transfected with the control mimic, AllStars Neg. siRNA tagged with Alexa Flour 488 (AF488), following the transfection methods outlined in section 2.11. One sample was used as a mock; therefore the cells underwent the transfection process, without the addition of the control mimic. Forty-eight hours post-transfection, media was aspirated, and the coverslips were washed with DPBS. The coverslip was then fixed with 4% paraformaldehyde (pH 7.2-7.4) (1.3M Paraformaldehyde, 2mM $MgCl_2$, 1.25mM egtazic acid (EGTA) (pH 8), 1X Phosphate-Buffered Saline (PBS)) and washed again with DPBS. Subsequently, the coverslip was mounted onto a slide using Dako Fluorescence Mounting Medium and observed using an Axioskop 2 MOT with Axiocam Carl Zeiss microscope to take fluorescent images. All images taken of the AF488 dye, used an excitation of 493nm and an emission of 520nm at magnifications of either 100X or 400X. These images allowed for the evaluation of transfection efficiency with the miRNA mimic by observing the location and intensity of fluorescence of the control mimic compared to brightfield images of the cells.

2.13 Clariom™ Assays

The Clariom™ Assays (ThermoFisher Scientific, ON) were conducted by the Génome Québec Innovation Center (McGill, Montreal, QC). RNA was isolated from transfected or un-transfected cells and quantified as described in section 2.4. Once isolated, the RNA was diluted in RNase-Free water to 85ng/µL as recommended in the Sample Preparation User Guide for Gene Expression Analysis Services provided by the Genome Québec Innovation Centre. RNA quality was initially assessed by the Genome Québec Innovation Centre, by Bioanalyzer and NanoDrop™.

Upon passing quality controls, RNA was used for hybridization with the Clariom™ D Assay (human) (Applied Biosystems, ThermoFisher Scientific, ON) for the VIVA-1, VIVA-2 and MDA-MB-134VI comparisons, or the Clariom™ S Assay (human) (Applied Biosystems, ThermoFisher Scientific, ON) for the specific miRNA inhibitor and mimic transfected cells.

It should be noted for the transfected cell samples; modulation of miRNA levels was confirmed using specific miRNA qPCR as described in section 2.9 to ensure sufficient modulation of miR-23c and miR-23b-3p levels following transfection with mimic or hairpin inhibitor prior to sending for analysis to the Génome Québec Innovation Center. Once the Clariom™ assays were completed, the resulting data was analyzed using the Transcriptome Analysis Console (TAC) Software (ThermoFisher Scientific, ON) which performs sample normalization and statistical analysis to compare data sets and identify targets and pathways (appliedbiosystems and ThermoFisher Scientific, 2017)(ThermoFisher Scientific, ON).

2.14 Invasion Chamber and Transwell® Migration Assays

Prior to commencing this investigation, the MDA-MB-330 cell line was tested for their invasive capabilities at 24 and 48hr, with 48hr found to be the best reflection of their invasive capabilities. The minimally invasive cell lines had been tested for their invasive capabilities at 48hr which did not result in many invasive cells; therefore, due to their slow growth seen in culture, 1-week invasion was tested and found to be the best representation of their invasive capabilities. Growth Factor Reduced Corning® Matrigel® Invasion Chamber 24-well plate 8.0 micron (invasion chamber) (Corning, Corning, NY) were used to test cell invasion, which was performed using an adapted recommended manufacture's protocol. All assays were conducted in duplicate. Prior to plating cells, the invasion chambers were rehydrated for 2hr in cell line specific culture

conditions with 0.5mL reduced FBS media ranging from 1-5% depending on the cell line. The media was then aspirated from the invasion chambers and the cells were plated within the insert at approximately $5x10^4$ cells per chamber. The invasion chambers were plated with 0.5mL reduced (1-5%) FBS media within the insert and 0.75mL of 5-20% FBS containing cell line specific culture media on the bottom, thus creating a gradient of FBS. Chambers were incubated in culture conditions for either 48hr or one week depending on the cell line. Once the time point was completed, the invasion chamber membranes were stained and imaged for quantification.

An exception to the methods described above, are those used to execute Figure 3. Four conditions with various FBS concentration gradients were conducted, an outline depicting these conditions can be found in Figure 3A. Two of the conditions were set up as follows. The cells were plated inside the invasion chambers as previously described; however, the bottom portion of the invasion chamber had either 10% or 20% FBS containing culture media. The other two conditions were conducted after serum starving the MDA-MB-330s overnight in 0% FBS containing culture media. The next day, the cells were plated in the top of the invasion chambers with 1% FBS containing culture media and the bottom of the invasion chamber had either 10% or 20% FBS containing culture media.

Cell migration assays were conducted using Transwell® Permeable supports 6.5mm insert 24 well plate 8.0μm polycarbonate membrane (Transwell®) (Costar, Corning, Corning, NY); however, were coated with 10μg/mL fibronectin (Sigma-Aldrich, Oakville, ON) and incubated at 4ºC overnight. Prior to cell seeding, the fibronectin coated Transwells® were rehydrated in 0.1mL cell line specific culture media containing 5% FBS for approximately two hours in the incubator at 37°C and 5% CO_2. The media was then aspirated from the Transwells® and the cells were plated within the Transwell® at $5x10^4$ cells/well in 0.1mL cell specific culture media with 5% FBS, and

0.6mL of cell specific culture media containing 20% FBS was added to the bottom of each Transwell® to create an effective FBS concentration gradient. Transwells® were then incubated at 37°C in 5% CO_2 for 24 or 48hr depending on the cell line.

Upon time point completion, the invasion/migration chambers were stained and imaged for quantification. Briefly, media from inside the chamber was aspirated, and a cotton swab was used to remove non-invading cells remaining on the surface of the inside portion of the membrane. After repeating this step a second time, this time dipping the cotton swab in the media, the chamber was placed in ~500μL of 100% methanol for 10-30s to fix cells to the membrane. Cells were then stained for about 30s with 0.5% Crystal Violet solution (12.3mM Crystal Violet (Fisher Scientific, ThermoFisher Scientific, ON), 25% Methanol), followed by three washes with water to remove excess stain, at which time staining was repeated to achieve a deeper stain.

For enumeration of invaded cells in invasion chambers, five random fields of view were imaged for each membrane at 100X using a Nikon Eclipse TE2000-U (Nikon, Mississauga, ON) and the number of invading cells was counted using the ImageJ (National Institutes of Health, Bethesda, MA) Cell Counter plugin (Kurt De Vos, University of Sheffield, Sheffield, UK). For cell migration through Transwells®, membranes were allowed to dry overnight after staining was complete and were then removed from the Transwells® and mounted on slides under coverslips using VectaMount® (Maravai LifeSciences, San Diego, CA). The slides were then imaged at 20X using the Aperio ScanScope® system (Leica Biosystems, Concord, ON), and the number of cells was counted from five representative images at the 20X field of view using the Aperio ImageScope software (Leica Biosystems, Concord, ON). After counting the number of migrating/invading cells, the data was either normalized to the control treatments and plotted, or raw counts were subsequently plotted.

As some variation was seen between biological replicates, invasion and migration assays were normalized to control conditions in most cases. The variation observed was believed to be in part due to the cell's conditions at the time of the assay, including passage number and degree of confluency prior to plating, in addition to differences in chambers between different lot and batch numbers. It was noted however, that the proportion of invading cells remained similar between different experimental conditions throughout biological replicates. Therefore, it was decided that normalization of the number of invading cells compared to the control would be the best representation of the data and would allow for statistical analysis across biological replicates to be conducted.

2.15 Isolating Cells from Invasion Chambers

The VIVA cell sub-populations were isolated from parental MDA-MB-134VI cells that had invaded through invasion chambers. Using methods described in section 2.14, MDA-MB-134VI cells were plated in 12 invasion chambers and incubated for 1-week at 37°C and 5% CO_2. To collect invaded cells, the media was aspirated from within the invasion chambers, and the non-invading cells on the top side of the membrane were scrubbed off using sterile cotton swabs. The invasion chambers were then transferred into a 24-well plate containing 1mL of DPBS per well, to wash the membranes. The invasion chambers were then moved to another 24-well plate containing 750µL of 0.05% trypsin-0.53mM EDTA per well to remove cells that had invaded through to the bottom side of the membrane. After trypsinization for 5min at 37°C and 5% CO_2, the invasion chamber was removed and 800µL of MDA-MB-134VI culture media was added to the well to neutralize the 0.05% trypsin-0.53mM EDTA. The media was then collected from all 12 wells of the 24-well plate and combined to be centrifuged at 1200 RPM for 5min using a

Thermo Scientific Sorval ST 8 centrifuge (ThermoFisher Scientific, ON) to pellet the cells. The media was then aspirated, and the pellet was resuspended in approximately 2mL of media and plated into 2 wells of a 24-well plate. The media was then changed approximately every two days. Once the cells had reached confluency, cells were harvested by trypsinization and used to seed gradually larger sized tissue culture dishes to allow cell growth and expansion. This sub-population of cells was named the VIVA-1 cell line.

To create the VIVA-2 sub-population, the VIVA-1 cell sub-population was subjected to the same invasion procedure as above and incubated for 1 week. The cells which had invaded to the bottom side of the invasion chambers after 7 days were isolated from the invading VIVA-1 cells, and serially expanded to generate the VIVA-2 sub-population. Both sub-populations grow in the same media and culture conditions as their parental MDA-MB-134VI cell line, as described in section 2.1.

2.16 Cell Growth and Viability Assay

To assess cell growth and viability of un-transfected cells (VIVA-1, VIVA-2, MDA-MB-134VI), cells were harvested by trypsinization and 2.5 x 10^4 cells/well were seeded in duplicate in a 24-well plate. For assessing growth and viability of transfected cells, MDA-MB-330 or MDA-MB-134VI cell lines were initially transfected in 6cm plates following the transfection protocol as described in section 2.11 and harvested by trypsinization and re-plated approximately 24hr later at a density of 2.5 x 10^4 cells/well in duplicate in 24-well plates. For the UACC-3133 cell line 24hr after transfection in 6cm dishes, cells were harvested by trypsinization and seeded at 2.0 x 10^4 cells/well in duplicate in a 24-well plate. To assess cell viability, cells in duplicate wells were independently harvested by trypsinization every two days after seeding and viable cells were

counted using Trypan blue solution (Sigma-Aldrich, Oakville, ON) staining and enumeration with the Vi-Cell™ XR. Duplicate values were then averaged and graphed.

2.17 Western Blot

To generate total protein lysates, the media was aspirated, and cells were washed twice at room temperature with DPBS. Cells were lysed following addition of protein lysis solution containing radioimmunoprecipitation assay (RIPA) Buffer (20mM Tris, 150mM NaCl, 1% NP-40, 1% Triton x100, 12.1mM Sodium Deoxycholate, 0.1% Sodium dodecyl sulfate (SDS), 0.2mL 1mM Ethylenediaminetetraacetic acid (EDTA)) and Protease Inhibitor Cocktail (0.2mM 4-(2-Aminoethyl)benzenesulfonyl fluoride hydrochloride (AEBSF), 0.03μM aprotinin, 11.6μM bestatin hydrochloride, 1.4μM N-(trans-Epoxysuccinyl)-L-leucine 4-guanidinobutylamide (E-64), 0.1μM leupeptin hemisulfate salt, 0.1mM EDTA) (Sigma-Aldrich, Oakville, ON). Cells were then scraped from the dish and transferred to an Eppendorf™ tube to be incubated on ice. The lysis was then vortexed for 10s in 5-10min intervals then incubated on ice for 30min. Subsequently, samples were centrifuged for 15min at 13500RPM at 4°C using an Axyspin R refrigerated microcentrifuge (Axygen, Corning, Corning, NY) to isolate the supernatant. Total protein in lysates was quantified using the Bio-Rad Protein Assay Dye Reagent Concentrate (Bio-Rad, Mississauga, ON), and absorbance was measured at 595nm using a BioMate 3 (ThermoFisher Scientific, ON) which then provided a protein quantification in mg/mL after performing a curve linear regression 2nd order. For subsequent analysis by western blot, 50μg of total protein was diluted in ddH_2O and mixed with 1X ß-mercaptoethanol based sample buffer (12.5mM Tris-HCl (pH 6.8), 4% glycerol, 0.4% SDS, 1% ß-mercaptoethanol, 0.01% bromophenol blue). The samples were then incubated at

100°C for 5min, placed on ice and then centrifuged at 4°C at 4000RPM using an Axyspin R refrigerated microcentrifuge (Axygen, Corning, Corning, NY) for 3min.

Using a Bio-Rad gel apparatus (Bio-Rad, Mississauga, ON), a 1.5mm 10% resolving SDS-Polyacrylamide gel electrophoresis (PAGE) (9.9% 30% Acrylamide/Bis Solution 29:1 (Bio-Rad, Mississauga, ON), 375mM Tris (pH 8.8), 0.1% SDS, 0.1% ammonium persulfate (APS), 0.04% Tetramethylethylenediamine (TEMED)) was made and left to polymerize for about 30min-1hr, then a 5% stacking Tris-Acrylamide gel (5% 30% Acrylamide/Bis Solution 29:1, 127M Tris (pH 6.8), 0.1% SDS, 0.1% APS, 0.1% TEMED) was made and was added to the top of the resolving gel and left to polymerize with a 15-well comb in place for about 10min. Protein samples were loaded into the wells of the Tris-Acrylamide gel and subjected to electrophoresis in 1X running buffer (24.8mM Tris Base, 192M glycine, 3.5mM SDS) at 140V in a Mini-PROTEAN® Tetra Cell (Bio-Rad, Mississauga, ON). A BLUeye Prestained Protein Ladder (FroggaBio Inc, Toronto, ON) was included in a separate lane of the gel, to facilitate identification of protein molecular weights. Following separation of proteins on the Tris-Acrylamide gel, proteins were transferred in 1X transfer buffer (31.25mM Tris base, 250mM glycine, 20% methanol) by electrophoresis at 100V for 90min using either a VWR AccuPower Model 500 (VWR International, Ville Mont-Royal, QC) or a Bio-Rad PowerPac™ HC power supply (Bio-Rad, Mississauga, ON) using the Tetra Blotting Module (Bio-Rad, Mississauga, ON), to an Immobilon®-P PVDF membrane (Millipore Ltd., Etobicoke, ON). The PVDF membrane had been pre-treated with methanol, ddH_2O, and 1X transfer buffer.

Upon completion of protein transfer, the non-specific sites on the PVDF membrane were blocked in blocking solution consisting of either 5% skim milk or bovine serum albumin (BSA) in 1X Tris-Buffered Saline with Tween (TBST) (1X Tris-Buffered Saline (TBS) (20mM Tris Base,

140mM NaCl (pH 7.6)), 0.1% Tween-20) for approximately 1hr at 4°C on a platform rocker. After blocking, membranes were incubated with specific primary antibody diluted in either 5% skim milk or 5% BSA in 1X TBST and incubated overnight at 4°C on a platform rocker. Primary antibody was then removed, and the membrane was washed three times with 1X TBST for approximately 5min each with agitation on an orbital shaker. Secondary antibody (Jackson ImmunoResearch Inc., West Grove, PA) specific to the species of the primary antibody diluted with 5% skim milk or 5% BSA in 1X TBST was then added to the membrane and incubated for approximately 1hr at room temperature on an orbital rocker. Secondary antibody was then removed, and the membrane was washed five times with 1X TBST for approximately 5min each time. Protein antibody conjugates were then visualized following addition of Bio-Rad Clarity™ Western ECL Substrate (Bio-Rad, Mississauga, ON) and subsequently imaged using either the Genegnome Syngene Bio Imaging imager (Syngene, Frederick, MD) or HyBlot CL® Autoradiography Film (Denville Inc., Saint-Laurent, QC) with a JP33 JPI Automatic X-ray film processor (JPI Healthcare, Plainview, NY). Dependant on location of the targeted protein, stripping buffer (200mM glycine, 291mM NaCl, 35mM SDS (pH2)) may have been used to remove the bound primary and secondary antibodies from the membrane. This was done by first washing the membrane in 1X TBST, then the addition of 5-10mL of stripping buffer for 5min three times while on an orbital shaker. The membrane was then washed twice with 1X TBST on an orbital shaker for 5min each wash. Primary antibody was either added again, or the membrane was stored in 1X TBST at 4°C when not in use.

Antibodies to specific protein targets used in western blot analysis are described below. Mouse monoclonal anti-human E-cadherin antibody was used at a 1:1000 dilution (610181, BD Pharmingen, BD Biosciences, Mississauga, ON). Mouse monoclonal anti-human ERα (6F11)

antibody was used at a dilution of 1:1000 (MA1-80216, Invitrogen, ThermoFisher Scientific, ON). Rabbit monoclonal anti-human HER2/ErB2 (29D8) antibody was used at a 1:1000 dilution (2165, Cell Signalling Technology Inc., New England Biolabs Ltd., Whitby, ON). Mouse monoclonal anti-human β-Actin antibody was used at a 1:2000 or 1:5000 dilution (A5316, Sigma-Aldrich, Oakville, ON). Secondary antibodies, Peroxidase AffiniPure Goat Anti-Mouse IgG (H+L) (115-035-146, Jackson ImmunoResearch Inc., West Grove, PA) and Peroxidase AffiniPure Goat Anti-Rabbit IgG (H+L) were used at a 1:2000 dilution (111-035-144, Jackson ImmunoResearch Inc., West Grove, PA).

2.18 Data Presentation and Statistics

The data in this thesis was graphed by choosing relevant types of graphs through Graph Pad Prism 5, 6 and 8 software (GraphPad Software, San Diego, CA). The appropriate statistical analysis was selected and calculated using the included Graph Pad Prism software (GraphPad Software, San Diego, CA). One-way ANOVA with Tukey's multiple comparisons was used to analyze datasets with multiple groups (GraphPad Statistics Guide, GraphPad Software, 2017). Comparison of two groups, control versus treatment or sub-population versus parental, was analyzed using an unpaired t test with Welch's correction (GraphPad Statistics Guide, GraphPad Software, 2017). A Two-way ANOVA with either Tukey's or Sidak's multiple comparisons was used to analyze multiple groups and factors (GraphPad Statistics Guide, GraphPad Software, 2017). All graphs unless otherwise specified, are plotted as mean values (GraphPad Statistics Guide, GraphPad Software, 2017). All error bars represent the standard error of the mean (SEM), and levels of significance are indicated with *, with the corresponding p value found in the figure's description.

Table 4: Symbols for Statistical Significance

ns	p value: >0.05
*	p value:≤0.05
**	p value: ≤0.01
***	p value: ≤0.001
****	p value: ≤0.0001
(GraphPad Software, 2009)	

Chapter 3: Results

3.1 Characterize and Identify the Invasive Capabilities of Four ILC Cell Lines

3.1.1 Protein Characterization of the ILC Cell Lines

There are a limited number of ILC cell lines available (Brinkley et al., 1980; Cailleau et al., 1974, 1978; Christgen and Derksen, 2015; Christgen et al., 2009; Domann et al., 2000; Ethier et al., 1993; Jambal et al., 2013) and unfortunately those that are accessible are poorly investigated (Tasdemir et al., 2018). Prior to commencing this investigation, four ILC cell lines were characterized to ensure a better understanding of the selected models. A protein analysis indicated that the selected ILC cell lines are each distinctly unique and possess markers of ILC. Figure 1 depicts the expression of some ILC markers, HER2, E-cadherin and ERα in the four ILC cell lines of this investigation (Arpino, Bardou, Clark, & Elledge, 2004; Moll & Mitze, 1993). All of the ILC cell lines were found to express HER2, and ERα to some level. The MDA-MB-330s have been shown previously to overexpress HER2 (Hollestelle et al., 2010), and this appears to be the case in Figure 1, as the MDA-MB-330 cell line has a large amount of HER2 expression compared to the other cell lines. The HER2 blot may appear overexposed, but this was done in order to visualize HER2 expression in the MDA-MB-134VI cell line. Although the literature suggests a lack of HER2 expression in both the MDA-MB-134VI (Christgen et al., 2009; Hollestelle et al., 2010) and the IPH-926 (Christgen et al., 2009) cell lines, we see what is believed to be normal expression of HER2 in the MDA-MB-134VIs; however, in the IPH-926s we see an expression that is between the levels MDA-MB-330 and MDA-MB-134VI. It appears that ERα has an increase in mass in the UACC-3133 cell line as seen by the slower migrating band, which may be a result of glycosylation or alternative splicing of the protein (Moore and AbD Serotec, 2009). IPH-926 were

characterized to be ER negative, but we occasionally see very low expression of ERα (Christgen et al., 2009). Expression of E-cadherin was limited to the MDA-MB-330 and UACC-3133 cell lines. Although the MDA-MB-330 have E-cadherin expression, it has been found to be non-functional as it and p120 have been relocated to the cytoplasm (Tasdemir et al., 2018). There does not seem to be literature suggesting that the UACC-3133 cell line has mutations in E-cadherin; however, there may be post-translational modifications contributing to the double bands present in Figure 1 (Jackson ImmunoResearch Laboratories, 2017; Mann and Jensen, 2003). Therefore, we may conject that the E-cadherin status of the UACC-3133 is unique and will be worth further investigation if it is to be continually used as an ILC cell line.

3.1.2 Characterization of the Invasive Capabilities of the ILC Cell Lines

In addition to confirming the specific protein profile of relevant ILC markers, the four ILC cell lines were tested for their invasive capabilities using Matrigel® coated 8 micron pore invasion chambers, since invasion is a marker of metastatic potential (Qian et al., 2017). Initial experiments assessed the invasive capabilities of the cell lines following 48hr of incubation with directed invasion towards increased serum concentrations in the lower well of the invasion assays. While pervious work had indicated little to no cell invasion for 3 of the 4 cell lines at 48hr, robust cell invasion of the MDA-MB-330 cell line was observed after 48hr (Figure 2A). Given the limited invasion of the remaining 3 cell lines at 48hr, we extended the incubation time in the invasion chambers to 7 days. All 3 cell lines had limited invasion after one week (Figure 2B), thus we deemed them minimally invasive for our subsequent studies. Since analysis of the minimally invasive cell lines was being conducted at 7 days, the MDA-MB-330 were tested for their invasion at a 7-day time point and the results were found to be too numerous to count. Therefore, for the

A

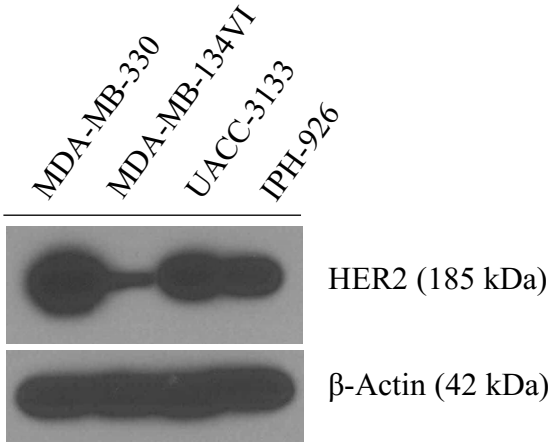
MDA-MB-330
MDA-MB-134VI
UACC-3133
IPH-926
HER2 (185 kDa)
β-Actin (42 kDa)

B

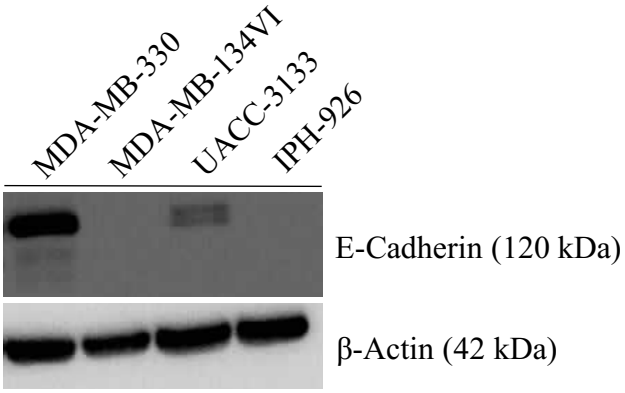
MDA-MB-330
MDA-MB-134VI
UACC-3133
IPH-926
E-Cadherin (120 kDa)
β-Actin (42 kDa)

C

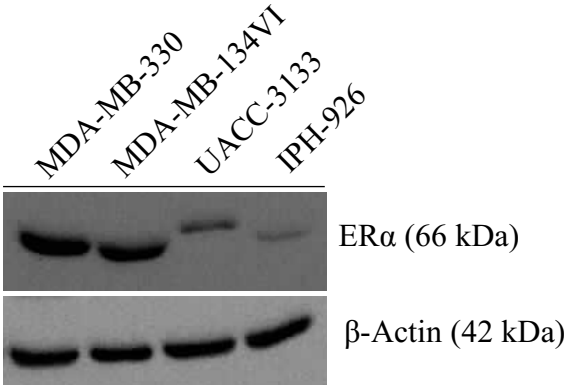
MDA-MB-330
MDA-MB-134VI
UACC-3133
IPH-926
ERα (66 kDa)
β-Actin (42 kDa)

Figure 1: Specific ILC marker expression in the four ILC cell lines.

Protein lysates were collected from plated cells with RIPA buffer. Subsequently, 50μg of protein was isolated from the cells and subjected to western blot analysis and probed with specific antibodies for various proteins of interest along with β-Actin as the loading control. (A) HER2 (B) E-cadherin (C) ERα (n=3 biological replicates).

remainder of the investigation we analyzed the invasive capabilities of the invasive MDA-MB-330 at 48hr and the minimally invasive cell lines at 7 days.

3.1.3 Confirmation of the Invasive Capabilities of the MDA-MB-330 Cell Line

Since conducting the characterization experiments at the beginning of this thesis, Tasdemir et al., (2018) published a paper establishing the invasive properties of select ILC cell lines, which included two of the ILC cell lines in this study (Tasdemir et al., 2018). They published that all the ILC cell lines they investigated in their paper had minimally invasive capabilities, including the MDA-MB-330 cell line (Tasdemir et al., 2018). As this was in contrast to the results shown in Figure 2 where the MDA-MB-330 cell line was found to be extremely invasive at 48hr, it was hypothesized that observed differences may be in part due to different cell culture or invasion assay methods between Tasdemir et al., (2018) and this thesis. Tasdemir et al., (2018) grew the MDA-MB-330 cell line in 10% FBS and 1:1 DMEM and Leibovitz's, which is a different culture method than recommended by ATCC® (American Type Culture Collection, 2019b). According to ATCC®, the MDA-MB-330 media should consist of Leibovitz's and 20% FBS along with additional growth factors: EGF, insulin, and glutathione (American Type Culture Collection, 2019b). The culture methods outlined in this thesis are those suggested by ATCC®, with additional DMEM to adapt the MDA-MB-330s to CO_2 conditions, thereby making the media 1:1 DMEM and Leibovitz's (American Type Culture Collection, 2019b). In addition to these differences in cell culture media, the paper by Tasdemir et al., (2018) serum starved the MDA-MB-330 cell line overnight, then put the cells into a serum free invasion chamber with FBS as the chemoattractant. Additionally, the authors appeared to use a different FBS gradient compared to that used in this thesis, and perhaps this was not sufficient to stimulate invasion while the selected gradient in this

A

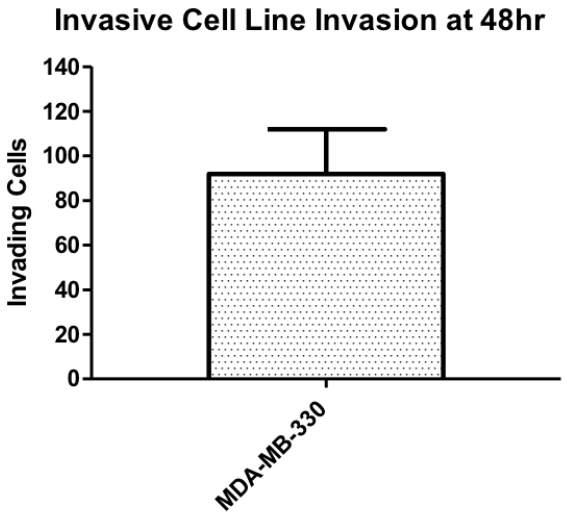
Invasive Cell Line Invasion at 48hr
Invading Cells
140
120
100
80
60
40
20
0
MDA-MB-330

B

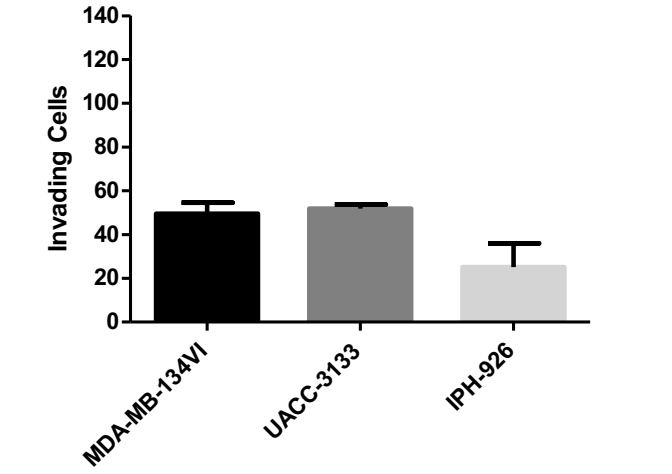
Minimally Invasive Cell Line Invasion at 1 Week
Invading Cells
140
120
100
80
60
40
20
0
MDA-MB-134VI
UACC-3133
IPH-926

Figure 2: Establishment of MDA-MB-330 as an invasive ILC cell line, and MDA-MB-134VI, UACC-3133 and IPH-926 as minimally invasive ILC cell lines.

The invasive capabilities of the four ILC cell lines was established through their ability to invade towards FBS through Matrigel® coated invasion chambers after 48hr or 7 days depending on the cell line. Invading cells were stained with crystal violet, counted from 5 representative images and plotted with the SEM. (A) The MDA-MB-330 are an invasive ILC cell line as they were able to invade within 48hr of platting in an invasion chamber. (B) The MDA-MB-134VI, UACC-3133 and IPH-926 are minimally invasive ILC cell lines as a limited number of cells were able to invade after one week within an invasion chamber (n=3 biological replicates).

thesis was. Each of these differences in methods may be possible reasons for discrepancies seen in the invasive capabilities of the MDA-MB-330s, therefore an experiment was conducted to substantiate the invasive nature of the MDA-MB-330 cell line.

MDA-MB-330 cells were serum starved overnight as was done in the paper by Tasdemir et al., (2018); however, all other growth factors normally found in the ATCC® recommended media were included (American Type Culture Collection, 2019b; Tasdemir et al., 2018). As it was feared the cells would not survive absolute serum free conditions for an extended period of time, we put the cells into invasion chambers with significantly reduced serum (1%) and the growth factors in the top of the chambers to maintain cell viability throughout the assay. To stimulate invasion, 10% and 20% FBS containing culture media was selected as the chemoattractant for the invasion chambers; these conditions are depicted in Figure 3A. These conditions were tested in comparison to those used in this thesis to ascertain the invasive capabilities of the MDA-MB-330s and to determine the most effective method of stimulating their invasive capabilities.

As seen in Figure 3B, the MDA-MB-330 cell line in our hands, remained invasive at all four tested conditions. This suggests that the growth conditions used in the paper by Tasdemir et al., (2018) may alter the properties of the MDA-MB-330 cell line and therefore their results may not be an accurate representation of the cell line's characteristics. This data does however, suggest that the 1:4 serum ratio used in this thesis ensures the greatest yield of invading MDA-MB-330 cells. This may be a consequence of the 5% FBS in the top chamber providing the best growth conditions for the cells throughout the course of the experiment, while ensuring a great enough FBS gradient to entice invasion. Figure 3B additionally indicates that serum starving the MDA-MB-330 cell line overnight did not significantly alter the invasive capabilities of the cells. Though there is no significant difference in the number of invading cells when comparing low serum

conditions, to those used in this thesis, it is believed that the results in this thesis may be a better representation of the invasive capabilities of the MDA-MB-330 cell line. This is considered to be a result of the growth conditions used in this thesis as they were compliant with those established by ATCC® and associated with trends for the highest levels of cell invasion (American Type Culture Collection, 2019b).

3.2 miRNA Genome Profile Invasive and Minimally Invasive ILC Cell Lines and Validate the Differential Expression of Specific miRNA

3.2.1 miRNA Genome Profile of the Invasive Compared to Minimally Invasive ILC Cell Lines

Once the invasive capabilities of the cell lines were established, comparison of their miRNA profiles could be executed. To generate the miRNA profile of each of the ILC cell lines, a miRNome analysis was conducted from three independent biological replicates of each cell line. The miRNome analysis compared the expression of 1066 miRNAs (QIAGEN, 2013) between the invasive and minimally invasive ILC cell lines (Figure 4). As seen in Figure 4, volcano plots generated from plotting the fold-change versus the p value of each miRNA indicated that there are a number of miRNA with differential expression in the invasive compared to minimally invasive ILC cell lines. It was noted that most of the significantly differentially regulated miRNA appear to be upregulated, while only one miRNA had significantly decreased expression in the invasive compared to minimally invasive ILC cell lines. From the miRNome analysis miRNAs were selected for further investigation into their potential role in regulating ILC cell line invasion based on greater than 2-fold differential expression and statistical significance (p value <0.05) in the invasive compared to minimally invasive ILC cell lines. From these miRNAs, miRNAs were selected and prioritized for further analysis with preference towards miRNAs with suspected roles

A

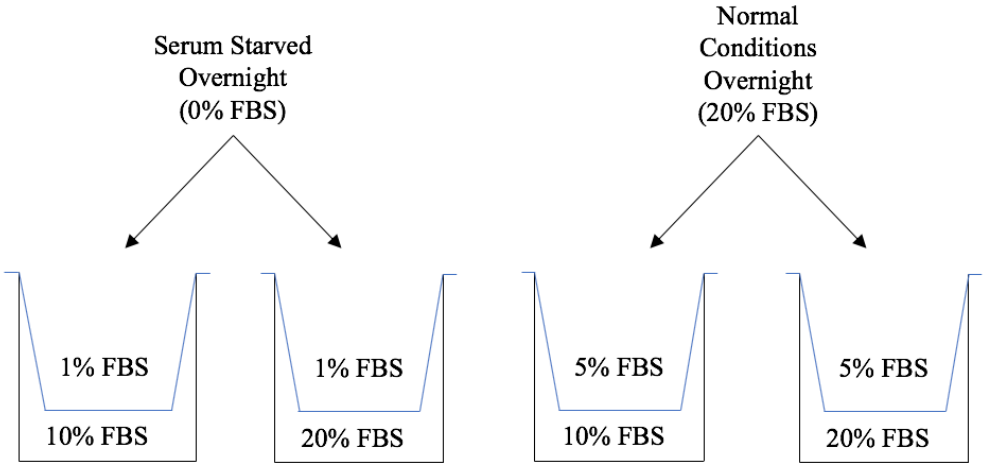
Serum Starved
Overnight
(0% FBS)
Normal
Conditions
Overnight
(20% FBS)
1% FBS
10% FBS
1% FBS
20% FBS
5% FBS
10% FBS
5% FBS
20% FBS

B

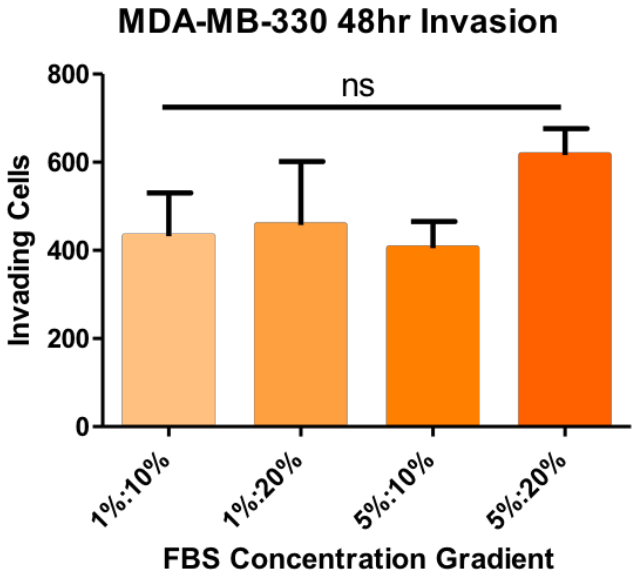
MDA-MB-330 48hr Invasion
ns
Invading Cells
800
600
400
200
0
1%:10%
1%:20%
5%:10%
5%:20%
FBS Concentration Gradient

Figure 3: Confirmation of the most effective media conditions to promote ILC cell line invasion.

The FBS concentration gradient used throughout this thesis yields the greatest number of invading MDA-MB-330 cells. The invasive capabilities of the MDA-MB-330 cell line was confirmed through Matrigel® coated invasion chambers at 48hr. Low serum conditions were tested against those used throughout this thesis, by using different concentration gradients of FBS. Cells were kept in their normal growth media, with changes made to the amount of FBS within the media. After the 48hr time point was completed, invading cells were stained with crystal violet, counted from 5 representative images and plotted with the SEM. (A) Image outlining the methods used to conduct this experiment. (B) First two columns: cells were serum starved overnight in 0% FBS containing media, they were then plated with 1% FBS within the chamber and either 10% or 20% FBS in the bottom of the chamber. Last two columns: cells were platted with 5% FBS media in the top chamber and either 10% or 20% FBS in the bottom of the chamber (n=2 biological replicates, with n=2 technical replicates, One-way ANOVA with Tukey's multiple comparisons). ns, p value >0.05.

in regulating cancer and metastasis (An et al., 2015; Begum et al., 2015; Liu and Wang, 2019; Shi and Teng, 2015; Wong and Wang, 2015; Zaman et al., 2012; Zhang et al., 2018).

3.2.2 Validation of Select miRNA Identified in the miRNome Analysis

Selected from the miRNome analysis were miR-23c, miR-23b-3p and miR-28-5p for further investigation into their significantly increased expression in the invasive compared to minimally invasive ILC cell lines. The miRNome analysis established miR-23c with a fold change of 35.5 (p value 0.03), miR-23b-3p with a fold change of 29.9 (p value 0.04) and miR-28-5p with a fold change of 4.6 (p value 0.02). Through independent biological replicates of cell line RNA, cDNA was generated to assess the levels of these specific miRNA by qPCR. Figure 5 depicts the relative quantification of the three selected miRNA within the four ILC cell lines. All three miRNAs validated within the four cell lines, with all three having increased expression within the invasive MDA-MB-330 cell line compared to the three minimally invasive ILC cell lines. Although miR-28-5p had increased expression in the invasive compared to minimally invasive ILC cell lines, it was found to only have significantly increased expression in the MDA-MB-330 compared to the MDA-MB-134VI and not the other two cell lines. Due to the variable expression of miR-28-5p in the minimally invasive cell lines which does not seem to correlate with their invasive capabilities, there was doubt in its validity to be a regulator of ILC cell line invasion. Therefore, it was not selected for further investigation into its participation in ILC cell line invasion; however, it was kept in mind as a potential component of a miRNA signature of ILC metastasis. Since both miR-23c and miR-23b-3p were found to validate with significantly increased expression in the invasive compared to all three minimally invasive cell lines, and had literature suggesting roles in regulating cancer and metastasis, these miRNA were selected for

MDA-MB-330 vs. MDA-MB-134VI & IPH-926 & UACC-3133

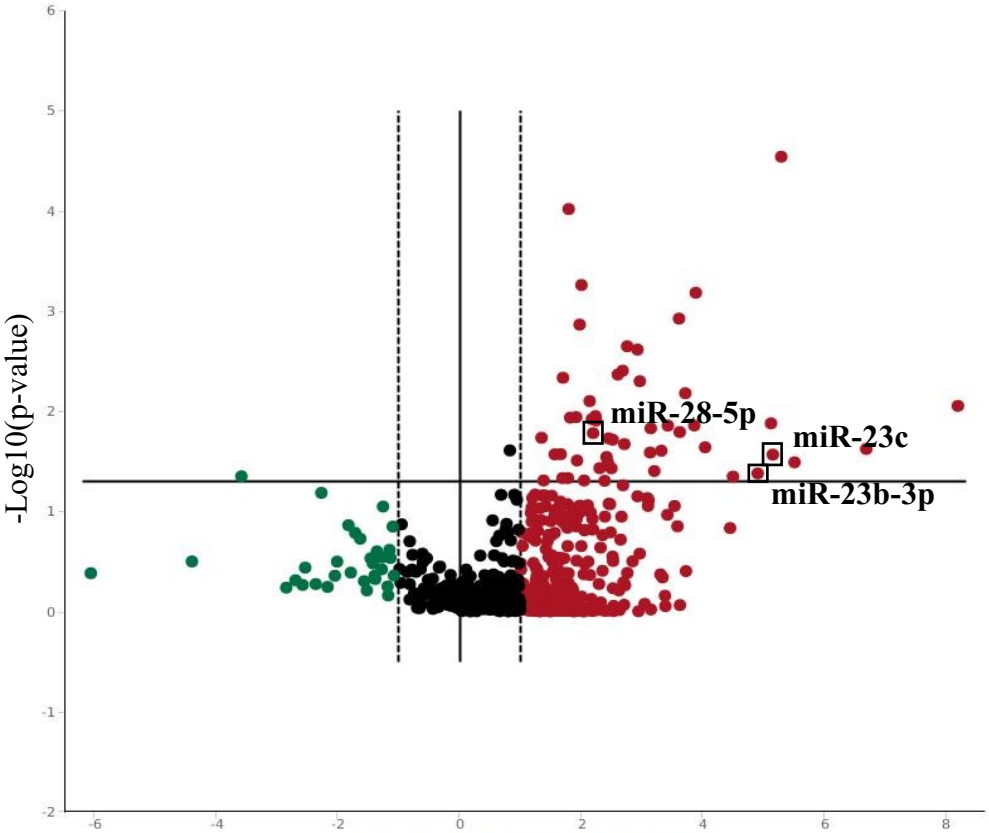

Log2(FC of MDA-MB-330/MDA-MB-134VI & IPH-926 & UACC-3133

Figure 4: Volcano plot comparing miRNA levels in invasive compared to minimally invasive ILC cell lines.

RNA was isolated from plated cells, and cDNA was made using the specific miRNome buffer. miRNome analysis was completed using qPCR-based methods and normalized to the six provided controls. miRNAs selected for further investigation into their expression in the invasive compared to minimally invasive ILC cell lines are marked: miR-23c, miR-23b-3p and miR-28-5p (n=3 biological replicates). Boundary of 2-fold change and p value of 0.05.

further investigation into their potential role in regulating ILC cell line invasion (An et al., 2015; Begum et al., 2015; Liu and Wang, 2019; Shi and Teng, 2015; Wong and Wang, 2015; Zaman et al., 2012; Zhang et al., 2018).

Due to their increased expression in the invasive compared to minimally invasive ILC cell lines, it was hypothesized that miR-23c and miR-23b-3p may play a role in regulating ILC invasion and metastasis. Therefore, the role of miR-23c and miR-23b-3p in ILC was assessed through evaluating subsequent invasion, migration and cell growth upon modulation of their levels within the ILC cell lines. This was achieved through the transfection of miRNA hairpin inhibitors and mimics to decrease and increase the levels of miR-23c and miR-23b-3p within the ILC cell lines, respectively.

3.3 Modulate Levels of miR-23c and miR-23b-3p and Investigate Their Role in ILC Cell Line Invasion

3.3.1 Decreased miR-23c Levels in the MDA-MB-330 Cell Line Results in Decreased Invasion

As previous observations suggested miR-23c was significantly increased in the invasive MDA-MB-330 cell line compared to the minimally invasive cell lines, the MDA-MB-330s were thus transfected with hairpin inhibitors to miR-23c to decrease its levels, or a non-targeting hairpin inhibitor control. Initially a range of concentrations (20, 50 and 100nM) of miR-23c hairpin inhibitor was evaluated to identify the most effective dose for efficient suppression. RNA was isolated from transfected cells and subjected to qPCR to determine the resulting relative quantification of miR-23c. As seen in Figure 6A, it was discovered that a 50nM dose of miR-23c hairpin inhibitor resulted in a significant decrease in the amount of miR-23c in the MDA-MB-330 cell line as compared to that observed in cells transfected with a similar amount of control non-

A

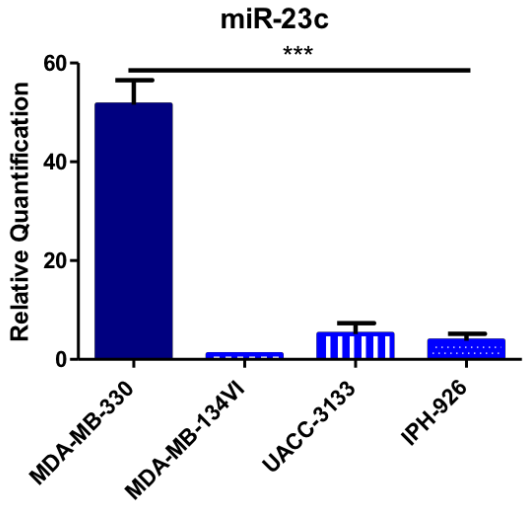
miR-23c
***
Relative Quantification
60
40
20
0
MDA-MB-330
MDA-MB-134VI
UACC-3133
IPH-926

B

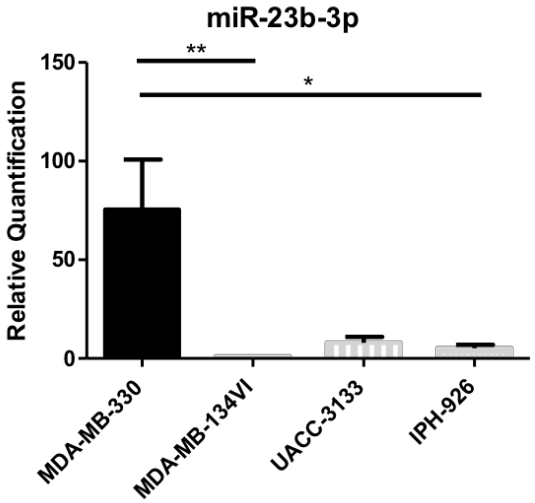
miR-23b-3p
**
*
Relative Quantification
150
100
50
0
MDA-MB-330
MDA-MB-134VI
UACC-3133
IPH-926

C

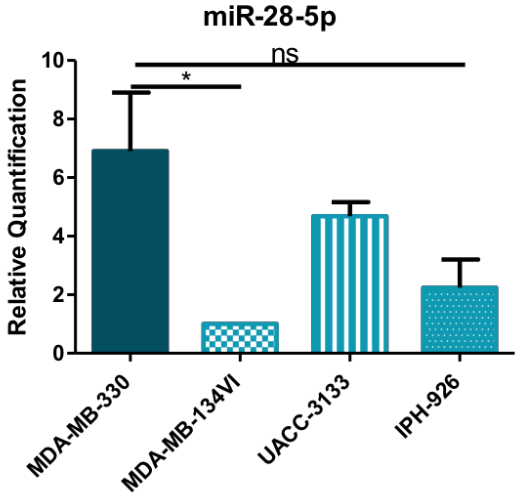
miR-28-5p
ns
*
Relative Quantification
10
8
6
4
2
0
MDA-MB-330
MDA-MB-134VI
UACC-3133
IPH-926

Figure 5: Candidate miRNA miR-23c, miR-23b-3p and miR-28-5p have increased expression in the invasive compared to minimally invasive ILC cell lines.

RNA was isolated from the four ILC cell lines and cDNA was generated to run a qPCR analysis of the expression of the selected miRNAs. Samples were normalized to SNORD95, and to the MDA-MB-134VI cell line which was selected as the relative experimental sample. Relative quantification of the miRNA within the ILC cell lines was graphed along with the SEM for (A) miR-23c (n=4 biological replicates, p value <0.0001), (B) miR-23b-3p (n=4 biological replicates, p value 0.0039) and (C) miR-28-5p (n=3 biological replicates, p value 0.0145). Significance was determined using a One-way ANOVA with Tukey's multiple comparisons. ns, p value >0.05, * p value ≤0.05, ** p value ≤0.01, *** p value ≤0.001.

targeting hairpin inhibitor. The other two doses tested decreased the amount of miR-23c in the cells; however, this was not to the point of statistical significance. Based on these results, we subsequently transfected MDA-MB-330 cells with a 20nM and 50nM dose of hairpin inhibitor, and 24hr post-transfection seeded cells in invasion chamber assays to test the effect of miRNA modulation on the invasive capabilities of MDA-MB-330 cells. As can be seen in Figure 6B, under conditions where miR-23c levels are significantly decreased in the MDA-MB-330 cell line (50nM of hairpin inhibitor), there is a significant decrease in the invasive capabilities of these cells. Although a slight trend for reduced cell invasion was observed when miR-23c levels were modestly decreased following transfection of cells with the 20nM dose of hairpin inhibitor, this was not statistically significant. When the ability of MDA-MB-330 cells to migrate was tested with modulated levels of miR-23c, migration was slightly decreased at the 20nM dose (Figure 6C), but this was not statistically significant, nor were any significant changes observed when the 50nM dose of hairpin inhibitor was used. In addition, no change in cell viability or growth over time was observed following transfection of cells with either dose of miR-23c hairpin inhibitor (Figure 6D).

3.3.2 Decreased miR-23b-3p Levels in the MDA-MB-330 Cell Line Results in Decreased Invasion

The effect of altered miR-23b-3p levels was tested in MDA-MB-330 cells in a similar manner to that described for miR-23c. To test the efficiency of miRNA depletion, cells were initially transfected with various doses (20, 50, 100nM) of miR-23b-3p or non-targeting hairpin inhibitor. RNA was isolated 48hr post-transfection, cDNA was made, and samples were subjected to qPCR. Levels of miR-23b-3p were significantly decreased at the three tested doses of hairpin inhibitor compared to the non-targeting hairpin inhibitor in the MDA-MB-330 cell line (Figure 7A). Subsequently, 20nM and 50nM doses of hairpin inhibitor were tested for their effects on the

A

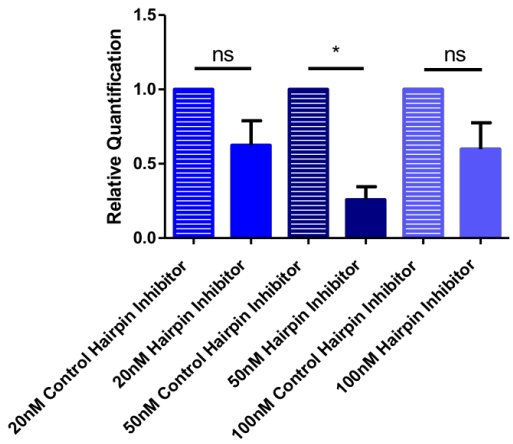
MDA-MB-330 with miR-23c Hairpin Inhibitor
Relative Quantification
1.5
1.0
0.5
0.0
ns
*
ns
20nM Control Hairpin Inhibitor
20nM Hairpin Inhibitor
50nM Control Hairpin Inhibitor
50M Hairpin Inhibitor
100nM Control Hairpin Inhibitor
100nM Hairpin Inhibitor

B

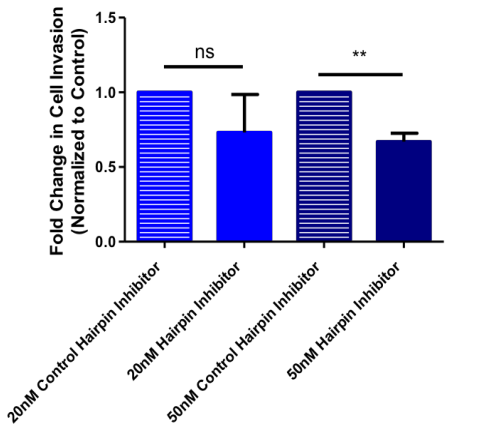
MDA-MB-330 with miR-23c Hairpin Inhibitor 48hr Invasion
Fold Change in Cell Invasion (Normalized to Control)
1.5
1.0
0.5
0.0
ns
**
20nM Control Hairpin Inhibitor
20nM Hairpin Inhibitor
50nM Control Hairpin Inhibitor
50nM Hairpin Inhibitor

C

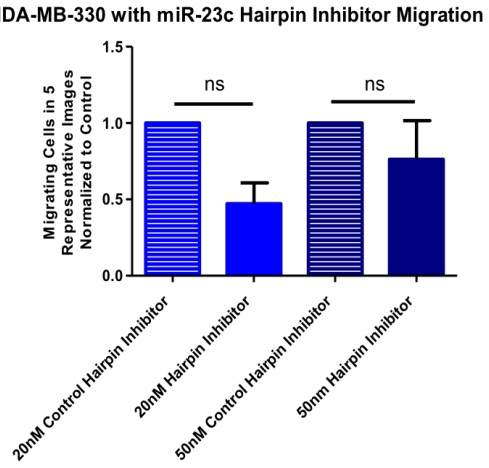
MDA-MB-330 with miR-23c Hairpin Inhibitor Migration
Migrating Cells in 5 Representative Images Normalized to Control
1.5
1.0
0.5
0.0
ns
ns
20nM Control Hairpin Inhibitor
20nM Hairpin Inhibitor
50nM Control Hairpin Inhibitor
50nm Hairpin Inhibitor

D

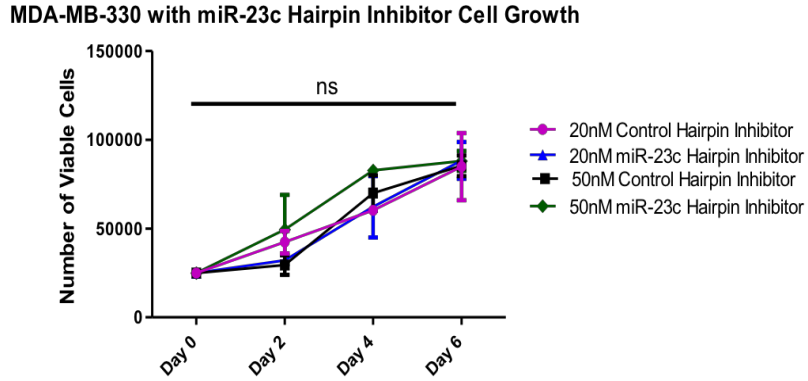
MDA-MB-330 with miR-23c Hairpin Inhibitor Cell Growth
Number of Viable Cells
150000
100000
50000
0
ns
Day 0
Day 2
Day 4
Day 6
20nM Control Hairpin Inhibitor
20nM miR-23c Hairpin Inhibitor
50nM Control Hairpin Inhibitor
50nM miR-23c Hairpin Inhibitor

Figure 6: Depletion of miR-23c levels is associated with reduced MDA-MB-330 cell invasion.

Significant decrease in the levels of miR-23c in the MDA-MB-330 cell line results in a significant decrease in the invasive capabilities of the cell line; however, does not significantly change the cell line's migratory abilities or viability over time. (A) RNA was collected 48hr post-transfection with a miR-23c or non-targeting hairpin inhibitor at multiple doses. Subsequently, cDNA was made and miR-23c levels were evaluated by qPCR. Samples were normalized to SNORD95 and controlled to the non-targeting control hairpin inhibitor. Mean relative quantification was plotted along with the SEM (n=3 biological replicates, unpaired t test with Welch's correction, p value 0.0134). (B) Cells were transfected with a miR-23c or non-targeting hairpin inhibitor and 24hr post-transfection were plated in invasion chambers. Following incubation for 48hr, invasion chamber membranes were stained with crystal violet, and the number of invading cells was counted from 5 representative images and the mean was plotted along with the SEM (n=3 biological replicates, unpaired t test with Welch's correction and n=4 biological replicates, unpaired t test with Welch's correction, p value 0.0099). (C) Twenty-four hours post-transfection with a miR-23c or non-targeting hairpin inhibitor, cells were plated in fibronectin coated Transwells® and left to incubate for an additional 24hr. Transwells® were then stained, the number of migrating cells in 5 representative images was counted, and the data was plotted as mean number of cells with associated SEM (n=3 biological replicates, unpaired t test with Welch's correction). (D) Twenty-four hours post-transfection with a miR-23c or non-targeting hairpin inhibitor, cells were plated to assess cell viability over time. Cell viability was established by trypan blue exclusion 2 days after seeding and every 2 days after for 6 days. Mean number of viable cells was calculated and graphed over time with the associated SEM (n=2 biological replicates, Two-way ANOVA with Tukey's multiple comparisons). ns, p value >0.05, * p value ≤0.05, ** p value ≤0.01.

invasive capabilities of MDA-MB-330 cells. A resulting significant decrease in the invasive capabilities of the cells at 48hr was seen at the 20nM dose of miR-23b-3p hairpin inhibitor as compared to the non-targeting control hairpin inhibitor (Figure 7B). Although the 50nM dose of hairpin inhibitor resulted in a significant decrease in the levels of miR-23b-3p, and a corresponding decrease in the cells ability to invade was observed, this did not reach statistical significance. In contrast to cell invasion, transfected MDA-MB-330 cells did not exhibit any significant changes in cell migration when miR-23b-3p levels were decreased (Figure 7C). In addition, no change was seen in cell viability upon inhibition of miR-23b-3p in the MDA-MB-330 cell line (Figure 7D). Therefore, the results of miR-23c and miR-23b-3p inhibition within the MDA-MB-330 cell line concludes that both miRNAs play a role in regulating MDA-MB-330 cell line invasion without inherently affecting their cell growth, viability, or their basal migratory rates.

3.3.3 Increased miR-23c Levels in the MDA-MB-134VI Cell Line Results in Increased Invasion

Confirming miR-23c and miR-23b-3p play a role in regulating MDA-MB-330 cell line invasion led to the speculation that reciprocal results would be seen in the MDA-MB-134VI cell line following transfection of cells with miRNA mimics. Increasing levels of miR-23c and miR-23b-3p in the MDA-MB-134VI cell line was done through the use of synthetic miRNA mimics. To evaluate the appropriate doses of mimic to be used for subsequent experiments, the miR-23c mimic was tested at three doses (1,10, and 20nM). Following cell transfection, RNA was collected 48hr later to make cDNA, which was then tested for the levels of miR-23c by qPCR. Though not significant, transfection of cells with the miR-23c mimic was able to drastically increase the amount of miR-23c in the MDA-MB-134VI cell line at the three tested doses when compared to cells transfected with control non-targeting mimic (Figure 8A). Cells were plated within invasion

A

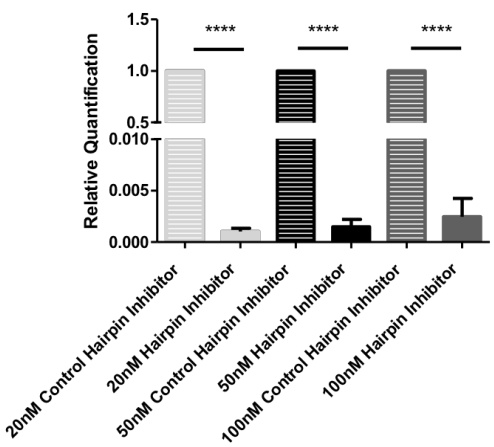
MDA-MB-330 with miR-23b-3p Hairpin Inhibitor
Relative Quantification
1.5
1.0
0.5
0.010
0.005
0.000
****
****
****
20nM Control Hairpin Inhibitor
20nM Hairpin Inhibitor
50nM Control Hairpin Inhibitor
50nM Hairpin Inhibitor
100nM Control Hairpin Inhibitor
100nM Hairpin Inhibitor

B

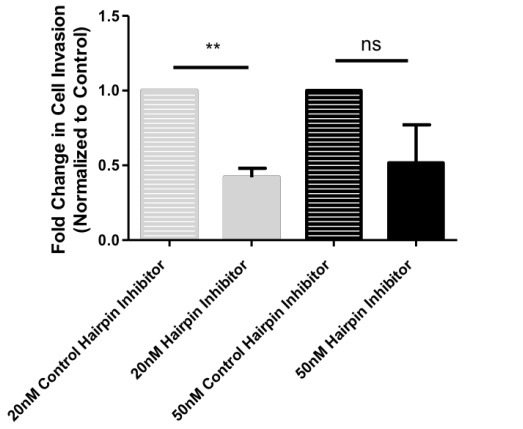
MDA-MB-330 with miR-23b-3p Hairpin Inhibitor 48hr Invasion
Fold Change in Cell Invasion (Normalized to Control)
1.5
1.0
0.5
0.0
**
ns
20nM Control Hairpin Inhibitor
20nM Hairpin Inhibitor
50nM Control Hairpin Inhibitor
50nM Hairpin Inhibitor

C

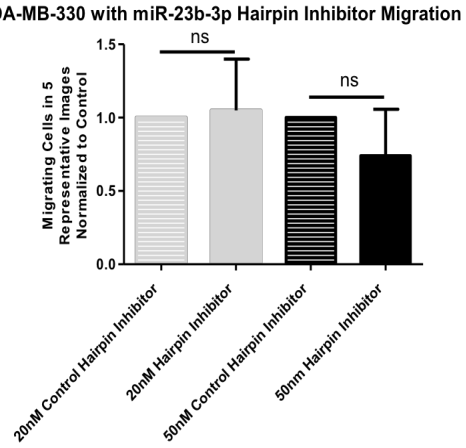
MDA-MB-330 with miR-23b-3p Hairpin Inhibitor Migration
Migrating Cells in 5 Representative Images Normalized to Control
1.5
1.0
0.5
0.0
ns
ns
20nM Control Hairpin Inhibitor
20nM Hairpin Inhibitor
50nM Control Hairpin Inhibitor
50nm Hairpin Inhibitor

D

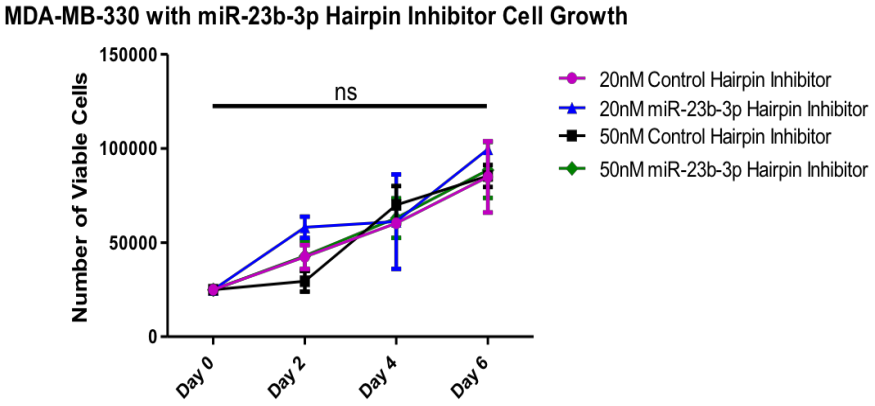
MDA-MB-330 with miR-23b-3p Hairpin Inhibitor Cell Growth
Number of Viable Cells
150000
100000
50000
0
ns
Day 0
Day 2
Day 4
Day 6
20nM Control Hairpin Inhibitor
20nM miR-23b-3p Hairpin Inhibitor
50nM Control Hairpin Inhibitor
50nM miR-23b-3p Hairpin Inhibitor

Figure 7: Depletion of miR-23b-3p levels is associated with reduced MDA-MB-330 cell invasion.

Significant decrease in the levels of miR-23b-3p following transfection of cells with 20nM of hairpin inhibitor in the MDA-MB-330 cell line results in a corresponding significant decrease in the invasive capabilities of the cell line, but does not significantly change the MDA-MB-330 cell line's migratory abilities or viability over time. (A) RNA was collected 48hr post-transfection with a miR-23b-3p or non-targeting hairpin inhibitor at multiple doses. Subsequently, cDNA was made and miR-23b-3p levels were measured by qPCR. Samples were normalized to SNORD95, and then to the control non-targeting hairpin inhibitor. Mean relative quantification was plotted along with the SEM (n=3 biological replicates, unpaired t test with Welch's correction, p value <0.0001). (B) Cells were transfected with a miR-23b-3p or non-targeting hairpin inhibitor and 24hr post-transfection were plated in invasion chambers followed by incubation for an additional 48hr. Invasion chamber membranes were then stained with crystal violet, and the number of invading cells was counted from 5 representative images and plotted as mean invaded cells along with the associated SEM (n=4 biological replicates, unpaired t test with Welch's correction, p value 0.0023 and n=3 biological replicates, unpaired t test with Welch's correction). (C) Twenty-four hours post-transfection with a miR-23b-3p or non-targeting hairpin inhibitor, cells were plated in fibronectin coated Transwells® and left to incubate for an additional 24hr. Transwells® were then stained, the number of migrating cells in 5 representative images was counted, and the data was plotted as mean with associated SEM (n=3 biological replicates, unpaired t test with Welch's correction). (D) Twenty-four hours post-transfection with a miR-23b-3p or non-targeting hairpin inhibitor, cells were plated for cell viability. Cell viability was established by trypan blue exclusion 2 days after seeding and every 2 days after for 6 days. Number of viable cells was calculated and graphed as mean over time with the associated SEM (n=2 biological replicates, Two-way ANOVA with Tukey's multiple comparisons). ns, p value >0.05, ** p value ≤0.01, **** p value ≤0.0001.

chambers 24hr post-mimic transfection, and the cells ability to invade was quantified 1 week later. The resulting increase in miR-23c levels translated into a modest increase in the MDA-MB-134VIs' invasive capabilities at the 1nM dose of mimic; however, this did not reach statistical significance when compared to transfection with similar doses of non-targeting control mimic (Figure 8B). No change was observed in the cells ability to invade when using the 10nM dose of mimic. When investigating the role of miR-23c on the cells ability to migrate, no significant change was seen at any of the tested concentrations of mimic (Figure 8C). In addition, no change was seen in the MDA-MB-134VI cell line growth or viability over time upon increased miR-23c levels with either 1nM or 10nM miR-23c mimic (Figure 8D).

3.3.4 Increased miR-23b-3p Levels in the MDA-MB-134VI Cell Line Results in Increased Invasion

In a similar manner, we tested the effects of increased levels of miR-23b-3p in the MDA-MB-134VI cell line. Initially, three tested doses of miR-23b-3p mimic (1, 10, 20nM) were transfected into MDA-MB-134VI cells, and RNA was isolated 48hr post-transfection. cDNA was then generated and resulting miR-23b-3p levels were quantified by qPCR. A substantial dose-dependent increase (>50 fold) in levels of miR-23b-3p was seen in the MDA-MB-134VI cell line when compared to non-targeting mimics; however, this increase was only significant at the 1nM dose (Figure 9A). Thus, the effects of increased miR-23b-3p at a 1nM and 10nM dose of mimic on the MDA-MB-134VI cell line was tested using Matrigel® coated invasion chambers. Cell invasion was increased by 2-fold at the 1nM dose of miR-23b-3p mimic; however, this did not reach statistical significance. No significant change was seen in the invasive capabilities of the cells at the 10nM dose of mimic as well (Figure 9B). The ability of transfected MDA-MB-134VI cells to migrate and grow was unchanged at both doses of miR-23b-3p mimic as compared to

A

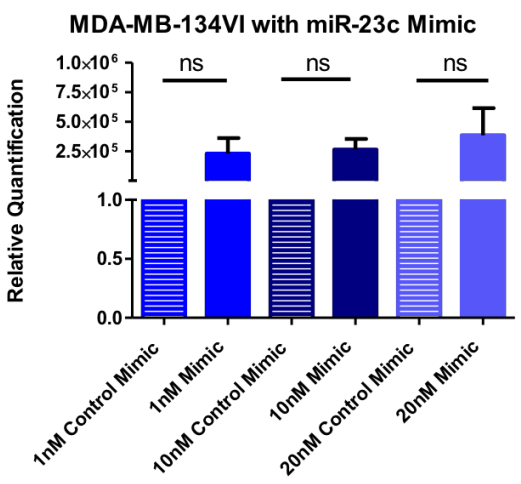
MDA-MB-134VI with miR-23c Mimic
Relative Quantification
1.0x10^6
7.5x10^5
5.0x10^5
2.5x10^5
1.0
0.5
0.0
ns
ns
ns
1nM Control Mimic
1nM Mimic
10nM Control Mimic
10nM Mimic
20nM Control Mimic
20nM Mimic

B

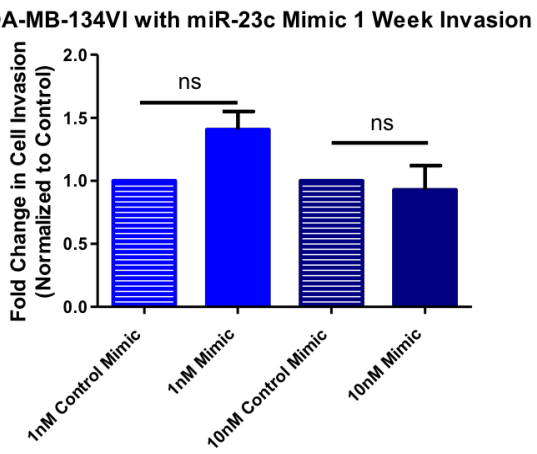
MDA-MB-134VI with miR-23c Mimic 1 Week Invasion
Fold Change in Cell Invasion (Normalized to Control)
2.0
1.5
1.0
0.5
0.0
ns
ns
1nM Control Mimic
1nM Mimic
10nM Control Mimic
10nM Mimic

C

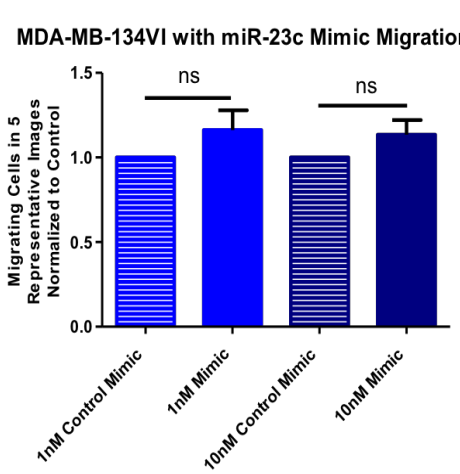
MDA-MB-134VI with miR-23c Mimic Migration
Migrating Cells in 5 Representative Images Normalized to Control
1.5
1.0
0.5
0.0
ns
ns
1nM Control Mimic
1nM Mimic
10nM Control Mimic
10nM Mimic

D

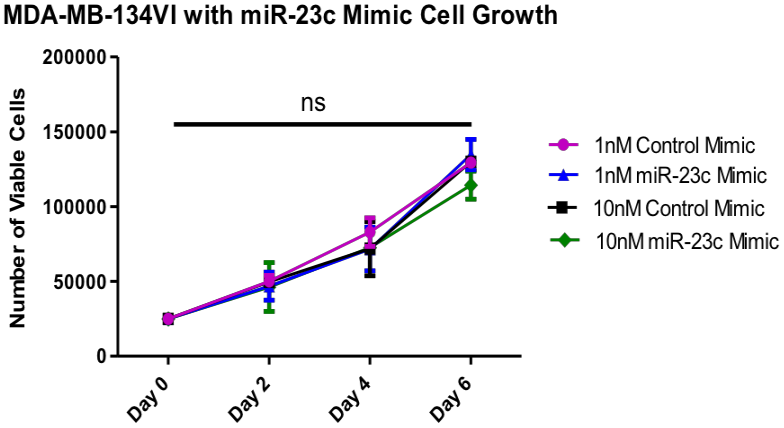
MDA-MB-134VI with miR-23c Mimic Cell Growth
Number of Viable Cells
200000
150000
100000
50000
0
ns
Day 0
Day 2
Day 4
Day 6
1nM Control Mimic
1nM miR-23c Mimic
10nM Control Mimic
10nM miR-23c Mimic

Figure 8: Increased miR-23c levels results in increased MDA-MB-134VI cell invasion.

Increased cell invasion was observed with increased miR-23c levels in MDA-MB-134VI cells following transfection with 1nM of mimic; however, no significant change was seen in the cell's migratory abilities and no change was seen to cell viability and growth over time. (A) RNA was collected 48hr post-transfection with a miR-23c or non-targeting mimic at multiple doses. Subsequently, cDNA was made and miR-23c levels were measured by qPCR. Samples were normalized to SNORD95, and then to the control non-targeting mimic. Mean relative quantification was plotted along with the SEM (n=3 biological replicates, unpaired t test with Welch's correction). (B) Cells were transfected with a miR-23c or non-targeting mimic and 24hr post-transfection were plated in invasion chambers to incubate for 1 week. Invasion chamber membranes were stained with crystal violet, and the number of invading cells was counted from 5 representative images and plotted as the mean along with the associated SEM (n=3 biological replicates, unpaired t test with Welch's correction). (C) Twenty-four hours post-transfection with a miR-23c or non-targeting mimic, cells were plated in fibronectin coated Transwells® and left to incubate for 48hr. Transwells® were then stained, the number of migrating cells in 5 representative images was counted, and the data was plotted as the mean with the SEM (n=3 biological replicates, unpaired t test with Welch's correction). (D) Twenty-four hours post-transfection with a miR-23c or non-targeting mimic, cells were plated for cell viability. Cell viability was established by trypan blue exclusion 2 days after seeding and every 2 days after for 6 days. Number of viable cells was calculated and graphed over time as the mean number of viable cells with the SEM (n=2, Two-way ANOVA with Tukey's multiple comparisons). ns, p value >0.05.

cells with the non-targeting mimic (Figure 9C&D). These results support the contention that miR-23c and miR-23b-3p may regulate MDA-MB-134VI invasion.

Unfortunately the findings pertaining to miR-23c and miR-23b-3p within the MDA-MB-134VI cell line have deceptive p values (Amrhein et al., 2019). The data displays a consistent trend in increased levels of miR-23c and miR-23b-3p and subsequent increased invasion upon transfection with mimics, however the results do not reach significance. When miR-23c and miR-23b-3p levels were increased within the MDA-MB-134VI cell line, substantial variability was seen between biological replicates and significance was not achieved despite a consistent increase in the levels of these miRNAs. These results are however, concordant with the biological changes observed upon transfection of miRNA hairpin inhibitors, supporting the relevancy of these findings despite not reaching statistical significance. Although the p values of these experiments indicate no change, the concordance and consistency of our data suggests cell invasion is modulated by these miRNAs and moreover it has been suggested that p value is not always an appropriate indicator of biological relevancy (Amrhein et al., 2019).

3.3.5 Evaluating the Efficacy of the Mimics

As we consistently saw substantial increases in the level of specific miRNA following transfection of the MDA-MB-134VI cell line with mimics but did not see any statistical significance in the modulation of cell invasion, we confirmed the efficiency of transfection using the non-targeting control mimic tagged with an AF488. This non-targeting control mimic permitted visualization of the subcellular localization of small RNA molecules following transfection of MDA-MB-134VI cells by immunofluorescence. This doubt in transfection efficiency was due to a paper by Thomson et al., (2013) which stated that the amount of functional

A

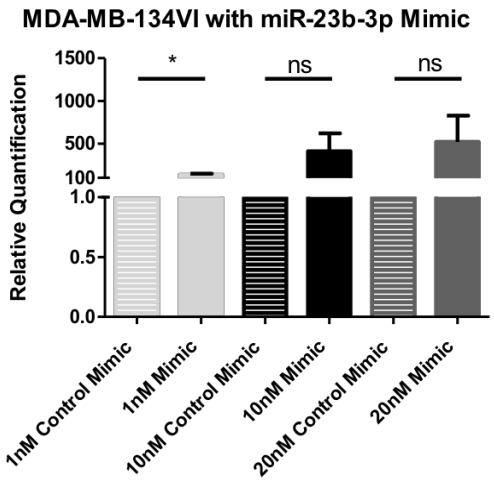
MDA-MB-134VI with miR-23b-3p Mimic
Relative Quantification
1500
1000
500
100
1.0
0.5
0.0
*
ns
ns
1nM Control Mimic
1nM Mimic
10nM Control Mimic
10nM Mimic
20nM Control Mimic
20nM Mimic

B

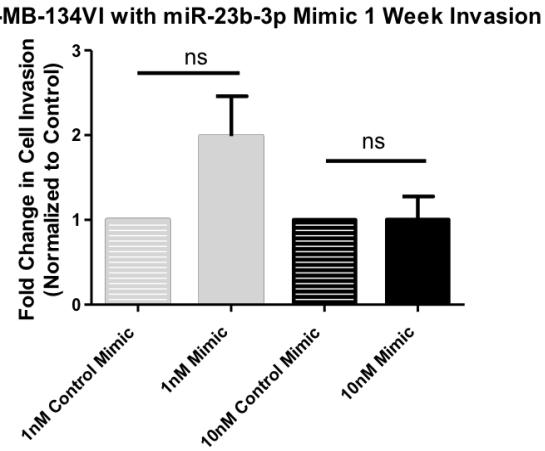
MDA-MB-134VI with miR-23b-3p Mimic 1 Week Invasion
Fold Change in Cell Invasion (Normalized to Control)
3
2
1
0
ns
ns
1nM Control Mimic
1nM Mimic
10nM Control Mimic
10nM Mimic

C

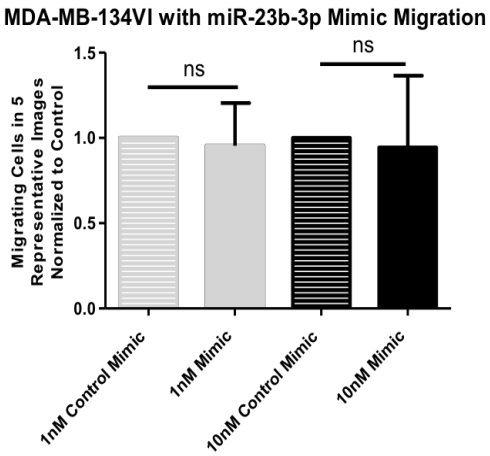
MDA-MB-134VI with miR-23b-3p Mimic Migration
Migrating Cells in 5 Representative Images Normalized to Control
1.5
1.0
0.5
0.0
ns
ns
1nM Control Mimic
1nM Mimic
10nM Control Mimic
10nM Mimic

D

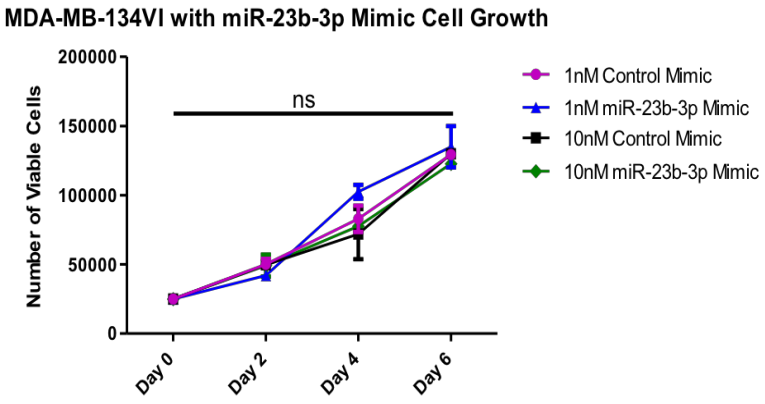
MDA-MB-134VI with miR-23b-3p Mimic Cell Growth
Number of Viable Cells
200000
150000
100000
50000
0
ns
Day 0
Day 2
Day 4
Day 6
1nM Control Mimic
1nM miR-23b-3p Mimic
10nM Control Mimic
10nM miR-23b-3p Mimic

Figure 9: Increased miR-23b-3p levels results in increased MDA-MB-134VI cell invasion.

Increased invasion was seen upon higher levels of miR-23b-3p at the 1nM dose of mimic within the MDA-MB-134VI cell line. No significant change was seen in the cell's migratory abilities upon increased levels of miR-23b-3p and no change was seen to cell viability and growth over time. (A) RNA was collected 48hr post-transfection with a miR-23b-3p or non-targeting mimic at multiple doses. Subsequently, cDNA was made and miR-23b-3p levels were measured by qPCR. Samples were normalized to SNORD95, and to the control non-targeting mimic. Mean relative quantification was plotted along with the SEM (n=3 biological replicates, unpaired t test with Welch's correction, p value 0.0104). (B) Cells were transfected with a miR-23b-3p or non-targeting mimic and 24hr post-transfection were plated in invasion chambers to incubate for 1 week. Invasion chambers were stained with crystal violet, and the number of invading cells was counted from 5 representative images and plotted as the mean along with the associated SEM (n=3 biological replicates, unpaired t test with Welch's correction). (C) Twenty-four hours post-transfection with a miR-23b-3p or non-targeting mimic, cells were plated in fibronectin coated Transwells® and left to incubate for 48hr. Transwells® were then stained, the number of migrating cells in 5 representative images was counted, and the data was plotted as the mean with the SEM (n=3 biological replicates, unpaired t test with Welch's correction). (D) Twenty-four hours post-transfection with a miR-23b-3p or non-targeting mimic, cells were plated for cell viability. Cell viability was established by trypan blue exclusion 2 days after seeding and every 2 days after for 6 days. Number of viable cells was calculated and the mean with associated SEM was graphed over the time (n=2 biological replicates, Two-way ANOVA with Tukey's multiple comparisons). ns, p value >0.05, * p value ≤0.05.

miRNA cannot be depicted in its quantification by qPCR. Thomson et al., (2013) also explained in their paper that transfection of mimics may result in their accumulation in non-functional areas of the cell. Transfected MDA-MB-134VI cells were therefore observed for their uptake of the non-targeting control mimic (Figure 10). The images of Figure 10 indicate that the non-targeting control mimic was able to enter the cells in what seems to be a dose dependent manner; however, there appears to be punctate staining, indicating a higher concentration of non-targeting control mimic in those areas of the cell. This punctate staining reflects the images included in the paper by Thomson et al., (2013) that shows that most transfected mimics end up near or in lysosomes and are not integrated with Argonaute, thereby rendering them non-functional. Though these images do depict the non-targeting control mimic entering the cell, there is no indication of the amount of functional mimic (Thomson et al., 2013) within the MDA-MB-134VI cell line that may be targeting cellular mRNA targets thereby effectively influencing cell phenotypes. The large amount of punctate staining suggests that perhaps the mimics are being sequestered in vesicles rendering them ineffective as elucidated by Thomson et al., (2013).

Although the results of increased miR-23c and miR-23b-3p levels within the MDA-MB-134VI cell line were not significant, perhaps due to the issues presenting with the mimic (Thomson et al., 2013), the data indicates that these miRNAs may promote MDA-MB-134VI invasion. The findings in the MDA-MB-134VI cell line are concordant with that which was seen in the MDA-MB-330 cell line whereby inhibition of miR-23c and miR-23b-3p using hairpin inhibitors appears to reduce cell invasion. Additionally, no change was seen in the MDA-MB-134VI's ability to migrate or proliferate, which is again congruent with the MDA-MB-330 data. It can therefore be concluded that miR-23c and miR-23b-3p play a role in regulating MDA-MB-330 and MDA-MB-134VI invasion without affecting basal cell growth, viability or migratory rates.

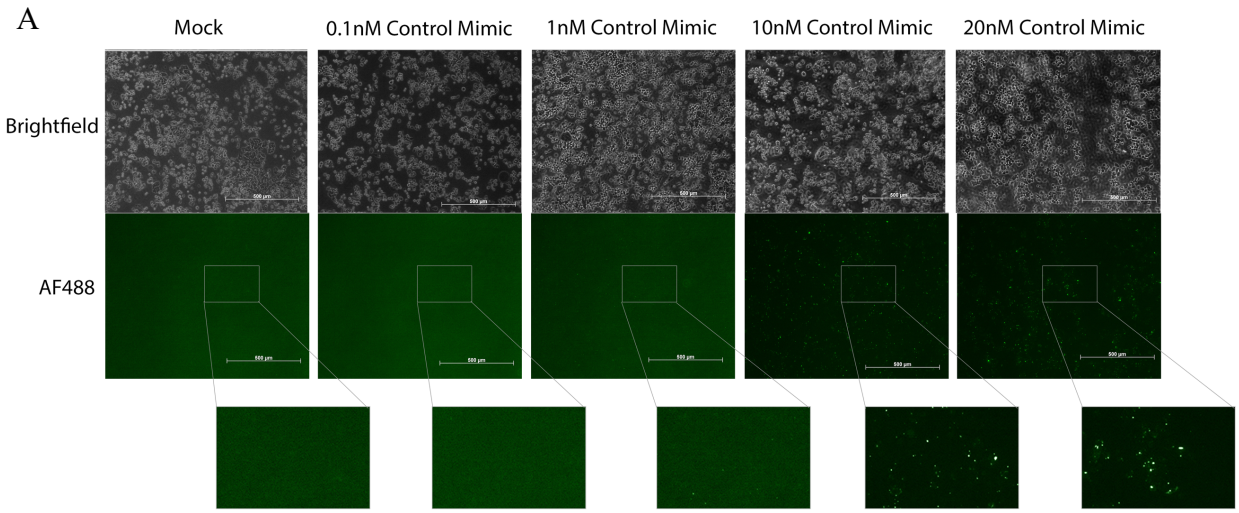
A
Mock
0.1nM Control Mimic
1nM Control Mimic
10nM Control Mimic
20nM Control Mimic
Brightfield
AF488

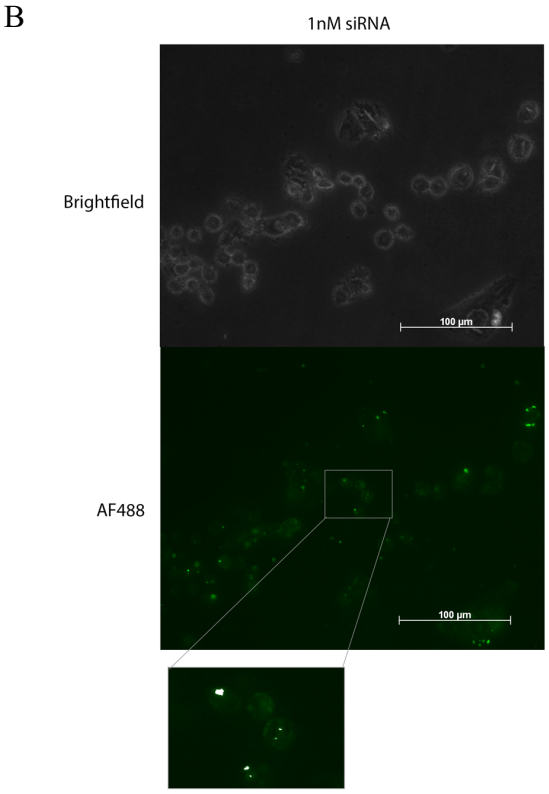
B
1nM siRNA
Brightfield
AF488
100 µm
100 µm

Figure 10: Immunofluorescence of the non-targeting control mimic in the MDA-MB-134VI cell line suggests its accumulation within vesicles.

Cells were plated on coverslips and transfected with the AllStars Neg. siRNA tagged with AF488. Cells were then fixed in 4% paraformaldehyde 48hr post-transfection and mounted on slides. Images were taken with an excitation of 493nm and an emission of 520nm. (A) Taken at 100X, multiple doses of the non-targeting control mimic including a mock, were tested for their transfection efficiency: 0.1nM, 1nM, 10nM, 20nM. The same digital magnification factor was used throughout (n=1, scale bar is 500μm). (B) Taken at 400X to observe the efficacy of transfection of the MDA-MB-134VI cell line with the control mimic at a 1nM dose, as it is the most promising dose of mimic throughout this thesis (n=1, scale bar is 100μm).

3.3.6 Increased miR-23c and miR-23b-3p Levels in the UACC-3133 Cell Line Results in Decreased Invasion

Since it was found that miR-23c and miR-23b-3p regulate MDA-MB-330 and MDA-MB-134VI invasion, it was hypothesized that similar results would be seen in the UACC-3133 cell line with transfection of mimics. As presented in Figure 5, the minimally invasive UACC-3133 cell line has significantly lower levels of both miR-23c and miR-23b-3p than the MDA-MB-330 cell line. As such, mimics were used to increase the levels of both miR-23c and miR-23b-3p in the UACC-3133 cell line and their effect on the cells invasive capabilities were observed. From previous work with the MDA-MB-134VI cell line, the decision was made to pursue this investigation at the 1nM dose of mimic given it was the most effective concentration used previously.

When the UACC-3133 cell line was treated with 1nM of miR-23c mimic, a substantial increase (~10^6-fold) was seen in its' levels when compared to cells transfected with control non-targeting mimic (Figure 11A). When treating the cells with 1nM miR-23b-3p mimic, an approximate 10-fold increase in its levels was seen; this was substantially lower than that seen with the miR-23c mimic. When UACC-3133 cells with altered miR-23c and miR-23b-3p levels were tested in invasion chambers, there was no increase in the invasive capabilities of these cells at one week compared to the non-targeting control mimic (Figure 11B). It appeared rather, that there was a slight decrease in the invasive capabilities of the UACC-3133 cell line upon increasing the levels of either miR-23c or miR-23b-3p. To establish whether the variation seen in the invasive capabilities of the UACC-3133 cell line with modulated levels of miR-23c and miR-23b-3p could be affected by changes in the cells growth rate, a viability assay was conducted. The viability assay found that the growth of the UACC-3133 cell line with increased levels of miR-23c and miR-23b-3p did not significantly change over time (Figure 11C). Therefore, increased levels of miR-23c

and miR-23b-3p within the UACC-3133 cell line results in a slight decrease in the invasive capabilities of the cell line.

3.4 Identification of Putative Targets of miR-23c and miR-23b-3p that May Contribute to Changes in the Invasive Capabilities of the MDA-MB-330 and MDA-MB-134VI Cell Lines

3.4.1 Clariom™ Assays of the MDA-MB-134VIs with Increased miR-23c and miR-23b-3p Levels Identified Possible Targets of the miRNAs

Although the UACC-3133 cell line invasion data did not confirm the findings seen in the MDA-MB-134VI cell line, perhaps due to issues with the mimic (Thomson et al., 2013), our previous data in the MDA-MB-330 and MDA-MB-134VI cell lines suggests a possible role of miR-23c and miR-23b-3p in ILC cell line invasion. Thus, possible pathways regulated by these miRNA may identify protein targets that contribute to ILC cell line invasion. To identify key pathways and possible protein targets of miR-23c and miR-23b-3p, the MDA-MB-134VI cell line was transfected with 1nM of miR-23c, miR-23b-3p, or non-targeting control mimic. RNA was then isolated 48hr post-transfection and sent for Clariom™ Assays at the Génome Québec Innovation Center (McGill University). Once the data output was received, it was analyzed using the recommended TAC software. The results received from the Clariom™ Assays are displayed in the volcano plots of Figure 12. The datasets were analyzed based on p values rather than FDR p values, focusing on targets that were found to be ≥2-fold significantly downregulated when miR-23c and miR-23b-3p levels were increased, as these have the highest likelihood of being direct putative targets, in addition to those targets that were found to be ≥2-fold significantly downregulated in both miRNA datasets. Targets were also selected and prioritized based on the literature indicating any possible role they may have in cancer, breast cancer or metastasis. Potential targets were further investigated for their expression levels in the cell lines with

A

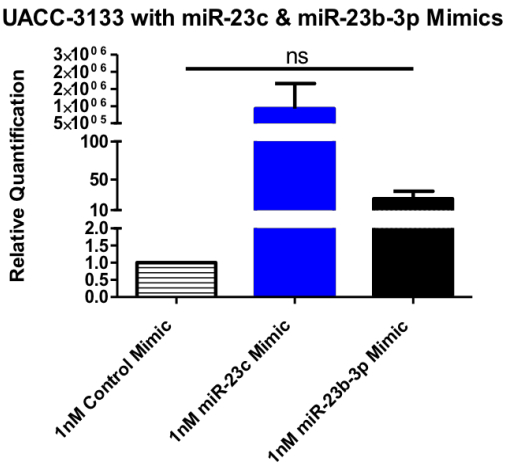
UACC-3133 with miR-23c & miR-23b-3p Mimics
Relative Quantification
ns
1nM Control Mimic
1nM miR-23c Mimic
1nM miR-23b-3p Mimic

B

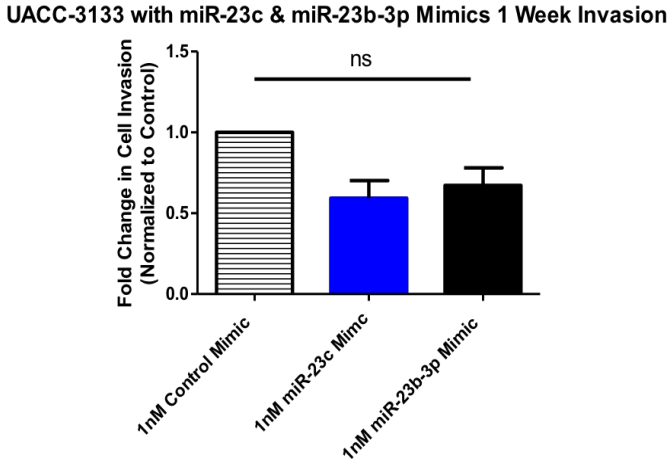
UACC-3133 with miR-23c & miR-23b-3p Mimics 1 Week Invasion
Fold Change in Cell Invasion (Normalized to Control)
ns
1nM Control Mimic
1nM miR-23c Mimc
1nM miR-23b-3p Mimic

C

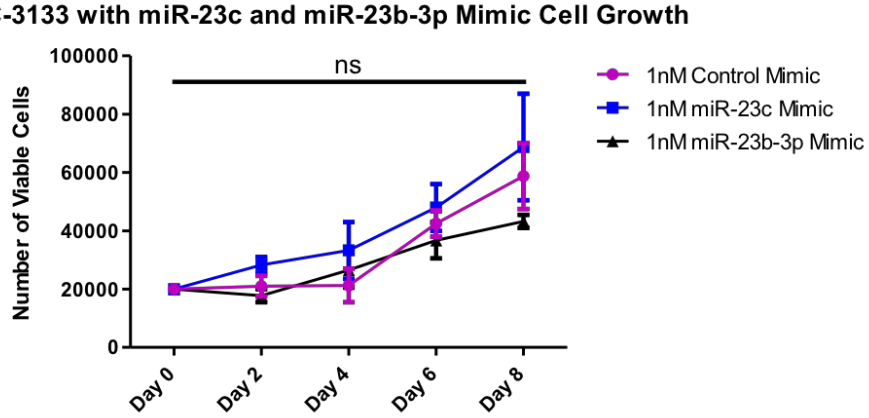
UACC-3133 with miR-23c and miR-23b-3p Mimic Cell Growth
Number of Viable Cells
ns
Day 0
Day 2
Day 4
Day 6
Day 8
1nM Control Mimic
1nM miR-23c Mimic
1nM miR-23b-3p Mimic

Figure 11: Increased miR-23c and miR-23b-3p levels in the UACC-3133 cell line results in decreased invasion.

Increased levels of miR-23c and miR-23b-3p in the UACC-3133 cell line resulted in a slight decrease in the cell line's invasive capabilities, with no significant change to its growth and viability over time. (A) Cells were treated with 1nM miR-23c and miR-23b-3p mimics, and 48hr post-transfection RNA was collected. Once RNA was isolated, cDNA was made and the levels of miR-23c and miR-23b-3p were measured by qPCR. Samples were normalized to SNORD95, and to the control non-targeting mimic. The relative quantification of each sample was calculated and graphed as the mean along with associated SEM (n=3 biological replicates, unpaired t test with Welch's correction). (B) miR-23c and miR-23b-3p mimics were transfected into UACC-3133 cells, and 24hr post-transfection the cells were plated in invasion chambers. After an incubation of 1-week, the invasion chambers were stained with crystal violet, and the number of invading cells were counted from 5 representative images and graphed as the mean with the SEM (n=3 biological replicates, unpaired t test with Welch's correction). (C) UACC-3133 cells were plated for a viability assay 24hr post-transfection with miR-23c and miR-23b-3p mimics. Cell viability was measured using trypan blue exclusion 2 days post-seeding and every 2 days after for 8 days. The number of cells was calculated, and the mean and associated SEM were plotted over time (n=2 biological replicates, Two-way ANOVA with Tukey's multiple comparisons test). ns, p value >0.05.

modulated levels of miR-23c and miR-23b-3p to confirm this matches the results obtained from the Clariom™ Assays.

3.4.2 Targets Identified from the MDA-MB-134VI Clariom™ Assays with Increased miR-23c and miR-23b-3p Levels did not Validate in the MDA-MB-134VI Cell Line

A short list of putative mRNA targets identified from the Clariom™ Assays were further investigated within the ILC cell lines to validate whether they may be possible targets of miR-23c and miR-23b-3p that may have contributed to the changes observed in ILC cell line invasion. It was speculated that targets of miR-23c and miR-23b-3p would have significantly decreased expression following increased levels of miR-23c and miR-23b-3p due to transfection with mimic. Thus, the MDA-MB-134VI cell line was treated with miR-23c and miR-23b-3p mimics, and 48hr post-transfection RNA was collected followed by cDNA generation. A qPCR was conducted to identify the resulting relative quantification of the targets after transfection with miR-23c and miR-23b-3p mimics compared to the cells treated with equal amounts of a non-targeting control mimic. From the selected targets, those that initially looked promising in the MDA-MB-134VI cell line with mimic were SV2A, ARHGEF1, CA11, as they were found to be altered in both the miR-23c and miR-23b-3p Clariom™ Assay datasets; and SULF1, CHPT1, CHRD which were selected from the miR-23c dataset. Further investigation into these targets; however, showed that none had validated, as presented in Figure 13. Although SV2A and ARHGEF1 showed decreased levels of expression associated with increased amounts of miR-23c or miR-23b-3p (via transfection of 1nM mimic) the change was not statistically significant. At the 10nM dose, increases were seen in the expression of the targets, except for SULF1 and CA11 with miR-23b-3p mimic. This increase in expression is opposite to what was seen in the Clariom™ Assay data, as the targets were selected based on their decreased expression in either or both of the datasets. It may have been expected

A

MDA-MB-134VI with 1nM miR-23c Mimic vs. MDA-MB-134VI with 1nM Control Mimic

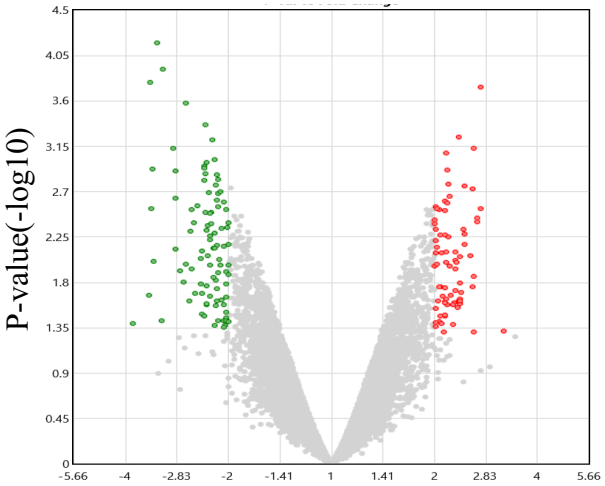

B

MDA-MB-134VI with 1nM miR-23b-3p Mimic vs. MDA-MB-134VI with 1nM Control Mimic

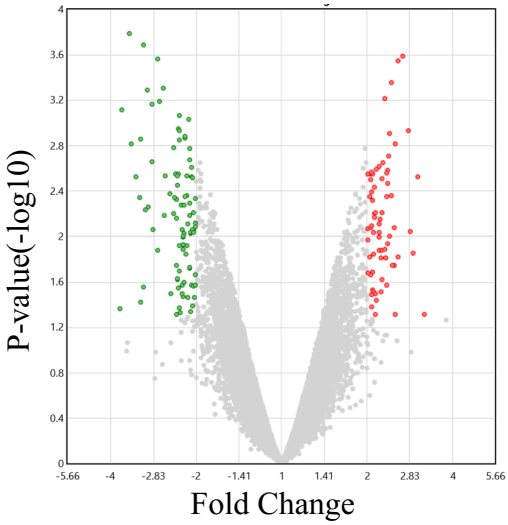

Figure 12: Volcano plots depicting resulting gene expression upon increased miR-23c and miR-23b-3p levels in the MDA-MB-134VI cell line compared to the non-targeting control mimic.

These plots identify a number of mRNAs with significant differential expression upon modulation of miR-23c and miR-23b-3p levels within the MDA-MB-134VI cell line. MDA-MB-134VI cells were transfected with 1nM of miR-23c or miR-23b-3p mimic as well as the non-targeting control mimic. RNA was isolated 48hr post-transfection, and samples were prepared according to the guidelines provided by Génome Québec Innovation Center (McGill University). Once ready, RNA was shipped for Clariom™ S Assays to be conducted by the Génome Québec Innovation Center at McGill University. The data was then sent back and was analyzed using the provided TAC software to generate the volcano plots. (A) miR-23c and (B) miR-23b-3p volcano plot data was analyzed to identify any possible targets found to be ≥2-fold significantly downregulated in both datasets, and those targets that were significantly differentially regulated in either dataset (n=2 biological replicates). Boundary of 2-fold change, p value <0.05.

that none of the mRNA targets would have decreased expression at the 10nM dose of either miR-23c or miR-23b-3p mimic, since no change was seen in the invasive capabilities of the MDA-MB-134VI cell line at the 10nM dose of either mimic (Figure 8B & 9B). Another reason that these targets did not validate may be due to the suspected issue with the mimics, perhaps the mimics are not producing higher functional levels of miR-23c and miR-23b-3p (Thomson et al., 2013) capable of interfering effectively with mRNA targets. Additionally, these results may be false positives from the Clariom™ Assay, rather than issues with the mimic. Due to the lack of validation of the targets in the MDA-MB-134VI cell line, it was hypothesized that perhaps these targets would show significant changes in the MDA-MB-330 cell line following transfection with hairpin inhibitors as was seen in the invasion data (Figure 6B & 7B).

3.4.3 Targets Identified from the MDA-MB-134VI Clariom™ Assays with Increased miR-23c and miR-23b-3p Levels did not Validate in the MDA-MB-330 Cell Line

It was suspected that lower levels of miR-23c and miR-23b-3p in the MDA-MB-330 cell line would result in increased expression of the evaluated mRNA if they were direct targets of these miRNAs. As presented in Figure 14, all the tested targets showed increased expression at both doses of the miRNA hairpin inhibitors, with the exception of SV2A and ARHGEF1. At the 20nM dose of miR-23b-3p hairpin inhibitor, SV2A and ARHGEF1 did not appear to have increased expression compared to the non-targeting control hairpin inhibitor at the same concentration. These changes in target expression however, remained not significant and the only target to show a significant difference in its expression was SULF1 at the 20nM dose of miR-23b-3p hairpin inhibitor. Although statistically significant, the increase seen in SULF1 expression is quite minimal as it is less than 2-fold, therefore the biological relevancy is questionable. These validation experiments conducted in both the MDA-MB-134VI and MDA-MB-330 cell lines,

A

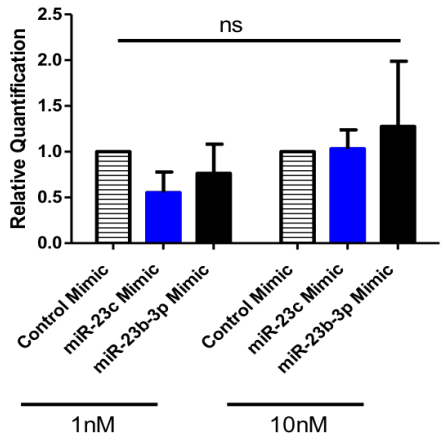
SV2A
ns
Relative Quantification
2.5
2.0
1.5
1.0
0.5
0.0
Control Mimic
miR-23c Mimic
miR-23b-3p Mimic
Control Mimic
miR-23c Mimic
miR-23b-3p Mimic
1nM
10nM

B

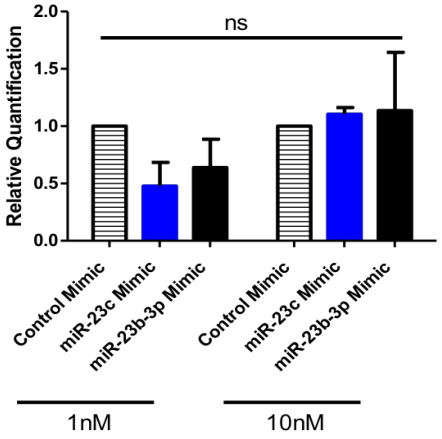
ARHGEF1
ns
Relative Quantification
2.0
1.5
1.0
0.5
0.0
Control Mimic
miR-23c Mimic
miR-23b-3p Mimic
Control Mimic
miR-23c Mimic
miR-23b-3p Mimic
1nM
10nM

C

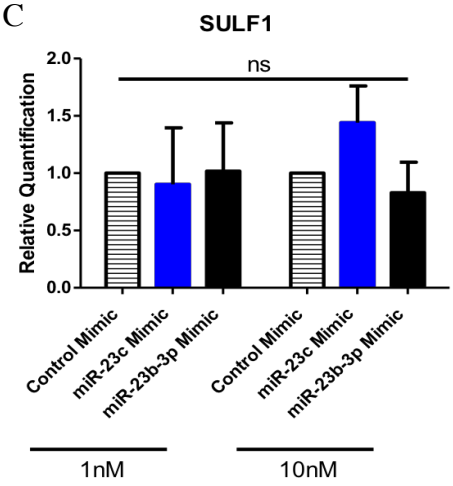
SULF1
ns
Relative Quantification
2.0
1.5
1.0
0.5
0.0
Control Mimic
miR-23c Mimic
miR-23b-3p Mimic
Control Mimic
miR-23c Mimic
miR-23b-3p Mimic
1nM
10nM

D

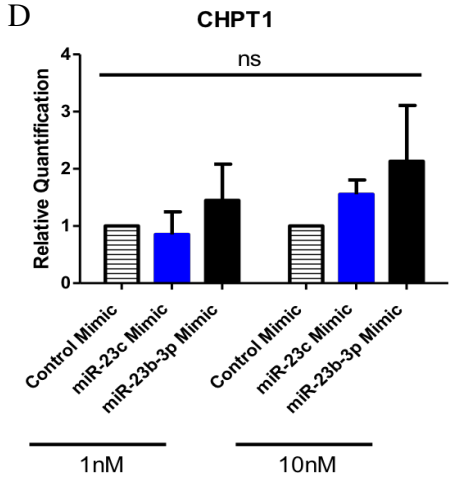
CHPT1
ns
Relative Quantification
4
3
2
1
0
Control Mimic
miR-23c Mimic
miR-23b-3p Mimic
Control Mimic
miR-23c Mimic
miR-23b-3p Mimic
1nM
10nM

E

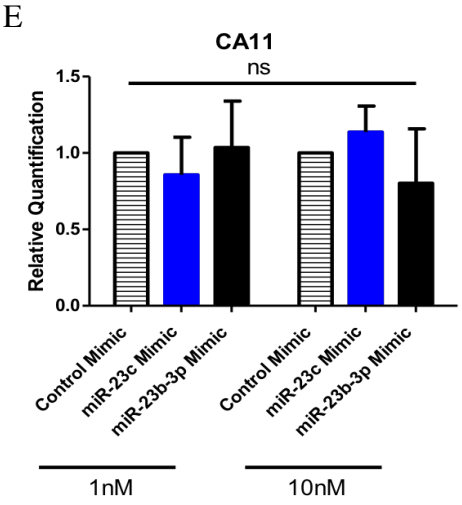
CA11
ns
Relative Quantification
1.5
1.0
0.5
0.0
Control Mimic
miR-23c Mimic
miR-23b-3p Mimic
Control Mimic
miR-23c Mimic
miR-23b-3p Mimic
1nM
10nM

F

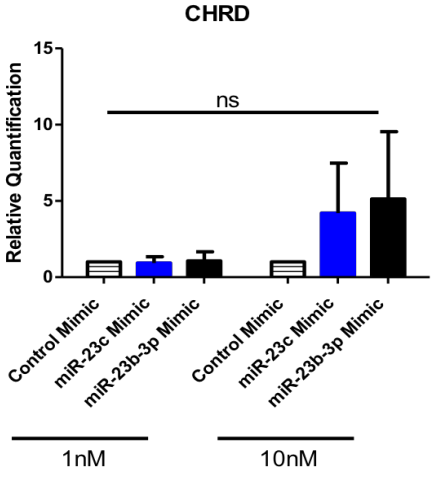
CHRD
ns
Relative Quantification
15
10
5
0
Control Mimic
miR-23c Mimic
miR-23b-3p Mimic
Control Mimic
miR-23c Mimic
miR-23b-3p Mimic
1nM
10nM

Figure 13: Quantification of potential mRNA targets of miR-23c and miR-23b-3p in MDA-MB-134VI cells transfected with mimic.

Targets identified through the Clariom™ Assays of the MDA-MB-134VI cell line treated with miR-23c and miR-23b-3p mimic did not validate. Cells were treated with either a 1nM or 10nM dose of miR-23c, miR-23b-3p, or control non-targeting mimic. After 48hr, RNA was collected, cDNA was made, and the targets' resulting expression was evaluated by qPCR. Samples were normalized to the selected control, β-Actin, and then normalized to the control non-targeting mimic. The relative quantification of each target was evaluated and plotted with the SEM. (A) SV2A and (B) ARHGEF1 at the 1nM dose did not validate despite slight decreases in expression when miR-23c and miR-23b-3p levels were increased. Potential targets (C) SULF1, (D) CHPT1, (E) CA11, and (F) CHRD were found to not validate at either dose of mimic (n=3 biological replicates, unpaired t test with Welch's correction). ns, p value >0.05.

concluded that none of the six selected targets from the MDA-MB-134VI Clariom™ Assay datasets appear to be direct targets of miR-23c and miR-23b-3p. In future experiments additional targets from the Clariom™ Assay data should be analyzed for possible targets of miR-23c and miR-23b-3p. These results however, prompted a Clariom™ Assay to be run on the MDA-MB-330s treated with miR-23c and miR-23b-3p hairpin inhibitor, given our concerns over the effective function of the mimics in the MDA-MB-134VI cell line.

3.4.4 Clariom™ Assays of the MDA-MB-330s with Decreased miR-23c and miR-23b-3p Levels Identified Possible Targets of miR-23c and miR-23b-3p

Since better results were seen with the use of hairpin inhibitors in the MDA-MB-330 cell line throughout this thesis, Clariom™ Assays were conducted to identify potential targets of miR-23c and miR-23b-3p that may play a role in regulating ILC cell line invasion. The MDA-MB-330 cell line was therefore treated with a 50nM dose of miR-23c, a 20nM dose of miR-23b-3p, and the corresponding doses of control non-targeting hairpin inhibitor. These doses were selected based on the resulting significant decrease in the invasive capabilities of the MDA-MB-330 cell line when treated with hairpin inhibitor, seen in Figure 6B and in Figure 7B. RNA was isolated 48hr post-transfection and sent for Clariom™ Assays to be performed by the Génome Québec Innovation Center at McGill University. The resulting dataset was evaluated through the provided TAC software and based on p values as opposed to FDR p values. Volcano plots identifying targets with ≥2-fold significant differential expression in the MDA-MB-330 cell line with decreased miR-23c and miR-23b-3p levels were generated (Figure 15).

The results of the MDA-MB-330 Clariom™ Assay were cross-referenced to the MDA-MB-134VI dataset, and the only target found to have significant differential expression in both datasets was HIPK1; however, it was found in the MDA-MB-134VI miR-23c dataset, and in the

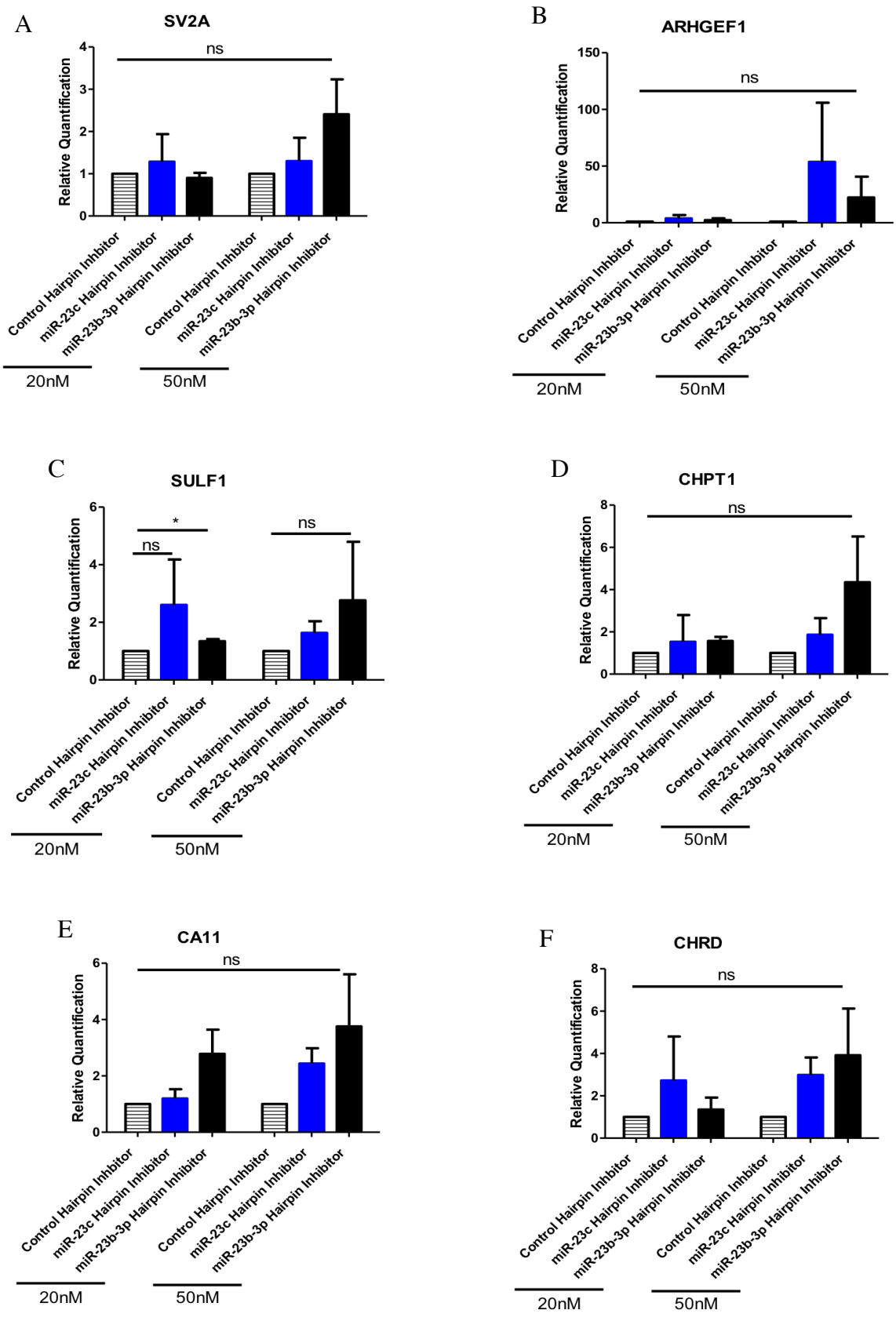
A
SV2A
Relative Quantification
ns
Control Hairpin Inhbitor
miR-23c Hairpin Inhibitor
miR-23b-3p Hairpin Inhibitor
20nM
50nM
B
ARHGEF1
C
SULF1
*
D
CHPT1
E
CA11
F
CHRD

Figure 14: Quantification of putative mRNA targets of miR-23c and miR-23b-3p in MD-MB-330 cells modified with specific hairpin inhibitors.

Targets were identified in the Clariom™ Assays of the MDA-MB-134VI cell line with increased levels of miR-23c and miR-23b-3p. Targets observed for their expression in the MDA-MB-330 cell line with decreased miR-23c and miR-23b-3p levels did not validate. The MDA-MB-330 cell line was transfected with 20nM or 50nM or miR-23c, miR-23b-3p or control non-targeting hairpin inhibitor. RNA was isolated 48hr post-transfection and cDNA was made, then analyzed by qPCR for the expression of the selected targets when miR-23c and miR-23b-3p levels were lowered in the MDA-MB-330 cell line. Samples were normalized to the selected control, β-Actin, and then normalized to the control non-targeting hairpin inhibitor. Relative quantification of each sample was plotted as mean with the SEM. (A) SV2A and (B) ARHGEF1 at the 20nM dose of miR-23b-3p hairpin inhibitor did not have increased expression. (C) SULF1 had a slight increase in expression at the 20nM dose of miR-23b-3p hairpin inhibitor that was found to be significant (p value 0.045). (D) CHPT1, (E) CA11, and (F) CHRD had increased expression at either dose of both miR-23c and miR-23b-3p hairpin inhibitor (n=3 biological replicates, unpaired t test with Welch's correction). ns, p value >0.05, * p value ≤0.05.

MDA-MB-330 miR-23b-3p dataset. The MDA-MB-330 miR-23c and miR-23b-3p datasets were cross-referenced to each other as well, to identify any common targets that may regulate ILC cell line invasion and none were found. Although there are no targets that were found to match in the MDA-MB-330 Clariom™ Assay datasets with decreased levels of miR-23c and miR-23b-3p there were; however, a number of targets that were significantly differentially regulated when levels of miR-23c and miR-23b-3p are decreased. Therefore, targets that had literature indicating a possible role in cancer, breast cancer or metastasis were noted for future investigations as outlined in Table 5.

Though miR-23c and miR-23b-3p are from the same family, and located on different chromosomes, they only differ at 2-3nt (Granados-López et al., 2017; Kozomara et al., 2019), suggesting they may be paralogous sequences (Griffiths-Jones et al., 2006). Paralogous sequences and miRNA families share some targets however, our results from the MDA-MB-134VI and MDA-MB-330 Clariom™ Assays indicate that these miRNA likely have different targets that respectively play a role in regulating ILC cell line invasion (Granados-López et al., 2017; Jeong et al., 2017). Therefore, future investigation into the potential targets of miR-23c and miR-23b-3p identified in the Clariom™ Assays should focus on differing targets, while not completely neglecting similar targets.

3.5 Evaluation of miRNA Expression in Metastatic and Non-Metastatic Patient ILC FFPE Tissues

3.5.1 Mean miR-23c and miR-23b-3p Expression in Metastatic Compared to Non-Metastatic ILC Does Not Reflect the Findings of the ILC Cell Lines

Since our data suggested that miR-23c and miR-23b-3p were found to regulate ILC cell line invasion, we tested whether their expression levels were associated with patient metastasis, and thus tested their expression levels in archival primary surgical specimens from newly

A

MDA-MB-330 with 50nM miR-23c Hairpin Inhibitor vs.
MDA-MB-330 with 50nM Control Hairpin Inhibitor

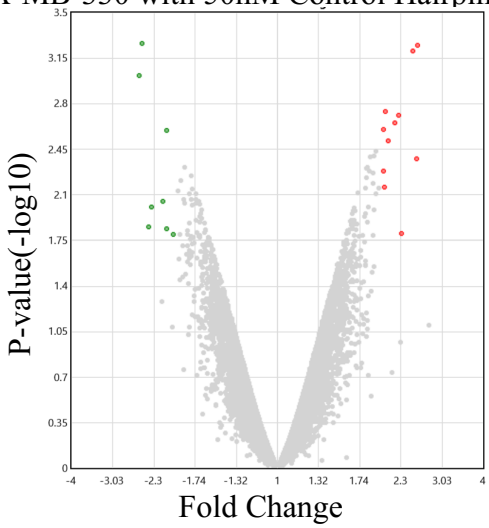

B

MDA-MB-330 with 20nM miR-23b-3p Hairpin Inhibitor
vs. MDA-MB-330 with 20nM Control Hairpin Inhibitor

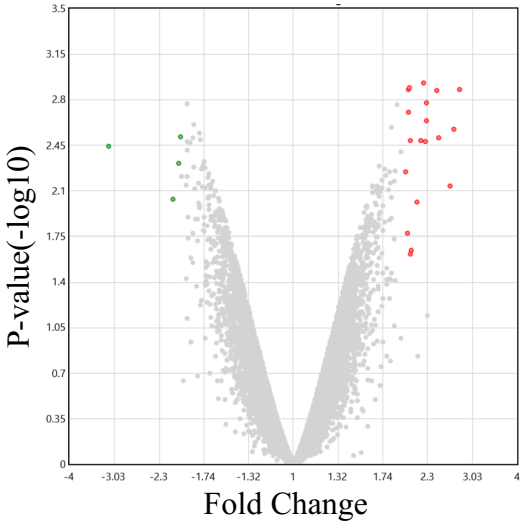

Figure 15: Volcano plots of differential gene expression in MDA-MB-330 cells with decreased miR-23c and miR-23b-3p levels compared to the non-targeting control hairpin inhibitor.

Volcano plots depicting targets with ≥2-fold significant differential expression in the MDA-MB-330 cell line with decreased miR-23c and miR-23b-3p levels identified from Clariom™ Assays. The MDA-MB-330 cell line was transfected with 50nM miR-23c, 20nM miR-23b-3p and the respective control non-targeting hairpin inhibitors at the same concentrations. RNA was isolated 48hr post-transfection and prepared following the guidelines outlined by the Génome Québec Innovation Center (McGill University). The samples were then sent to the Génome Québec Innovation Center at McGill University to be run on Clariom™ S Assays. Once the data was returned, it was analyzed using the provided TAC software and volcano plots were generated. (A) 50nM miR-23c compared to 50nM non-targeting control hairpin inhibitor and (B) 20nM miR-23b-3p compared to 20nM non-targeting control hairpin inhibitor volcano plot data were then evaluated to identify any possible targets found to be ≥2-fold significantly downregulated in either dataset (n=2 biological replicates). Boundary of 2-fold change, p value <0.05.

miR-23c Hairpin Inhibitor Clariom™ Assay Dataset		
Target	**Fold Change**	**p value**
EPHA4	2.49	0.0006
SPINK13	2.07	0.0018
IF127	2.11	0.003
USP13	2.3	0.0157
miR-23b-3p Hairpin Inhibitor Clariom™ Assay Dataset		
Target	**Fold Change**	**p value**
MAP4	2.24	0.0012
SYNE1	2.28	0.0023
HIPK1	2.46	0.0031
MX1	2.02	0.0169
DACH1	2.06	0.0243

Table 5: Potential targets identified from the MDA-MB-330 cell line with decreased levels of miR-23c and miR-23b-3p Clariom™ Assays.

Data was analyzed through the provided TAC software using p values rather than FDR p values, which provided a list of targets with ≥2-fold significant differential expression in the MDA-MB-330 cell line with lower levels of either miR-23c or miR-23b-3p compared to the control non-targeting hairpin inhibitor. From the software output, the above list of targets was created based on available previous literature indicating the target's possible role in cancer, breast cancer, invasion or metastasis.

diagnosed ILC with >5-10 years follow-up. It was anticipated that the results and trends seen in the ILC cell lines would translate to patient ILC, wherein miR-23c and miR-23b-3p are markers of metastatic ILC. A cohort of 13 metastatic and 13 non-metastatic patient ILC FFPE tissues were studied for their levels of miR-23c and miR-23b-3p expression using qPCR. As presented in Figure 16A, mean miR-23c expression was found to be lower in metastatic compared to non-metastatic ILC. This is opposite to what was speculated, as the cell line data suggested an increase in expression should be seen in the metastatic compared to non-metastatic samples. Mean miR-23b-3p expression however, was slightly higher in metastatic compared to non-metastatic ILC (Figure 16B). These results are closer to what was expected, as the cell line data proposes increased expression of miR-23b-3p in the invasive/metastatic compared to non-invasive/non-metastatic samples. Though these miRNAs may not be robust indicators of metastatic potential in patients, their role in regulating ILC cell line invasion suggests that interrogation of their targets may identify important regulatory proteins or pathways of metastatic ILC in patients.

3.5.2 miRNome Analysis of Patient ILC FFPE Tissues Depicts the Differential Expression of miRNA in Metastatic Compared to Non-Metastatic ILC

Since the analysis of miR-23c and miR-23b-3p did not yield expected results in patient samples, it is possible that our initial investigation was biased towards miRNA expression differences associated with MDA-MB-330 cells as opposed to invasive ILC, highlighting potential flaws due to a limited availability of invasive ILC cell lines. As such, miRNAs with more relevancy may be concealed, which prompted a miRNome analysis comparing metastatic and non-metastatic ILC FFPE tissues (Figure 17). The 13 metastatic and 13 non-metastatic samples used in this analysis, had a number of miRNAs with significant differential expression between the two cohorts. Similar to results shown in Figure 16A, the miRNome analysis found miR-23c expression

A

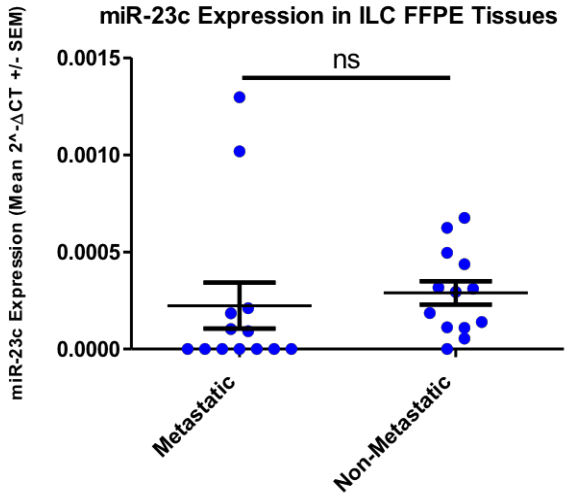
miR-23c Expression in ILC FFPE Tissues
miR-23c Expression (Mean 2^-ΔCT +/- SEM)
0.0015
0.0010
0.0005
0.0000
ns
Metastatic
Non-Metastatic

B

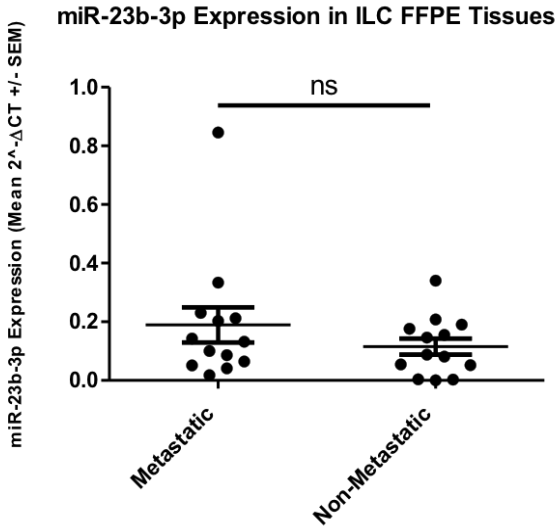
miR-23b-3p Expression in ILC FFPE Tissues
miR-23b-3p Expression (Mean 2^-ΔCT +/- SEM)
1.0
0.8
0.6
0.4
0.2
0.0
ns
Metastatic
Non-Metastatic

Figure 16: No significant difference was seen in the expression levels of miR-23c and miR-23b-3p in metastatic compared to non-metastatic ILC patient FFPE tumours.

Mean miR-23c and miR-23b-3p show a not significant decrease and increase in expression respectively in FFPE archival primary surgical specimens from newly diagnosed ILC with 5-10 years follow-up. RNA was isolated from 13 metastatic and 13 non-metastatic ILC FFPE tumour samples and cDNA was then made followed by preamplification. After confirming the preamplification was efficient, miRNA expression was evaluated by qPCR. Samples were normalized to SNORD95, then mean 2^-ΔCt was calculated and plotted along with the SEM to compare expression of (A) miR-23c and (B) miR-23b-3p in metastatic and non-metastatic ILC FFPE patient tissue samples (n=13 metastatic samples, n=13 non-metastatic samples, unpaired t test with Welch's correction). ns, p value >0.05.

had a 0.3-fold (p value 0.06) decrease in metastatic compared to non-metastatic ILC. Surprisingly, miR-23b-3p expression as detected by the miRNome analysis only had a slight fold increase of 1.2 (p value 0.9); which suggests the results in Figure 16B are due to an outlying result. Despite the inability to confirm roles of miR-23c and miR-23b-3p in ILC metastasis in patient samples, the results obtained from the miRNome analysis, provided a number of miRNA targets with potential roles in regulating ILC metastasis that may be further investigated in future studies.

3.5.3 miR-28-5p Warrants Further Investigation into it's Possible Role in Regulating ILC Invasion and Metastasis

While analyzing the miRNome analysis of the ILC FFPE tissues, a particular miRNA stood out, miR-28-5p. The patient archival surgical specimen miRNome analysis indicated that miR-28-5p may be worth further investigation as it had a fold change of 2.1 (p value 0.1) (Figure 17). Initially, miR-28-5p had been selected for further validation from the cell line miRNome due to its significantly increased fold change of 4.6 (p value 0.02) in the invasive compared to minimally invasive ILC cell lines (Figure 4). Upon further investigation into its expression in the ILC cell lines using qPCR, increased levels in the invasive compared to minimally invasive cell lines was confirmed; however, it was only significantly higher in the MDA-MB-330 compared to the MDA-MB-134VI cell line (Figure 5C). Due to its lack of statistical significance across all three minimally invasive ILC cell lines, it was not pursued initially with respect to its effects on ILC cell line invasion. However, given the small sample size used to date for the patient miRNome analysis, it is possible that miR-28-5p expression differences could reach significance. Presently, miR-28-5p does have increased expression in the invasive compared to minimally invasive ILC cell lines, thus it could potentially regulate ILC invasion/metastasis or contribute to a signature of metastatic potential. Therefore, we validated this hypothesis in the FFPE tissue samples by qPCR. As seen

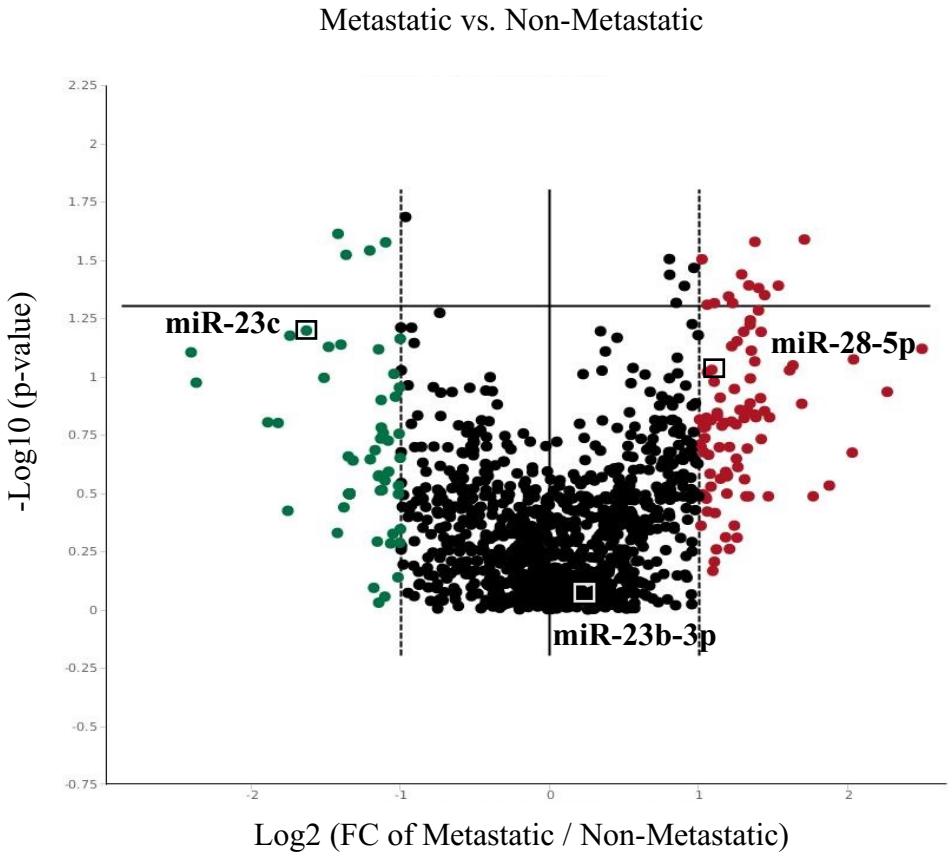
Metastatic vs. Non-Metastatic
-Log10 (p-value)
Log2 (FC of Metastatic / Non-Metastatic)
miR-23c
miR-28-5p
miR-23b-3p
2.25
2
1.75
1.5
1.25
1
0.75
0.5
0.25
0
-0.25
-0.5
-0.75
-2
-1
0
1
2

Figure 17: miRNome analysis comparing the expression of miRNAs in metastatic and non-metastatic ILC patient FFPE tumour specimens.

RNA was isolated from 13 metastatic and 13 non-metastatic ILC patient FFPE tumour samples, cDNA was then made using the specific miRNome buffer followed by preamplification. The miRNome analysis was then conducted using qPCR-based methods and normalized to the six provided controls. miR-23c, miR-23b-3p and miR-28-5p are indicated on the volcano plot (n=13 metastatic, n=13 non-metastatic). Boundary of 2-fold change and p value 0.05.

in Figure 18, mean miR-28-5p expression was found to be higher in metastatic compared to non-metastatic patient FFPE tissues (p value 0.051). Perhaps upon increasing the size of this cohort, miR-28-5p will be found to be a potential marker of metastatic ILC. Due to its increased expression within the ILC cell lines, as well as the patient dataset, it is proposed that miR-28-5p is investigated in the future as a possible regulator or biomarker of metastatic ILC.

3.6 Compare the Invasive Capabilities of the VIVA-1 and VIVA-2 Sub-Populations to the Parental MDA-MB-134VI Cell Line

3.6.1 Isolation of MDA-MB-134VI Cells that Invaded Through an Invasion Chamber Created the More Invasive VIVA-1 and VIVA-2 Sub-Populations

As mentioned throughout this thesis, there are a limited number of ILC cell lines available (Christgen and Derksen, 2015; Jambal et al., 2013; Tasdemir et al., 2018), specifically more invasive ones as our work to date has only confirmed the MDA-MB-330 cell line as an invasive ILC cell line. As it remains possible that our findings have been biased towards specific differences reflective of MDA-MB-330 biology and not necessarily invasive ILC, over the course of this investigation the need for more invasive ILC cell lines has become more apparent. As such, our lab has attempted to take steps towards generating additional ILC cell lines through patient tumour samples, and patient-derived xenograft models. Unfortunately, due to the slow growing nature of ILC (Reed et al., 2015; Yoder et al., 2007) these discoveries are still underway.

In parallel to isolating new ILC cell lines from patient derived tissues, we attempted to isolate more invasive sub-populations of cells from a pre-existing minimally invasive ILC cell line. It was believed that this would create a more invasive sub-population for ILC investigations in a time conscious manner and lead to the identification of novel targets and pathways that may regulate ILC invasion/metastasis. It was speculated that if we isolated cells that had invaded

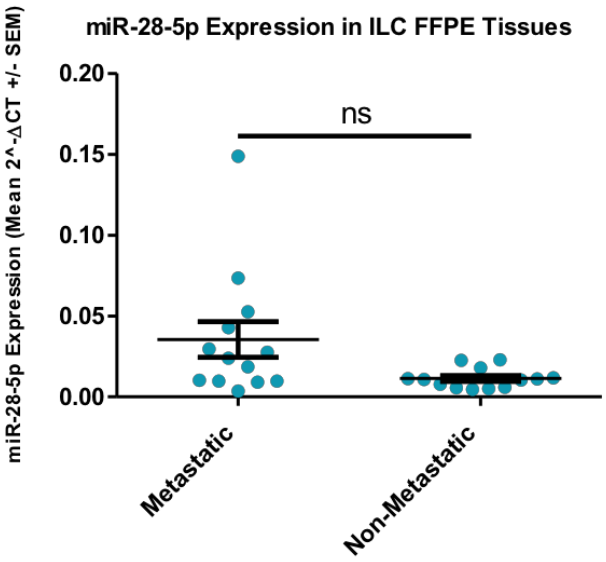
miR-28-5p Expression in ILC FFPE Tissues
miR-28-5p Expression (Mean 2^-ΔCT +/- SEM)
0.20
0.15
0.10
0.05
0.00
ns
Metastatic
Non-Metastatic

Figure 18: Mean miR-28-5p expression is increased in metastatic compared to non-metastatic ILC patient FFPE archival tumour specimens.

Mean miR-28-5p expression is not significantly increased in the metastatic compared to non-metastatic FFPE archival primary surgical specimens from newly diagnosed ILC with 5-10 years follow-up. Though not significant presently, with additional samples it is believed that the current p value at 0.051 will reach the point of significance. RNA was isolated from 13 metastatic and 13 non-metastatic ILC FFPE tumour samples and cDNA was then made followed by preamplification. After confirming the preamplification was efficient, miRNA expression was evaluated by qPCR. Samples were normalized to SNORD95, then mean 2^-ΔCt was calculated and plotted along with the SEM to compare expression of miR-28-5p in metastatic and non-metastatic ILC FFPE patient tissue samples. (n=13 metastatic samples, n=13 non-metastatic samples, unpaired t test with Welch's correction). ns, p value >0.05.

through an invasion chamber and expanded them, we could rescue a more invasive sub-population. Thus, Matrigel® coated invasion chambers were seeded with MDA-MB-134VI cells which were allowed to invade over a 7-day period. At this time, cells which had invaded were isolated from the bottom of the invasion chamber membrane by trypsinization and subsequently expanded. This led to the production of the VIVA-1 sub-population. After the VIVA-1 cells had been expanded, the process was repeated by seeding the VIVA-1 cells into invasion chambers and isolating the cells that had invaded at 1-week. This resulted in the generation of the VIVA-2 sub-population. Once these sub-populations had been developed, they could be characterized to ensure their use as a more invasive model of ILC in ensuing experiments and investigations.

As the primary goal was to create cells that had higher invasive capabilities, the VIVA sub-populations were plated in Matrigel® coated invasion chambers to compare their ability to invade at selected time points (48hr and 1-week) compared to their parental MDA-MB-134VI cell line (Figure 19). The VIVA-1 cell line was found to have about a 3.5-fold increase in cell invasion at 48hr (p value 0.1885, Figure 19A) and one week (p value 0.0403, Figure 19B) compared to the parental MDA-MB-134VIs. The invasive capabilities of the VIVA-2 cell line were found to have an approximate 2-fold increase at 48hr (p value 0.0401, Figure 20A) and a 2.5-fold increase at one week (p value 0.1029, Figure 20B) compared to the MDA-MB-134VI parental cell line. These increased invasive capabilities compared to the parental cell line confirm we were able to isolate two more invasive sub-populations from the MDA-MB-134VI cell line. These sub-populations were thus further profiled to ensure they still maintain characteristics of the parental MDA-MB-134VI cell line.

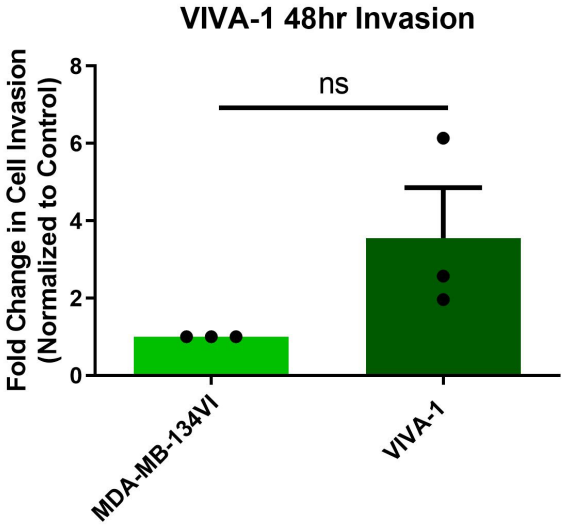
VIVA-1 48hr Invasion
Fold Change in Cell Invasion (Normalized to Control)
ns
0
2
4
6
8
MDA-MB-134VI
VIVA-1

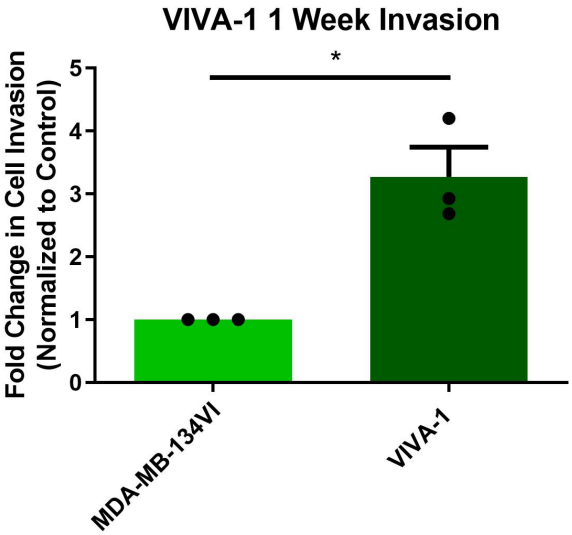
VIVA-1 1 Week Invasion
Fold Change in Cell Invasion (Normalized to Control)
*
0
1
2
3
4
5
MDA-MB-134VI
VIVA-1

Figure 19: VIVA-1s are a more invasive sub-population isolated from the MDA-MB-134VI cell line.

The VIVA-1s were seeded into Matrigel® coated invasion chambers with FBS acting as the chemoattractant. At either 48hr or 7-days after plating, the invasion chambers were stained with crystal violet, and the number of invading cells was counted from 5 representative images. The number of invading cells was plotted along with the SEM. The VIVA-1 sub-population is (A) more invasive than its parental cell line at 48hr; however, (B) their invasive capabilities are significantly greater at one week (p value 0.0403) (n=3 biological replicates, unpaired t test with Welch's correction). ns, p value >0.05, * p value ≤0.05.

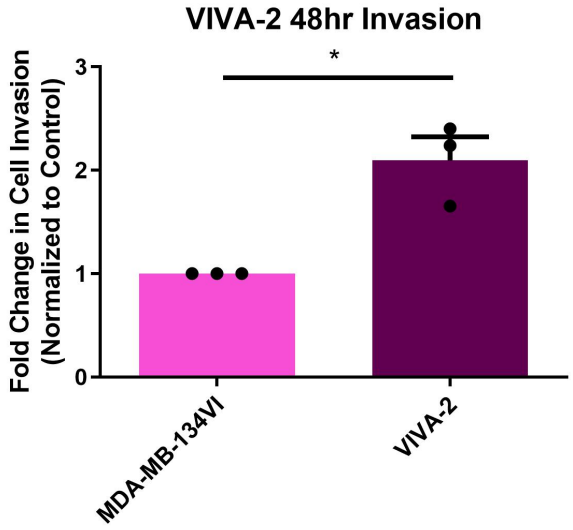
VIVA-2 48hr Invasion
*
Fold Change in Cell Invasion
(Normalized to Control)
3
2
1
0
MDA-MB-134VI
VIVA-2

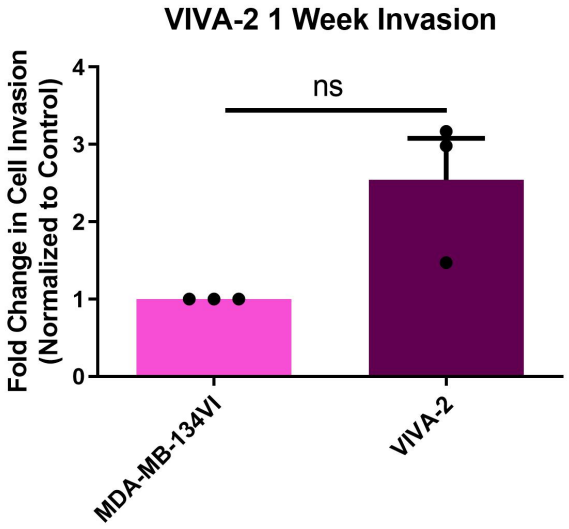
VIVA-2 1 Week Invasion
ns
Fold Change in Cell Invasion
(Normalized to Control)
4
3
2
1
0
MDA-MB-134VI
VIVA-2

Figure 20: The VIVA-2s are a more invasive sub-population isolated from the MDA-MB-134VI cell line.

The VIVA-2s were seeded into Matrigel® coated invasion chambers with FBS acting as the chemoattractant. At either 48hr or 7-days after plating, the invasion chambers were stained, the number of invading cells was counted from 5 representative images, and the results were plotted along with the SEM. The VIVA-2 sub-population is (A) significantly more invasive than its parental cell line at 48hr (p value 0.0401); however, (B) their increased invasive capabilities were not found to be significant at 7-days (n=3 biological replicates, unpaired t test with Welch's correction). ns, p value >0.05, * p value ≤0.05.

3.7 Characterize the VIVA Sub-Populations in Comparison to the Parental MDA-MB-134VI Cell Line

3.7.1 Growth of the VIVA Sub-Populations is Not Significantly Different from the Parental MDA-MB-134VIs

Following confirmation that the VIVA sub-populations were more invasive than the parental MDA-MB-134VI cell line, a cell viability assay was conducted to ensure the changes seen in the cells invasive capabilities were not due to altered cell growth. Given the selected time points of the invasion assays, changes in cell growth could be a contributing factor. Therefore, cell growth was analyzed through the measurement of viable cells over time. Cell viability was measured every two days after plating, and the number of viable cells was enumerated through a combination of trypan blue staining and a cell counter. It was found that the VIVA-1 sub-population had similar cell growth to the parental MDA-MB-134VI cell line (Figure 21A). Although there was a slightly reduced number of viable cells over time of the VIVA-2s compared to the parental MDA-MB-134VIs, this did not reach statistical significance (Figure 21B). This data further establishes that the VIVAs are more invasive sub-populations of the MDA-MB-134VI parental cell line, and that altered cell growth and viability are not significantly contributing to this invasive phenotypic difference.

3.7.2 The VIVAs Protein Profile Appears to be the Same as the Parental MDA-MB-134VIs

In addition to evaluating the cell growth rate of the VIVA sub-populations in comparison to the parental MDA-MB-134VI cell line, their protein profile was also confirmed with respect to common ILC markers. This was done to confirm the VIVAs still maintained a protein profile resembling the parental MDA-MB-134VI cell line and that of an ILC cell line. The expression of the ILC markers, HER2, E-cadherin and ERα (Arpino et al., 2004; Moll & Mitze, 1993) were therefore examined in the VIVA sub-populations compared to the parental MDA-MB-134VI cell

A

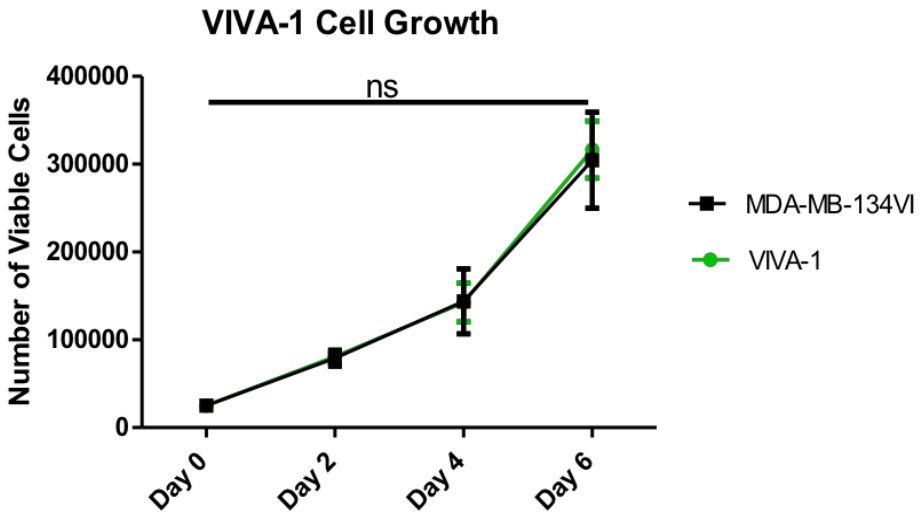
VIVA-1 Cell Growth
ns
Number of Viable Cells
400000
300000
200000
100000
0
Day 0
Day 2
Day 4
Day 6
MDA-MB-134VI
VIVA-1

B

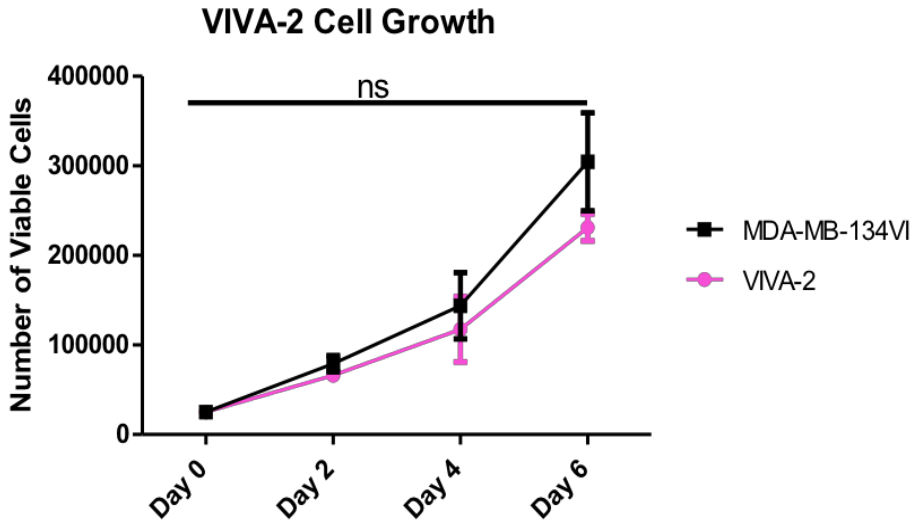
VIVA-2 Cell Growth
ns
Number of Viable Cells
400000
300000
200000
100000
0
Day 0
Day 2
Day 4
Day 6
MDA-MB-134VI
VIVA-2

Figure 21: Cell growth and viability over time did not significantly differ between the VIVA sub-populations and the parental MDA-MB-134VI cell line.

The VIVA sub-populations were plated, and cell viability was measured every 2 days thereafter for 6 days. Cell viability was measured through trypan blue staining and a cell counter that quantified viable cells. The number of viable cells within the plate was calculated and graphed over the course of the 6 days along with the SEM. It was discovered that the (A) VIVA-1 cells had similar and the (B) VIVA-2 cells had slightly but not significant decreased cell growth over time compared to the parental MDA-MB-134VI cell line (n=3 biological replicates per graph, Two-way ANOVA with Sidak's multiple comparisons). ns, p value >0.05.

line. As presented in Figure 22, across three biological replicates, the E-cadherin and ERα status of the VIVA sub-populations does not appear to differ from the parental MDA-MB-134VIs. Although there is some overexposure and what seems to be some slight variability in the expression of HER2, all that can be said is that both VIVA sub-populations maintain HER2 expression. We thus concluded that the VIVAs maintain the same ILC protein profile as the parental MDA-MB-134VI cell line, and characteristics of an ILC cell line.

3.8 Analyze the miRNA and mRNA expression profiles of the VIVAs in Comparison to the Parental MDA-MB-134VI Cell Line

3.8.1 miRNome Analysis of the VIVAs Compared to the Parental MDA-MB-134VIs Identified Numerous miRNAs with Differential Expression

In order to better understand important mechanisms by which the VIVA sub-populations have conferred increased invasive abilities, both miRNome and gene expression analyses were conducted. The miRNome analyses were executed with the use of cDNA made from RNA isolated from plated VIVA and MDA-MB-134VI cells. Analysis of the array data produced volcano plots that evaluate the miRNAs fold changes and p values. Figure 23 is comprised of volcano plots presenting the distinct miRNA profiles of the VIVA-1 (Figure 23A) and the VIVA-2 (Figure 23B) sub-populations compared to the parental MDA-MB-134VI cell line. As presented in their individual miRNomes', the VIVA-1 and VIVA-2 sub-populations differ in miRNA expression from the parental MDA-MB-134VI cell line. When the VIVAs are analyzed together compared to the MDA-MB-134VIs (Figure 23C) a number of miRNAs with similar expression in both sub-populations were identified based on their differential expression in the VIVAs compared to the MDA-MB-134VI cell line. Many of these miRNAs have significantly decreased expression in the VIVAs compared to the MDA-MB-134VIs. Perhaps these miRNAs are those that generally

A

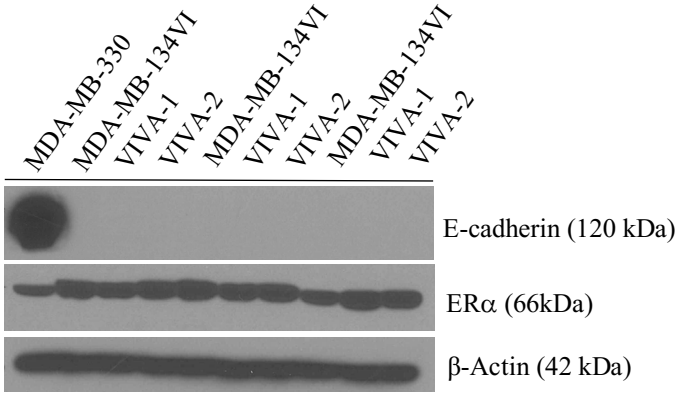
MDA-MB-330
MDA-MB-134VI
VIVA-1
VIVA-2
MDA-MB-134VI
VIVA-1
VIVA-2
MDA-MB-134VI
VIVA-1
VIVA-2
E-cadherin (120 kDa)
ERα (66kDa)
β-Actin (42 kDa)

B

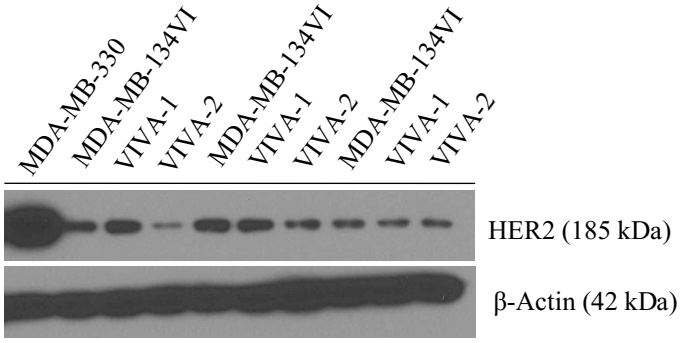
MDA-MB-330
MDA-MB-134VI
VIVA-1
VIVA-2
MDA-MB-134VI
VIVA-1
VIVA-2
MDA-MB-134VI
VIVA-1
VIVA-2
HER2 (185 kDa)
β-Actin (42 kDa)

Figure 22: The VIVAs appear to maintain expression of ILC protein markers compared to the parental MDA-MB-134VI cell line.

Protein lysates were collected from plated cells with RIPA buffer. Subsequently, 50μg of protein was isolated from the cells and was subjected to western blot analysis with β-Actin as the loading control. The VIVAs maintained (A) E-cadherin, ERα and (B) HER2 expression compared to the parental MDA-MB-134VI cell line (n=3 biological replicates included in each western blot).

modulate the increased invasive capabilities of the VIVA sub-populations. On another note, when comparing the VIVA-2s, who have significantly increased invasive capabilities at 48hr, to the VIVA-1s there is again a number of miRNAs with differential expression between the two sub-populations. In this analysis comparing the two VIVA sub-populations to each other, it is interesting that only one miRNA has significantly greater than 2-fold differential expression between the sub-populations. This miRNA was miR-4289 (fold change 2.5, p value 0.049), however it was found to have a fold change of 0.3 (p value 0.047) in the VIVA-1 compared to MDA-MB-134VI and a fold change of 0.9 (p value 0.5) in the VIVA-2 compared to MDA-MB-134VI datasets. Perhaps this miRNA plays a role initiating the increased invasive capabilities of the VIVA-2s compared to the VIVA-1s. Therefore, it is suggested that miR-4289 may be worth further investigation into its role in regulating VIVA-2 invasion. These miRNome analyses suggest that upon isolation of both VIVA sub-populations there were a number of miRNAs with differential expression within the sub-populations, that may be responsible for their increased invasive capabilities, although it appears that few of these are common between the two sub-populations.

3.8.2 Comparison of the Patient ILC FFPE miRNome to the Cell Line and VIVA miRNomes Identified miRNAs Worth Further Investigation

After completing the miRNome analysis of the VIVA sub-populations, we thought that it would be ideal to compare their miRNome analysis to the patient FFPE tissue miRNome and the MDA-MB-330 vs. MDA-MB-134VI miRNome to identify miRNA that may regulate ILC invasion/metastasis. Therefore, the expression of miRNAs with significant differential expression in the metastatic compared to non-metastatic patient FFPE tissue miRNome were compared across the other three miRNome analyses of this thesis (Table 6). Though only significant in the patient

A

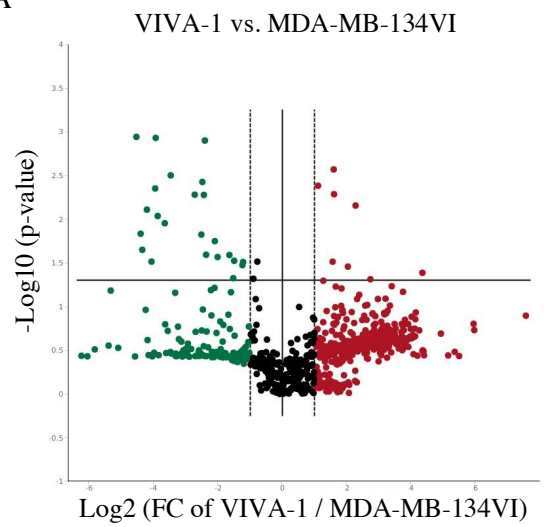
VIVA-1 vs. MDA-MB-134VI
-Log10 (p-value)
Log2 (FC of VIVA-1 / MDA-MB-134VI)

B

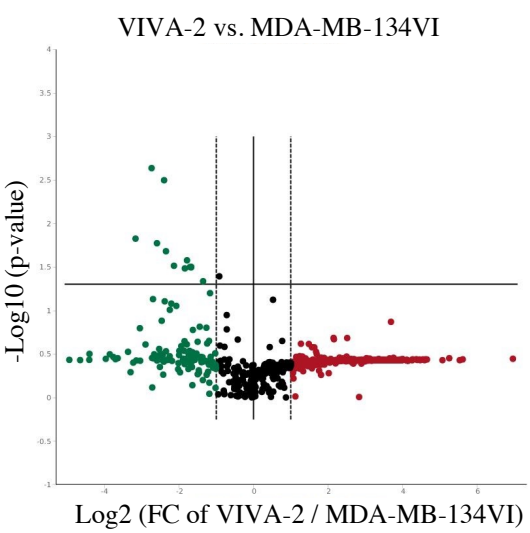
VIVA-2 vs. MDA-MB-134VI
-Log10 (p-value)
Log2 (FC of VIVA-2 / MDA-MB-134VI)

C

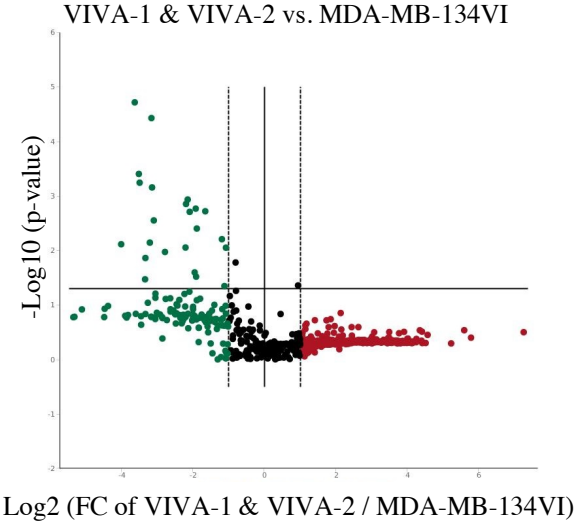
VIVA-1 & VIVA-2 vs. MDA-MB-134VI
-Log10 (p-value)
Log2 (FC of VIVA-1 & VIVA-2 / MDA-MB-134VI)

D

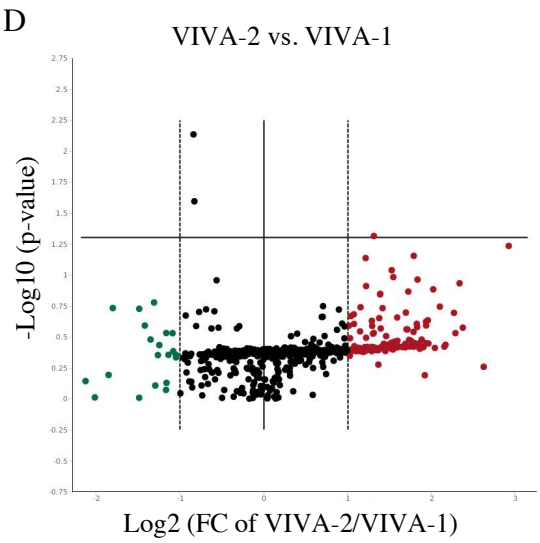
VIVA-2 vs. VIVA-1
-Log10 (p-value)
Log2 (FC of VIVA-2/VIVA-1)

Figure 23: Volcano plots depicting miRNA expression of the VIVA sub-populations.

RNA was isolated from plated VIVA cells, and cDNA was made using the specific miRNome buffer. miRNome analyses were completed using qPCR-based methods and normalized to SNORD68 and SNORD95. There are a number of miRNAs with ≥2-fold significant differential expression in the (A) VIVA-1 and (B) VIVA-2 sub-populations compared to the parental MDA-MB-134VI cell line. (C) When comparing the two sub-populations to the parental cell line, a number of miRNAs were found to have significantly decreased expression; however, when comparing (D) the VIVA-2s to the VIVA-1s there was only one miRNA with ≥2-fold significant differential expression (n=3 biological replicates). Boundary of 2-fold change and p value of 0.05.

dataset, miR-517-5p presents as an interesting target, as its expression is increased in all four datasets. This suggests that perhaps this may be a regulator of ILC invasion/metastasis, or rather a possible biomarker of metastasis. miR-29a-3p, miR-331-3p and miR-339-5p have significantly increased expression in the patient dataset; however, miR-29a-3p has a fold regulation of about 1, whereas miR-331-3p and miR-339-5p have fold regulations of around 1.5 in the MDA-MB-330 vs. MDA-MB-134VI dataset. Since, miR-331-3p and miR-339-5p have fold regulations around 1.5, they may be more promising as they are in the same direction as the patient dataset; perhaps, they may be worth investigating as we have seen different expression of miRNA when they are evaluated by qPCR. Although their expression is in the opposite direction in the VIVA datasets, this is not too concerning as they are sub-populations of a minimally invasive cell line and perhaps these are not miRNA that regulate the VIVAs increased invasive capabilities but may regulate ILC invasion/metastasis. These miRNAs may contribute to a possible signature of ILC metastasis, and their investigation in the ILC cell lines may present possible targets and pathways that may regulate ILC invasion/metastasis.

3.8.3 miR-23c, miR-23b-3p and miR-28-5p Expression Varies in the VIVAs

As miR-23c and miR-23b-3p were found to regulate MDA-MB-330 and MDA-MB-134VI invasion, we speculated differences in miR-23c and miR-23b-3p expression may be associated with the increased invasive ability of the VIVA sub-populations compared to the parental MDA-MB-134VI cell line (Figure 24). Therefore, it was believed that like the more invasive MDA-MB-330 cell line, the VIVAs would have increased expression of miR-23c and miR-23b-3p. miR-23c expression was found to be similar in the VIVA-1s compared to the parental MDA-MB-134VI cells. There was an approximate 3-fold increase in levels of miR-23c in the VIVA-2 cells compared

miRNA	Metastatic vs. Non-Metastatic		MDA-MB-330 vs. MDA-MB-134VI		VIVA-1 vs. MDA-MB-134VI		VIVA-2 vs. MDA-MB-134VI	
	Fold Regulation	p value	Fold Regulation	p value	Fold Regulation	p value	Fold Regulation	p value
miR-517-5p	2.3	0.03	2.99	0.4	8.6	0.2	13.0	0.4
miR-29a-3p	2.7	0.04	1.18	0.4	-12.5	0.3	-7.2	0.3
miR-331-3p	2.6	0.02	1.54	0.4	-1.5	0.99	-2.1	0.2
miR-339-5p	3.0	0.04	1.69	0.4	-1.9	0.6	-2.9	0.2

Table 6: Comparison of miRNAs with significant differential expression in the metastatic compared to non-metastatic patient ILC FFPE tumour sample, the ILC cell line and VIVA miRNome analyses.

The table was created after controlling all the miRNomes to SNORD95 and all the cell line miRNomes to the MDA-MB-134VI cell line. After further validation, these miRNAs may be found to be possible regulators of ILC invasion/metastasis, or rather may contribute to a signature of metastatic potential of ILC. It is possible as well, that the pathways these miRNAs regulate may be therapeutic targets or regulators of ILC invasion/metastasis. These miRNA are worth further investigation by qPCR in both the ILC cell lines and the patient ILC FFPE tumour samples.

to the MDA-MB-134VI parental cells. Pertaining to miR-23b-3p, it was found to have a significant decrease in expression in the VIVA-1 sub-population compared to the parental MDA-MB-134VI cell line; however, a slight decrease in miR-23b-3p expression was seen in the VIVA-2 sub-population. The significant decrease in miR-23b-3p expression in the VIVA-1s is opposite to what was observed in the more invasive MDA-MB-330s cells, where we saw increased miR-23b-3p levels compared to that found in MDA-MB-134VIs. As a result of its increased expression in the patient datasets, miR-28-5p's expression in the VIVA sub-populations was also investigated. Although miR-28-5p was reduced in the VIVA-1 sub-population, no change was seen in miR-28-5p expression in the VIVA-2 sub-population compared to the MDA-MB-134VI cell line either. This data suggests that these miRNAs are not key regulators of the VIVAs increased invasive capabilities, and other modulators which remain to be identified are more likely contributing to their differential invasive ability.

3.8.4 Clariom™ Assays of the VIVAs Compared to the Parental MDA-MB-134VI Cell Line Identified Numerous Targets that may be Responsible for the VIVAs Increased Invasive Capabilities

To identify pathways that may be responsible for the VIVAs increased invasive capabilities, Clariom™ Assays were conducted on the VIVA-1 and VIVA-2 sub-populations compared to the parental MDA-MB-134VI cell line. RNA was collected from plated cells and was isolated following the guidelines provided by the Génome Québec Innovation Center at McGill University. Once RNA quality was assured, it was sent to the Génome Québec Innovation Center (McGill University) for Clariom™ Assays. The returned data was analyzed using the provided TAC software based on p values rather than FDR p values. This analysis generated volcano plots comparing mRNA expression between the individual VIVA sub-populations and the parental

A

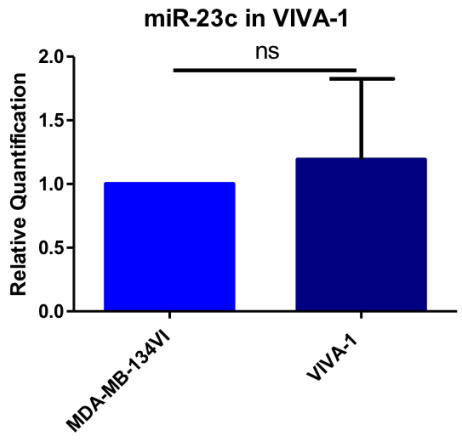
miR-23c in VIVA-1
ns
Relative Quantification
2.0
1.5
1.0
0.5
0.0
MDA-MB-134VI
VIVA-1

B

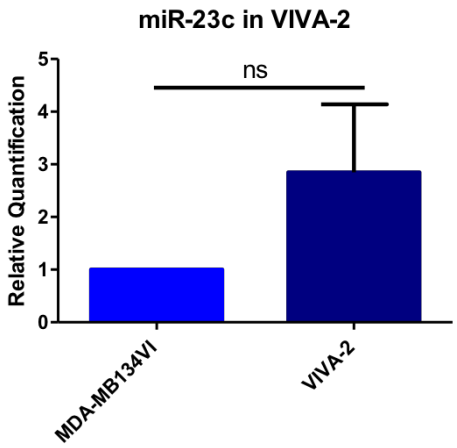
miR-23c in VIVA-2
ns
Relative Quantification
5
4
3
2
1
0
MDA-MB134VI
VIVA-2

C

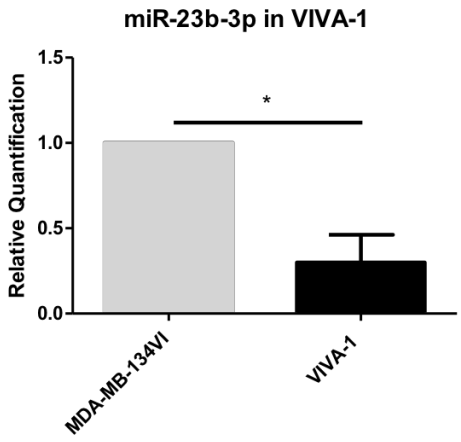
miR-23b-3p in VIVA-1
*
Relative Quantification
1.5
1.0
0.5
0.0
MDA-MB-134VI
VIVA-1

D

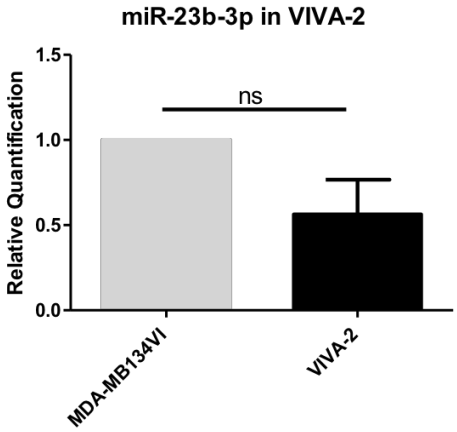
miR-23b-3p in VIVA-2
ns
Relative Quantification
1.5
1.0
0.5
0.0
MDA-MB134VI
VIVA-2

E

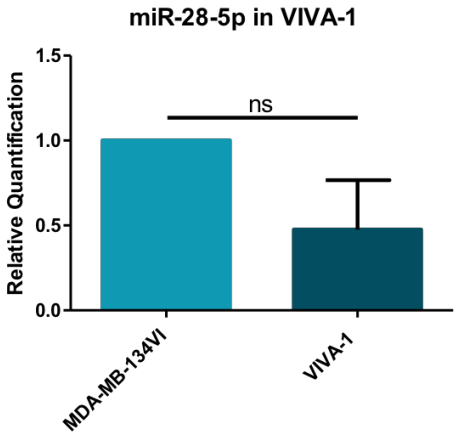
miR-28-5p in VIVA-1
ns
Relative Quantification
1.5
1.0
0.5
0.0
MDA-MB-134VI
VIVA-1

F

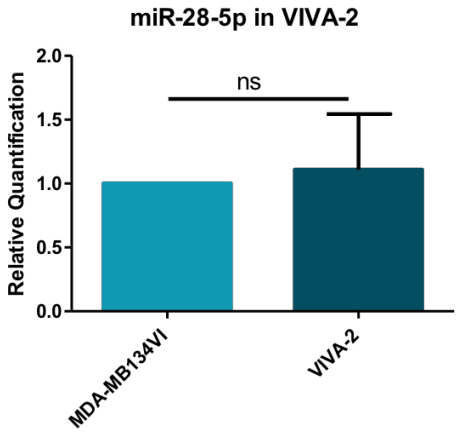
miR-28-5p in VIVA-2
ns
Relative Quantification
2.0
1.5
1.0
0.5
0.0
MDA-MB134VI
VIVA-2

Figure 24: Expression of miR-23c, miR-23b-3p and miR-28-5p in the VIVA sub-populations compared to the parental MDA-MB-134VI cell line.

RNA was isolated from plated cells, which was then used to generate cDNA. Subsequently, a qPCR analysis was conducted to evaluate the expression of select miRNAs within the VIVA sub-populations compared to the parental MDA-MB-134VIs. Relative quantification was calculated from the qPCR data and plotted with the SEM. The samples were normalized to SNORD95, and to the MDA-MB-134VI cell line. miR-23c was found to have no significant change in expression in the (A) VIVA-1 or (B) the VIVA-2 cells compared to the parental MDA-MB-134VI cell line. In comparison to the MDA-MB-134VIs, miR-23b-3p was found to have significantly decreased expression in the (C) VIVA-1s (p value 0.0495), whereas (D) the VIVA-2s were found to have no significant change in miR-23b-3p expression. miR-28-5p was found to have no significant difference in expression in either (E) the VIVA-1s or the (F) VIVA-2s compared to the MDA-MB-134VI parental cell line (n=3 biological replicates, unpaired t test with Welch's correction). ns, p value >0.05, * p value ≤0.05.

MDA-MB-134VI cell line (Figure 25). As is made apparent in the volcano plots of Figure 25, there are a number of mRNAs with ≥2-fold significant differential expression in the VIVA sub-populations compared to the MDA-MB-134VIs. From the volcano plots, a number of targets were selected for future investigations into their potential role in regulating the increased invasive capabilities of the VIVA sub-populations (Table 7). These targets were selected based on their ≥2-fold significant differential expression in the VIVA sub-populations compared to the parental MDA-MB-134VIs as well as any literature indicating a potential role in breast cancer or invasion/metastasis. The mRNA targets were preferentially selected for those that had ≥2-fold significant differential expression in both the VIVA-1 and VIVA-2 datasets. From both datasets, it was found that approximately 530 targets with ≥2-fold significant differential expression were in common between the VIVA-1s and the VIVA-2s. From these targets, the top ~40 targets with increased expression and the top ~30 targets with decreased expression were considered, as well as literature indicating roles in breast cancer or invasion/metastasis was searched. The selected mRNA targets are identified in Table 7, which depicts the fold change and the p value of each of the mRNA targets in the individual VIVA datasets. It is suggested that further research into the VIVA sub-populations, begin through the investigation of these selected targets.

A

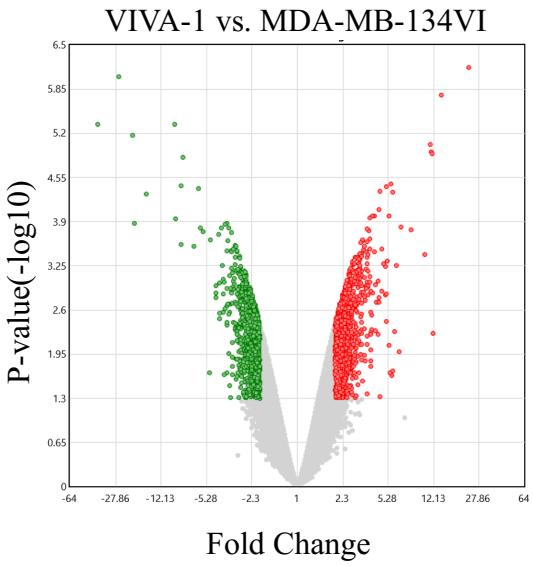
VIVA-1 vs. MDA-MB-134VI
P-value(-log10)
6.5
5.85
5.2
4.55
3.9
3.25
2.6
1.95
1.3
0.65
0
-64
-27.86
-12.13
-5.28
-2.3
1
2.3
5.28
12.13
27.86
64
Fold Change

B

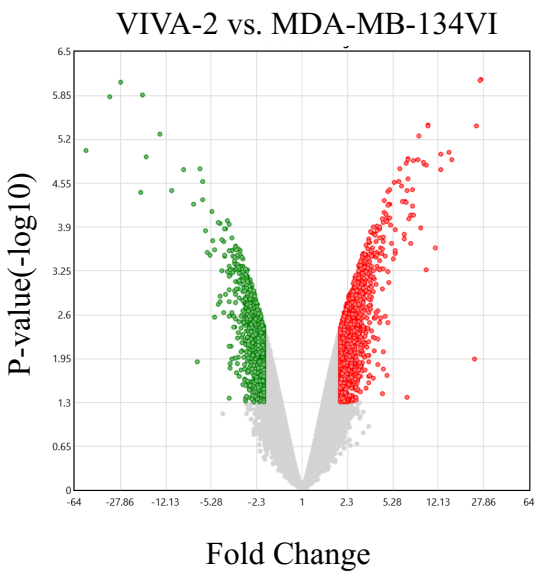
VIVA-2 vs. MDA-MB-134VI
P-value(-log10)
6.5
5.85
5.2
4.55
3.9
3.25
2.6
1.95
1.3
0.65
0
-64
-27.86
-12.13
-5.28
-2.3
1
2.3
5.28
12.13
27.86
64
Fold Change

Figure 25: Volcano plots depicting mRNA with ≥2-fold significant differential expression in the VIVA-1 and VIVA-2 sub-populations compared to the parental MDA-MB-134VI cell line.

RNA was isolated from plated cells and prepared following the guidelines provided by the Génome Québec Innovation Center (McGill University). After RNA quality was assured, Clariom™ D Assays were conducted by the Génome Québec Innovation Center at McGill University. The returned data was then evaluated using the provided TAC software, and the above volcano plots were generated. The volcano plots of the (A) VIVA-1s and (B) VIVA-2s compared to the MDA-MB-134VI cell line show a number of targets with ≥2-fold significant differential expression (n=2 biological replicates). Boundary of 2-fold change and p value of 0.05.

Target		VIVA-1 vs. MDA-MB-134VI		VIVA-2 vs. MDA-MB-134VI		Role in Metastasis ?
		Fold Change	p value	Fold Change	p value	
Calpain 2	CAPN2	11.38	9.23E-06	24.48	3.98E-06	(Miao et al., 2017)
Gastrin-releasing peptide receptor	GRPR	11.81	1.23E-05	15.51	1.23E-05	(Ananias et al., 2009)
Relaxin 2	RLN2	5.05	0.0014	12.67	1.04E-05	(Ma et al., 2015)
Doublecortin	DCX	4.25	0.0019	7.34	0.0002	(Santra et al., 2009)
Capping protein (actin filament), gelsolin-like	CAPG	6.66	0.0001	6.49	0.0002	(Westbrook et al., 2016)
Progesterone Receptor	PGR	4.14	0.005	5.52	0.0001	(Mcfall et al., 2018)
Chemokine (C-X-C motif) receptor 4	CXCR4	-26.4	9.09E-07	-27.6	8.8E-07	(Liang et al., 2005)
Annexin A1	ANXA1	-6.09	4.02E-05	-4.12	0.0001	(de Graauw et al., 2010)
Guanine nucleotide-binding protein G(i), α-1 subunit	GNAI1	-19.69	0.0001	-10.96	3.5E-05	(Yao et al., 2012)
Tenascin-C	TNC	-3.63	0.0041	-6.55	1.72E-05	(Hancox et al., 2009)

Table 7: mRNA targets with ≥2-fold significant differential expression in the VIVA sub-populations compared to the parental MDA-MB-134VI cell line.

Through the evaluation of p values opposed to FDR p values, it is believed that these mRNA targets warrant further investigation into their possible role in VIVA invasion and ILC invasion/metastasis due to their ≥2-fold significant differential expression as well as literature suggesting possible roles in breast cancer or invasion/metastasis.

Chapter 4: Discussion

4.1 miR-23c and miR-23b-3p Were Found to Modulate ILC Cell Line Invasion, While the VIVA Sub-populations Have Increased Invasive Capabilities Compared to Their Parental MDA-MB-134VIs

There is a drastic need for new biomarkers and therapeutic targets of ILC, therefore this thesis aims to identify miRNAs with roles in ILC cell line invasion that may act as biomarkers or therapeutic targets of metastatic ILC. Through a miRNome analysis of four ILC cell lines we were able to identify miRNAs with potential roles in ILC cell line invasion. Two miRNA, miR-23c and miR-23b-3p were found to modulate invasion in the ILC cell lines, while they were not found to alter migration or cell growth. Unfortunately, in metastatic compared to non-metastatic patient ILC FFPE tumours, miR-23c was found to have expression differences in the opposite direction compared to ILC cell lines, while miR-23b-3p was found to have expression in a direction similar to what was seen in the ILC cell lines but did not reach statistical significance. Although miR-23c and miR-23b-3p could regulate ILC cell line invasion *in vitro*, they do not appear to regulate ILC metastasis in patients, therefore we speculated that the findings in the ILC cell lines may be MDA-MB-330 specific as it is was the only invasive ILC cell line. Knowing that there is a lack of ILC cell lines available (An et al., 2018) we sought to create another model of invasive ILC. This led to the generation of the VIVA-1 and VIVA-2 sub-populations. The VIVA sub-populations were created from the isolation of MDA-MB-134VI cells that had invaded through Matrigel® coated invasion chambers. Both VIVA sub-populations were found to have increased invasive capabilities compared to their parental MDA-MB-134VI cell line. Further investigation into the properties of the VIVAs revealed that they maintained the cell growth rate and specific protein characteristics of their parental cell line; however, both miRNA and mRNA analysis showed many targets with significant differential expression. From the findings of this thesis, we have improved methods for

studying ILC *in vitro* and identified miR-23c and miR-23b-3p as regulators of ILC cell line invasion.

4.2 Further Investigation May Need to be Conducted Before Confirming the MDA-MB-330 Cell Line is an Invasive ILC Cell Line

In section 3.1.3, we confirmed the invasive capabilities of the MDA-MB-330 cell line (Figure 2&3). The reason for doubt with regards to the MDA-MB-330s invasive capabilities was due to a paper by Tasdemir et al., (2018) which had been published after commencing the work of this thesis. The study found that the tested ILC cell lines, which included the MDA-MB-330s, had minimal invasive capabilities in both Collagen I and Matrigel® (Tasdemir et al., 2018). We noticed however, that the media in which they cultured the MDA-MB-330s is not what is recommended by ATCC®, whereas the media used in this thesis, with the addition of DMEM to adapt the cells to CO_2, was recommended by ATCC® (American Type Culture Collection, 2019b; Tasdemir et al., 2018). As discussed in section 3.1.3, we therefore tested different methods of stimulating invasion, and found there to be no significant difference in the invasive capabilities of the MDA-MB-330 cell line. The methods in this thesis appear to be the best conditions to stimulate invasion; however, this is not significantly greater. Since it does not appear that serum starving the cells overnight or leaving the cells in limited serum within the invasion chambers, as was done in the paper by Tasdemir et al., (2018) reduces the invasive capabilities of the MDA-MB-330s, we then may speculate that perhaps the differences in media may be responsible. Therefore future experiments would be to confirm the invasive capabilities of the MDA-MB-330s with no growth factors in the media as well as serum starving the cells overnight (American Type Culture Collection, 2019b; Tasdemir et al., 2018). These conditions would mimic those used in the paper by Tasdemir et al., (2018) and it is believed that this would confirm that the varying methods used

to culture the cells and stimulate invasion were responsible for the drastic changes seen in MDA-MB-330 invasion. We may also confirm the differences in the invasive capabilities of the cells by approaching Tasdemir et al., (2018) for some of their MDA-MB-330s, which we would then compare to our MDA-MB-330s. In addition, the MDA-MB-330 cell line should be sent for authentication as was done in the paper by Tasdemir et al., (2018) to confirm genetically the cell lines are a match and that they are still the original cell line received from ATCC® (American Type Culture Collection, 2019c). Although there is some hesitation with regards to the invasive capabilities of the MDA-MB-330s due to the recently published paper by Tasdemir et al., (2018) we however, consistently see invasion of the MDA-MB-330 cell line at 48hr.

4.3 miR-23c, miR-23b-3p and miR-28-5p Were Selected Due to Previous Roles in Cancer, Invasion and Metastasis

4.3.1 miR-28-5p in the Literature in Comparison to Our Findings

The miRNAs selected from the cell line miRNome analysis (Figure 4&5) were elected for further investigation due to their significantly increased expression in the invasive compared to minimally invasive ILC cell lines, as well as their previously suggested roles in cancer and metastasis (An et al., 2015; Begum et al., 2015; Liu and Wang, 2019; Shi and Teng, 2015; Wong and Wang, 2015; Zaman et al., 2012; Zhang et al., 2018). miR-28-5p was not originally selected for investigation into its potential role in regulating ILC cell line invasion even though it was found to have increased expression in the invasive compared to minimally invasive cell lines (Figure 5C). The reason miR-28-5p was omitted from further investigation was that its increased expression in the invasive compared to minimally invasive ILC cell lines was only significantly different between the MDA-MB-330 and MDA-MB-134VI cell lines. Since both miR-23c and

miR-23b-3p had significantly increased expression in the invasive MDA-MB-330s compared to each minimally invasive ILC cell line, they were more promising targets and thus were selected for further investigation into their potential role in regulating ILC cell line invasion (Figure 5A&B). However, as our study progressed, we found that miR-28-5p has a higher mean expression in metastatic compared to non-metastatic patient ILC samples, therefore it is suggested that further investigation into its role in regulating ILC invasion and metastasis is conducted (Figure 18).

In colorectal cancer miR-28-5p was found to have significantly decreased expression, while increased levels of miR-28-5p resulted in decreased cell line migration and invasion (Almeida et al., 2012). In gastric cancer, miR-28-5p was found to have lower levels which was associated with reduced overall survival (Xiao et al., 2018); however, when miR-28-5p levels were increased in gastric cancer cell lines, decreases in cell invasion and migration resulted (Xiao et al., 2018). In hepatocellular carcinoma, miR-28-5p expression was found to act as a tumour suppressor, in that its decreased levels of expression were associated with aggressiveness, malignancy and recurrence (Shi and Teng, 2015). The findings of these studies were opposite to what was seen in our ILC data, which suggests that increased miR-28-5p expression may be associated with increased invasion/metastasis and therefore we would speculate a reduction in overall survival. It may be hypothesized that miR-28-5p plays a different role in ILC, and it is suggested that miR-28-5p still be considered for further investigation into its potential role in regulating ILC invasion/metastasis.

4.3.2 miR-23c in the Literature in Comparison to Our Findings

miR-23c was found to have significantly increased expression in the invasive compared to minimally invasive ILC cell lines and to modulate the invasive capabilities of the MDA-MB-330

and MDA-MB-134VI cell lines (Figure 5A,6B,8B). However, it had an opposite trend in patient ILC samples where its mean expression was not significantly reduced in the metastatic compared to non-metastatic ILC patient FFPE tumour samples (Figure 16A). A recent study found that miR-23c has decreased expression and targeted erbin (ERBB2IP) in hepatocellular carcinoma (Zhang et al., 2018). It has been shown that ERBB2IP interferes with ERα signaling in hepatocellular carcinoma (Wu et al., 2017). This study also looked at the expression of miR-23c among other cancers, including breast invasive carcinoma, and found its expression to correlate with tumourigenesis (Zhang et al., 2018). Based on these findings we examined the MDA-MB-330 Clariom™ Assay data to see if use of the miR-23c hairpin inhibitor resulted in any changes in expression of ERBB21P when miR-23c levels were decreased. There was found to be no significant change in the fold change (around 1) of ERBB2IP or ESR1 when miR-23c levels were decreased in the MDA-MB-330 cell line. Though ERBB2IP may be a direct target of miR-23c in the context of hepatocellular carcinoma (Zhang et al., 2018), it appears to not be directly regulated by miR-23c in ILC cell lines and as such other regulators may be at play.

4.3.3 miR-23b-3p in the Literature in Comparison to Our Findings

miR-23b-3p was found to have significantly increased expression in the invasive compared to minimally invasive ILC cell lines, and to modulate the invasive capabilities of the MDA-MB-330 and MDA-MB-134VI cell lines (Figure 5B,7B,9B). However, though not significant, it had slightly increased mean expression in the metastatic compared to non-metastatic ILC samples (Figure 16B), supporting its association with ILC cell line invasion. Other investigations found conflicting data, with low levels of miR-23b-3p found to be associated with metastasis correlating to worse prognosis in gastric cancer (An et al., 2015), and with increased invasion in osteosarcoma

(Liu et al., 2018), and pancreatic cancer (Wei et al., 2018). Despite these contrasts, there is literature that suggests miR-23b-3p expression is increased in aggressive non-small cell lung cancer with higher levels indicative of poor outcome relating to increased risk of recurrence and lower overall survival (Begum et al., 2015). Similar to our findings as well, in renal cell carcinoma decreased levels of miR-23b-3p was associated with decreased invasion and increased levels of its direct target PTEN (Zaman et al., 2012). Although PTEN is a commonly altered gene in ILC compared to IDC (Ciriello et al., 2015), neither the MDA-MB-330 or MDA-MB-134VI cell lines have known mutations in PTEN (Hollestelle et al., 2007). Examination of the gene expression dataset of MDA-MB-330 cells with decreased miR-23b-3p levels mediated by hairpin inhibitor transfection showed no change (-1.06-fold) in PTEN expression, suggesting the ability of miR-23b-3p to regulate ILC cell invasion is PTEN independent. Although some studies would contradict our findings regarding the association of miR-23b-3p with cell metastasis and invasion, others support our findings which suggests tumour cell type specific effects may contribute to the role of this miRNA in tumour invasion.

Together these findings suggests that the function of miRNA may be tissue (Lagos-Quintana et al., 2002) and cancer type dependent (Wang and Luo, 2015), and varied results could be observed in part due to the genetic landscape of various tumours. Despite previous findings pertaining to miR-23c and miR-23b-3p with regards to cancer, invasion, and metastasis, this thesis found that modulated levels of both miRNAs was associated with varying invasive capabilities within the ILC cell lines. Though miR-23c does not appear to be associated with metastatic potential in ILC patient FFPE tumour samples, miR-23b-3p appears more promising. Therefore, this thesis is the beginning of defining the role miR-23c and miR-23b-3p have in ILC specifically.

4.4 Hairpin Inhibitors Transfection Efficiency is Questionable

4.4.1 Hairpin Inhibitors Can Inhibit the qPCR Reaction and May Have Off-Target Effects

During the course of this thesis, we did not encounter substantial issues with the miR-23c and miR-23b-3p hairpin inhibitors as there was significant inhibition of the targeted miRNAs upon transfection with the specific hairpin inhibitors (Figure 6A,7A). Despite this, there was some variability upon analyzing the subsequent invasive capabilities of the MDA-MB-330 cell line treated with the hairpin inhibitor. As such, 4 independent biological replicates were completed, and with each replicate there was a consistent decrease in the invasive capabilities of the MDA-MB-330s at the 50nM dose of miR-23c and the 20nM dose of miR-23b-3p of hairpin inhibitor; however, it was not until the completion of the fourth replicate that they became statistically significant (Figure 6B,7B). The study by Thomson et al., (2013) found that qPCR is not an accurate indicator of the effects of hairpin inhibitors, as hairpin inhibitors can directly obstruct qPCR mediated detection of the target miRNA. The hairpin inhibitor can also be sequestered within vesicles, which may result in limited inhibition of the select miRNA (Thomson et al., 2013). Despite the complications that may indicate our measurements of the miRNA levels following hairpin inhibitor transfection of MDA-MB-330 may be inaccurate (Thomson et al., 2013), we found that compared to the control non-targeting hairpin inhibitor there was a significant decrease in the detected levels of miR-23c and miR-23b-3p which was sufficient to result in a significant decrease in the invasive capabilities of the cells (Figure 6B,7B). Therefore, we believe that our methods using hairpin inhibitors resulted in sufficient targeted decreases in miR-23c and miR-23b-3p levels, which is able to effectively result in downstream phenotypic alterations.

A study by Robertson et al., (2010) found cross-reactivity between hairpin inhibitors targeting the members of the let-7 family of miRNA. Additionally, they found effective hairpin

inhibitor concentrations were dependent on the amount of endogenous targeted miRNA present, and higher concentrations of hairpin inhibitor could result in greater off-target effects (Robertson et al., 2010). Accordingly, Robertson et al., (2010) found that reduced concentrations of hairpin inhibitors resulted in greater precision of the hairpin inhibitor for its target. From these findings, we may consider that the significant effects in inhibition of cell invasion seen at the 20nM dose of miR-23b-3p may be real due to a lower dose of hairpin inhibitor being used (Figure 7) (Robertson et al., 2010). However, as Robertson et al., (2010) suggested that hairpin inhibitors in excess could have off-target effects, we have to acknowledge that the significant decrease in cell invasion observed at the 50nM dose of miR-23c hairpin inhibitor may be due in part to off-target effects (Figure 6). Since miR-23c and miR-23b-3p are from the same family of miRNA and differ at only 2-3nt (Granados-López et al., 2017; Kozomara et al., 2019), it is possible the significant decrease seen in the invasive capabilities of the MDA-MB-330s at the 50nM dose of miR-23c hairpin inhibitor may be due to off-target effects of the hairpin inhibitor in part via targeting of miR-23b-3p (Robertson et al., 2010). This may explain in part why despite effects seen in the ILC cell lines with respect to modulation of cellular invasive ability following miR-23c hairpin transfection, these significant differences in miR-23c did not translate to the metastatic compared to non-metastatic patient ILC FFPE tumour samples (Figure 16&17). It is also possible that elevated expression of miR-23c and its association with cell invasion is a specific characteristic of the MDA-MB-330 cell line and not generalizable to ILC tumours, as unfortunately we were restricted to one invasive ILC cell line upon which our comparisons were made and could be therefore biasing our cell line results.

4.4.3 Hairpin Inhibitors May Saturate the miRNA Pathway Resulting in Toxicity

Issues with regard to short hairpin RNA (shRNA) toxicity has been seen in rat brain, where detrimental effects were observed in the tissues due to the use of shRNA (van Gestel et al., 2014). These effects were found to be a consequence of saturation of the miRNA pathway, resulting in decreased expression of miRNAs within the treated area (van Gestel et al., 2014). In a similar manner we may speculate that use of hairpin inhibitors could saturate the miRNA pathway machinery as well (van Gestel et al., 2014). In our investigation we only evaluated the expression of the specific miRNA and the control SNORD95, and we did not examine the expression of other cell specific miRNA which could have indicated issues with the miRNA pathway machinery following the use of the hairpin inhibitors (van Gestel et al., 2014). It is possible the results of significantly decreased invasion in the MDA-MB-330 with reduced miR-23c and miR-23b-3p levels were due to saturation of the miRNA pathway by the hairpin inhibitors (van Gestel et al., 2014), which consequently decreased the expression of multiple miRNAs resulting in the change in the MDA-MB-330s invasive capabilities. Therefore, other methods of miRNA inhibition, such as locked nucleic acid miRNA inhibitors (Thomson et al., 2013) or expression vectors (Merhautova et al., 2016), should be investigated for further examination of the roles miR-23c and miR-23b-3p have in regulating ILC invasion and metastasis.

4.5 Mimic Transfection Efficiency is Questionable

4.5.1 Mimics Were not Able to Significantly Increase Specific miRNA Expression

The lack of statistical significance achieved in the invasion assays of the MDA-MB-134VI cell line despite having seemingly increased levels of miRNA expression in cells via mimic transfection (Figure 8B&9B), led to the postulation that the transfection efficiency was not

adequate. Therefore, using a fluorescently tagged control mimic, we visualized subcellular localization of the mimics and found that although the mimic was entering into the cell, punctate staining suggested it was sequestered within vesicles (Figure 10) (Thomson et al., 2013). This was found to be similar to the results displayed in the paper by Thomson et al., (2013), where instead of miRNA mimics being functional which requires integration within the RISC and combining with Argonaute, the mimic was found in proximity to lysosomes. We may also speculate that this punctate staining may indicate that the miRNA are located within P-bodies, locations within the cytoplasm where miRNA may execute their post-transcriptional silencing (Lin and Gregory, 2015). It seems unlikely however, that the punctate staining observed is localization within P-bodies as the control mimic used in Figure 10 is non-targeting and should not target any mRNA found within the cell therefore deeming it non-functional (QIAGEN, 2015). Unfortunately we can only hypothesize at this moment, and further staining in conjunction with markers specific for lysosomes, Argonaute, and P-bodies will have to be conducted to determine whether they colocalize with the non-targeting control mimic (Thomson et al., 2013). Therefore, if the mimic is collecting within vesicles and is thus not functional (Thomson et al., 2013), then we may surmise that the mimic is unable to block its target mRNAs within cells, which could translate into the modest biological effects we observed in our study.

4.5.3 Despite Their Limitations Mimics Have Select Advantages

In addition to the concern with regards to the functionality of transfected miRNA mimics, there is apprehension with off-target effects due to the possibility of the passenger strand integrating with Argonaute (Thomson et al., 2013). In contrast to these findings, it has been suggested that miRNA mimics have greater post-transcriptional effects compared to their

endogenous miRNA due to greater integration within the RISC, as such the passenger strand should not produce off-target effects as was suggested in the paper by Thomson et al., (2013) (Merhautova et al., 2016). . One advantage of the use of miRNA mimics in cells is a lack of toxicity compared to use of hairpin inhibitors (Bader et al., 2010; van Gestel et al., 2014) as they have identical sequences to their endogenous miRNA counterparts thereby increasing miRNA that is already present within the cell at lower levels, and targeting similar pathways (Bader et al., 2010).

4.5.4 Transfection Efficiency May Have Varied Between Replicates

It is also possible that the variability we observed in our studies could be attributed to varying transfection efficiencies across biological replicates. Due to the slow growing nature of the four ILC cell lines *in vitro* (Christgen et al., 2009; Tasdemir et al., 2018), and relatively low RNA yields, we were unable to assess and confirm the transfection efficiency of the hairpin inhibitor and mimic for every experiment. We therefore opted to perform initial experiments optimizing the concentrations of mimic and hairpin inhibitor, which appeared to effectively modulate miRNA levels in cells prior to commencing downstream investigations (Figure 6A,7A,8A,9A). As such, the most effective concentrations observed in these experiments were used for subsequent downstream assays. We acknowledge that this lack of confirmation of effective mimic and hairpin inhibitor transfection may also contribute to the variability seen between replicates in invasion assays due to possible variation in transfection efficiency which could not be confirmed at every step.

4.6 The UACC-3133 Cell Line May Not be of ILC Origin

In addition to the MDA-MB-134VI cell line, we attempted to increase the sample size of our analysis in non-invasive ILC cell lines by testing the effects of miR-23c and miR-23b-3p overexpression in the UACC-3133 cell line. The UACC-3133 cell line was another of the minimally invasive cell lines, that according to ATCC® is of ILC origin (American Type Culture Collection, 2019d). Our initial results suggested that like other minimally invasive ILC cell lines tested, levels of miR-23c and miR-23b-3p were lower in the UACC-3133 cell line than in the invasive MDA-MB-330 line (Figure 5A&B). As such we predicted that overexpression of miR-23c and miR-23b-3p using mimic transfection should result in increased cell invasion similar to what was observed with the MDA-MB-134VI cell line. Unfortunately, using similar approaches in the UACC-3133 cell line, our results were opposite to the those seen in the MDA-MB-134VI cell line. Despite a >10,000-fold increase in miR-23c and a >10-fold increase in miR-23b-3p levels following transfection with mimics, statistical significance was not achieved which is similar to that seen in the MDA-MB-134VI cell line (Figure 8A&9A). We speculate this may be due in part to similar confounding issues as discussed previously (section 4.5.1) with respect to sequestration of mimics in vesicles (Thomson et al., 2013) as well as difficulties in transfection efficiency across biological replicates. Despite the non-significant but substantial increases in miRNA levels with mimic transfection of UACC-3133 cells, we observed a not significant decrease in the invasive capabilities of the cell line. This suggests that the results seen in the MDA-MB-330 and MDA-MB-134VI cell lines may be cell line specific, or potentially a product of the reduced mimic efficiency or off-target effects discussed in section 4.5. Although plausible arguments, the opposite effects of the miR-23c and miR-23b-3p mimics on UACC-3133 cell invasion could be an indication of different cellular origin. As seen in Supplementary Figure 2A and 2B, miR-23c and

miR-23b-3p expression did not correlate with the invasive capabilities of the tested IDC breast cancer cell lines. This suggests that perhaps the UACC-3133 cell line is not of ILC origin, but another subtype of breast cancer.

With regards to the UACC-3133 cell line, there does not seem to be any literature outlining the characteristics of the cell line. In fact, the only paper we could find pertaining to the cell line's derivation recorded that the UACC-3133 cell line was an adenocarcinoma isolated from plural effusions (Domann et al., 2000). This is consistent with ATCC®'s description of the cell line, apart from ATCC® establishing that the poorly differentiated adenocarcinoma was ILC like and had metastasized to the pleural fluid (American Type Culture Collection, 2019a). According to ATCC®, as we cannot find any other paper indicating so, the UACC-3133 cell line is ER low, PR negative, and HER2 positive (American Type Culture Collection, 2019a). Through western blot analysis from UACC-3133 cell lysate, the UACC-3133 cell line presented with a doublet in E-cadherin which may suggest post-translational modifications (Jackson ImmunoResearch Laboratories, 2017; Mann and Jensen, 2003), since there seems to be no papers indicating non-functional E-cadherin (Figure 1B). The protein profile of the UACC-3133 cell line does not suggest classical ILC (Arpino et al., 2004; Iorfida et al., 2012; Moll et al., 1993), but may indicate pleomorphic ILC (Jacobs et al., 2015; Rakha et al., 2013; Rosa-Rosa et al., 2019) or an alternative subtype of breast cancer origin. It is suggested that before conclusions are made with regards to the role of miR-23c and miR-23b-3p in the UACC-3133 cell line, and by association ILC, that further investigation into the cellular origin of the UACC-3133 cell line is conducted. Primary steps should begin with identifying mis-localization of p120 to the cytoplasm upon loss of E-cadherin function, as establishing the E-cadherin and p120 status associated with ILC (Sarrió et

al., 2004; Tasdemir et al., 2018) will provide a preliminary foundation for confirming the cellular origin of the UACC-3133 cell line.

4.7 Targets Identified From the MDA-MB-134VIs with Increased miR-23c and miR-23b-3p Clariom™ Assays Did not Validate

4.7.1 Only SULF1 was Found to Validate From the MDA-MB-134VI Clariom™ Assays

Despite potential experimental hurdles with the use of mimics and hairpin inhibitors to modulate miRNA levels in cells, they are standard methods widely used in the research community (Jiang et al., 2014; Liu et al., 2018; Qian et al., 2017). Moreover, use of these approaches did result in modulation of ILC cell line invasion, which led us to pursue gene expression analysis of mimic or hairpin inhibitor transfected cells in an attempt to identify relevant mRNA targets that may be regulating ILC cell line invasion and metastasis. From the Clariom™ Assays conducted, we attempted to validate whether mRNA targets identified from the MDA-MB-134VI Clariom™ Assays showed similar changes in expression upon modulation of miRNA in both the MDA-MB-134VI and MDA-MB-330 cell lines (Figure 13&14). These targets were selected based on their ≥2-fold significantly downregulated expression when miR-23c and miR-23b-3p levels were increased in addition to literature indicating potential roles in cancer, breast cancer or metastasis. For the most part we were unable to confirm modulation of mRNA expression following miRNA mimic or hairpin inhibitor transfection of cells. However, of the investigated targets, SULF1 at the 20nM dose of miR-23b-3p hairpin inhibitor in the MDA-MB-330s was the only target to validate. The significant increase in SULF1 expression was minimal (<2-fold) which we speculated could have limited biological impact (Figure 14C). It is possible that these targets did not validate when qPCR was used, due in part to their levels of expression in ILC cells as we believe the Clariom™

Assay may be more sensitive than qPCR. Moreover, qPCR uses an endogenous control mRNA, β-actin in our case, whereas the Clariom™ Assay uses the SST-RMA method for normalization (appliedbiosystems and ThermoFisher Scientific, 2017) which may account for variability of target expression between the Clariom™ Assay and qPCR.

4.7.2 SV2A was the Only Predicted Target of miR-23c and miR-23b-3p from the Selected Clariom™ Assay Targets

As previously discussed, miRNA can target multiple mRNAs (Schoolmeesters et al., 2009) and have tissue (Lagos-Quintana et al., 2002) as well as cancer specific expression (Wang and Luo, 2015). This may have contributed to the lack of validation of the targets identified in the MDA-MB-134VI Clariom™ Assays. It was considered that perhaps the mRNA targets were not validating in either the MDA-MB-134VI or MDA-MB-330 cell lines as they were not direct targets of miR-23c and miR-23b-3p, but rather downstream targets resulting from increased miR-23c and miR-23b-3p levels. Therefore, using miRDB a target prediction website, we looked up whether our selected targets were predicted direct targets of miR-23c and miR-23b-3p (Liu and Wang, 2019; Wong and Wang, 2015). The only target found to be a predicted target of miR-23c and miR-23b-3p was SV2A; however, it had a target score of 52 with either miRNA which is suggestive of less certainty in the match (Liu and Wang, 2019; Wong and Wang, 2015). The other evaluated targets were not found to be predicted targets of either miR-23c or miR-23b-3p (Liu and Wang, 2019; Wong and Wang, 2015). These findings indicate that these targets, apart from SV2A, may be downstream targets of the miRNAs or could be false positives or negatives from the Clariom™ Assays. Another reason could be the lack of confirmation of transfection efficiency prior to validating the expression of mRNA targets identified in the Clariom™ Assays by qPCR. Before sending the samples for Clariom™ Assays, we confirmed the transfection efficiency of the mimics

and hairpin inhibitors (Supplementary Figure 3&4). In order to confirm the transfection efficiency of the MDA-MB-330 cell line prior to being sent for Clariom™ Assay, the transfection was conducted using a larger number of cells due to low RNA yield. As mentioned prior, ILC cell lines are slow growing (Christgen et al., 2009; Tasdemir et al., 2018) and have low RNA yield, therefore it was difficult to confirm the transfection efficiency for the mRNA target validations for every biological replicate. It does appear however, that the selected mRNA targets were not direct targets of miR-23c and miR-23b-3p (Liu and Wang, 2019; Wong and Wang, 2015). As such, future investigations should observe possible direct targets, or rather regulated pathways that may be affected due to both direct and downstream targets of the miRNAs.

4.8 The Clariom™ Assays of the MDA-MB-330s with Decreased miR-23c and miR-23b-3p Levels Identified Modulated Pathways

4.8.1 Three Common Pathways Were Identified Between the miR-23c and miR-23b-3p MDA-MB-330 Clariom™ Assays

While the targets identified from the MDA-MB-134VI Clariom™ Assays did not validate in either the MDA-MB-134VI or MDA-MB-330 cell lines (Figure 13&14), other targets with ≥2-fold significant differential expression are available from both datasets (Table 5). Moving forward, preference will be given to targets identified from the dataset of the MDA-MB-330s transfected with hairpin inhibitor due to suspected issues with the mimic transfection (Figure 10). In addition, biological pathways with a number of differentially expressed mRNA may be worth investigating as they may lead to the discovery of downstream targets that are regulators of invasion, metastasis, and ILC. While we should consider common altered pathways shared between miR-23c and miR-23b-3p, those that are unique to one miRNA or the other should be evaluated as well. The highly regulated pathways from the MDA-MB-330s with decreased levels of miR-23c identified by the

Clariom™ Assay analysis were: G protein-coupled receptors (GPCR) class A Rhodopsin-like, nuclear receptor meta pathway, PI3K-Akt and focal adhesion. From the miR-23b-3p dataset, the highly regulated pathways were: PI3K-Akt, GPCR and focal adhesion. The common pathways modulated by both miR-23c and miR-23b-3p were PI3K-Akt, focal adhesion and GPCRs, which may suggest these are familial pathways of the miRNAs (Granados-López et al., 2017; Kozomara et al., 2019). Each of the identified pathways has a number of differentially regulated targets associated with decreased expression of miR-23c and miR-23b-3p which make them good candidate pathways for further investigation.

4.8.2 The Possible Role the Nuclear Receptor Pathway May Play in ILC Cell Line Invasion

Along these lines, previous studies support roles for many of these pathways as being altered in breast cancer (Cai et al., 2018; Feigin et al., 2014; Lin et al., 2015; Magnon et al., 2013; Provenzano et al., 2008; Yoeli-Lerner et al., 2005). The study conducted by Lin et al., (2015) found that a large number of nuclear receptors were present in breast cancer, this includes ERα and PR. The fact that nuclear receptors were a highly regulated pathway in the MDA-MB-330s with decreased miR-23c levels, may be an indication of the common expression of ER and PR in ILC (Arpino et al., 2004). One particular target from the nuclear receptor pathway stood out, serine peptidase inhibitor Kazal Type 13 (SPINK13) (Fijten et al., 2019; Slenter et al., 2018). SPINK13 was found to have a significant increase in expression in the MDA-MB-330 cell line when miR-23c levels were decreased (fold change 2.07, p value 0.0018). Although not significant in the MDA-MB-330s with decreased miR-23b-3p levels, SPINK13 had a slight increase in expression (fold change 1.26, p value 0.13). In ovarian cancer, increased SPINK13 expression correlated with increased overall survival (Cai et al., 2018). In addition, when SPINK13 levels were decreased,

consequent significant increase in ovarian cancer cell line invasion was seen (Cai et al., 2018). Through further investigation into SPINK13 and its role in invasion, it was found that its decreased expression may be associated with increased EMT (Cai et al., 2018). Though these findings were in ovarian cancer, they are extremely similar to what we see in the MDA-MB-330 cell line (Cai et al., 2018). Normally the MDA-MB-330 cell line is invasive; however, when miR-23c levels are decreased there is a significant decrease in the invasive capabilities of the MDA-MB-330s. From the Clariom™ Assay, it is apparent that when miR-23c levels are decreased, there is a significant 2-fold increase of SPINK13. Thus, we would hypothesize that SPINK13 has lower endogenous expression in the MDA-MB-330 cell line, which correlates with its invasive capabilities; however, when miR-23c expression is decreased, SPINK13 a possible target of miR-23c expression, is increased which results in decreased invasion (Cai et al., 2018). These results are promising, and SPINK13 is worth further investigation into its possible role in regulating MDA-MB-330 ILC cell line invasion. Therefore, the modulation of nuclear receptors may be a factor responsible for the changes seen in the invasive capabilities of the ILC cell lines with different levels of miR-23c and miR-23b-3p.

4.8.3 The PI3K-Akt Signaling Pathway May Have a Greater Role in ILC Cell Lines

ILC is known to have increased phosphorylation of Akt (Ciriello et al., 2015) and thus increased PI3K-Akt signaling (Ciriello et al., 2015; Michaut et al., 2016), which is why it being a top regulated pathway in the MDA-MB-330s with decreased levels of either miR-23c or miR-23b-3p may have been expected. Activated Akt, a component of the PI3K-Akt pathway has been shown to inhibit both invasion and migration in breast cancer (Yoeli-Lerner et al., 2005), thus indicating the potential effects of this pathway in regulating ILC cell line invasion. An interesting target that

was uncovered from the Clariom™ Assays was cholinergic receptor muscarinic 1 (CHRM1), as it was found to have significantly decreased expression when miR-23b-3p levels were decreased in the MDA-MB-330 cell line (fold change -1.9, p value 0.0017). Though this is in the opposite direction to what we would expect when miR-23b-3p levels are decreased, CHRM1 is part of both the GPCR and PI3K-Akt pathways (Conklin et al., 2018; Hanspers et al., 2018; Slenter et al., 2018). CHRM1 was found to be associated with invasion, while its reduction resulted in decreased metastasis and consequently increased survival in a mouse model of prostate cancer in the paper by Magnon et al., (2013). The results in the paper by Magnon et al., (2013), where decreased CHRM1 is associated with decreased metastasis are comparable to what we have seen in the MDA-MB-330 cell line, where decreased CHRM1 expression is a consequence of decreased miR-23b-3p levels, which results in significant decreased invasion. This data therefore suggests that CHRM1 is not a direct target of miR-23b-3p as we would expect that decreased miR-23b-3p levels would result in increased expression of its direct target; however, this may indicate that CHRM1 is a downstream target of miR-23b-3p which would explain its resulting decreased expression when miR-23b-3p levels are reduced. Accordingly, we would suggest future investigation into the possible role of CHRM1 in regulating ILC cell line invasion due its role in multiple pathways suspected to be modulated by miR-23c and miR-23b-3p.

4.8.4 The Common Pathways All Interact With One Another

Both the GPCR and focal adhesion pathways have been implicated in regulating breast cancer invasion and/or metastasis (Feigin et al., 2014; Provenzano et al., 2008). Since modulation of the focal adhesion pathway can contribute to changes in proliferation, invasion and migration due to its integration with numerous pathways (Provenzano et al., 2008), perhaps it is through the

focal adhesion pathway that downstream targets regulate ILC cell line invasion. The PI3K-Akt pathway is known to interact with the focal adhesion pathway (Provenzano et al., 2008), while the GPCR pathway has been found to correlate with the mTOR pathway, which the Akt pathway is known to interact with (Feigin et al., 2014). Therefore, all three common pathways identified from the Clariom™ Assays of the MDA-MB-330s with decreased levels of either miR-23c and miR-23b-3p communicate with one another, thus depicting the numerous targets and the downstream intricacy miR-23c and miR-23b-3p may have on ILC cell line invasion. Future investigations should observe the effects these pathways have on ILC as well as ILC cell line invasion. Perhaps in future experiments, if we were to treat with both miR-23c and miR-23b-3p hairpin inhibitors or mimics there would be a greater effect on these highly regulated pathways, thus creating greater downstream responses. As such, the hope of investigating these pathways is to identify possible therapeutic and diagnostic targets of ILC metastasis.

4.9 The Patient miRNome Analysis May be Comprised of Various ILC Subtypes and Cell Types

Despite promising findings of miR-23c and miR-23b-3p with respect to ILC cell line invasion, they did not appear to have statistically significant differences in their levels of expression in the small cohort of patient ILC FFPE tumours we analyzed. We may speculate that the reason miR-23c and miR-23b-3p did not validate within the patient ILC FFPE tumour dataset was because it does not regulate ILC metastasis in patients, or because effects we observed *in vitro* are cell line specific or due to suspected issues with use of the hairpin inhibitor and mimic approaches as previously discussed. Another reason however, may be attributed to the methods used to perform the patient ILC FFPE tumour miRNome analysis (Figure 16,17&18). When identifying ILC patient FFPE tumour samples for our investigation they were not separated by the

various ILC subtypes (Sinn and Kreipe, 2013), as gathering enough samples with metastatic and non-metastatic fates took precedence. Therefore our miRNome of metastatic compared to non-metastatic ILC may not be focused on the more prominent classical ILC (Hwang and Sahoo, 2016), but rather various ILC subtypes (Sinn and Kreipe, 2013). As pleomorphic ILC is more aggressive (Jacobs et al., 2015), it is possible that pooling of ILC subtypes (Sinn and Kreipe, 2013) within the miRNome analysis is misrepresenting the expression of miRNA within metastatic compared to non-metastatic ILC. As discussed previously, miRNA expression can vary based on numerous factors, including breast cancer subtype (Riaz et al., 2013). With the addition of more metastatic and non-metastatic ILC patient FFPE tumour samples, we may have sufficient sample size in the future to power the analysis to consider subtype specific miRNA expression associated with metastatic and non-metastatic ILC (Sinn and Kreipe, 2013).

Our present study may be limited by looking at only the primary tumour to identify miRNAs that may play roles in regulating ILC metastasis. Tumours are heterogenous (Hanahan and Weinberg, 2011), and within this heterogenous population are cells that have developed metastatic abilities (Navin et al., 2011). These metastatic cells will subsequently leave the primary tumour to derive the metastatic tumour (Hanahan and Weinberg, 2000; Navin et al., 2011). We would speculate that the cells which form the metastatic site comprise a small portion of the primary tumour (Navin et al., 2011), therefore our ability to detect miRNAs that may regulate ILC metastasis may be masked by miRNA expression in the bulk of the tumour epithelial or stroma cells (Allinen et al., 2004). Studies have found that only a limited number of miRNAs are found to have altered expression between the primary and the metastatic tumour (Schrijver et al., 2017). To identify these limited miRNA it would be prudent to look at cells that have intravasated into the blood and lymphatic system (Hanahan and Weinberg, 2011) and compare their expression to

the primary and metastatic tumours. The limited number of metastatic cells within the primary tumour (Navin et al., 2011), may contribute to the lack of validation of miR-23c and miR-23b-3p within the patient ILC FFPE cohort observed in our study.

While the varying subtypes of ILC (Sinn and Kreipe, 2013) used in this analysis may contribute to our findings, it is also possible that the scrape method used to isolate RNA from the tumour samples may be responsible for varying miRNA expression. The use of the scrape method was an alternative to the initial LCM method for isolating the tumour cells from the FFPE slides (section 2.5). We found the LCM extremely time consuming and resulted in lower quality RNA as a result. Although pathological assessment was used to identify areas of ILC tumour in each tissue section, which was isolated for subsequent analysis using the scrape method, due to the nature of ILC and the scrape method, our RNA would have included both tumour epithelial and stromal cell RNA (Allinen et al., 2004). While we tried to take areas enriched for tumour epithelium, it is impossible to avoid stromal cells using this method, and thus these alternative cell types may hinder the specificity of the miRNome analysis, and confound our potential signature of miRNA expression within metastatic compared to non-metastatic ILC (Allinen et al., 2004). A potential solution would be to find miRNA signatures of normal breast (Pal et al., 2015) and tumour stromal, basal and luminal cells and cross reference these signatures to our miRNome analysis of metastatic compared to non-metastatic ILC FFPE tissues to differentiate the expression of miRNAs in the tumour compared to the surrounding cells (Allinen et al., 2004; Pal et al., 2015). These additional precautions will allow for the continuation of the scrape method for isolating RNA from the FFPE tissue samples, which will allow for the derivation of a miRNA signature of metastatic compared to non-metastatic ILC in a time conscious manner.

4.10 VIVAs Have Increased Invasion, but it is Not Significant at All Time Points

During our study, it became apparent that there is a significant lack of invasive ILC cell lines (An et al., 2018) for preclinical evaluation and validation of our miRNA of interest. As a result, we embarked on a strategy to isolate and expand more invasive sub-populations from our minimally invasive MDA-MB-134VI cell line to use as a research tool in future studies. As shown in Figures 19 and 20, both the VIVA-1 and VIVA-2 cell sub-populations had altered invasive capabilities compared to their parental cell line. Although trends for increased invasion were observed at all time points examined, VIVA-1 invasion only reached statistical significance at 1-week post seeding, while VIVA-2 only reached statistical significance at 48hr post seeding. A reason the invasive capabilities of the VIVA-1s at 48hr (Figure 19A) and the VIVA-2s at 1-week (Figure 20B) did not reach statistical significance was due to the presence of outliers within the 3 biological replicates. Based on the method by which they were isolated, both the VIVA-1s and the VIVA-2s are heterogenous populations. It should be noted that biological replicates were all performed at increasing passage number of the sub-populations. We may speculate that if these sub-populations are heterogenous that the cells do not all possess the same characteristics and thus may have differential invasive capabilities, some of which may be lost or gained over time as certain cell clones may outgrow the others during routine passaging. These sub-populations were isolated not too long ago, and we are just beginning to characterize and study them, therefore we are not sure how these sub-populations will continue through further passages. It may be that the VIVAs lose their increased invasive capabilities or become more invasive over time, and we will have to investigate this further.

4.11 VIVA Clariom™ Assays Identified Possible Pathways Regulating ILC Cell Line Invasion

4.11.1 The VIVAs Shared Top Pathways

In an attempt to identify possible pathways regulating ILC cell line invasion, we performed gene expression analysis on both VIVA sub-populations compared to the parental MDA-MB-134VI cell line. From the Clariom™ Assays there were a number of mRNA targets with ≥2-fold significant differential expression between the VIVAs and their parental MDA-MB-134VI cell line (Figure 25). A list of targets suggested for further investigation due to their ≥2-fold significant differential expression in both VIVA sub-populations compared to the MDA-MB-134VIs, which have previously published roles in breast cancer and metastasis was compiled (Table 7). While these targets are interesting candidates, some of the top ≥2-fold regulated pathways in both VIVA sub-populations may have greater potential as they may regulate the VIVAs increased invasive capabilities which could provide insight into key modulators of ILC invasion and metastasis. The top ≥2-fold regulated pathways in the VIVAs compared to the parental MDA-MB-134VIs are miR-targeted genes, PI3K-Akt signaling and nuclear receptors. In future investigations pertaining to the VIVA sub-populations, research should focus on these top pathways as they may lead to discoveries pertaining to the increased invasive capabilities of the sub-populations compared to the MDA-MB-134VI parental cell line or rather ILC invasion and metastasis.

4.11.2 The Possible Role the VIVAs Top Pathways May Have in Regulating ILC Cell Line Invasion

miR-targeted genes as a top regulated pathway in the VIVAs, is not too surprising due to the number of differentially expressed miRNAs seen in the miRNome analysis of the VIVAs compared to the parental MDA-MB-134VIs (Figure 12). miRNA have been shown to have

differential expression that is both tissue specific (Lagos-Quintana et al., 2002) as well as cancer specific (Wang and Luo, 2015). Additionally, miRNA have multiple targets (Schoolmeesters et al., 2009) therefore the number of differentially expressed miRNA in the VIVAs compared to the parental cell line is indicative of all the modulated targets that may be responsible for their increased invasive capabilities; thereby making miR-targeted genes a highly regulated pathway within the VIVA sub-populations.

As previously discussed in section 4.8.3, ILC commonly has increased phosphorylation of Akt (Ciriello et al., 2015) and thus increased PI3K-Akt signaling (Ciriello et al., 2015; Michaut et al., 2016), which is why it being a top regulated pathway in the VIVAs compared to the MDA-MB-134VIs may have been expected. Again as was discussed previously, Akt has been shown to modulate both invasion and migration in breast cancer (Yoeli-Lerner et al., 2005), thus indicating the potential effects of this pathway in regulating VIVA invasion. In section 4.8.2 the potential effects of the nuclear receptor pathway were discussed in the context of ILC. To reiterate, numerous nuclear receptors are present in breast cancer and this is not limited to ERα and PR (Lin et al., 2015). In Table 7 we marked PR (PGR in the table) as a target worth further investigation in the VIVAs due to its significantly increased expression in the VIVA sub-populations compared to the parental MDA-MB-134VIs. While it is interesting that PR has differential mRNA expression in the VIVAs compared to the MDA-MB-134VIs it appears that ERα mRNA expression did not differentiate between the sub-populations and the parental cell line (Figure 22A). This increased regulation of the nuclear receptor pathway may be contributing to the increased invasive capabilities of the VIVAs as studies have found that targets of the nuclear receptor pathway and nuclear receptors are able to modulate invasion in cancer cell lines (Cai et al., 2018; Fijten et al., 2019; Lin et al., 2015; Slenter et al., 2018). The importance of both the PI3K-Akt and nuclear

receptor pathways in ILC has been displayed in its high regulation in the MDA-MB-330 as well as the VIVA Clariom™ Assay datasets. While individual targets may be worth investigating in the context of VIVA invasion, interrogating important pathways may illuminate additional regulators and therapeutic targets of ILC metastasis.

4.12 Conclusions

At present there is a lack of ILC cell lines for investigating ILC *in vitro* (An et al., 2018), more specifically invasive ILC cell lines. Through isolation of MDA-MB-134VI cells that had invaded through an invasion chamber assay after 1-week, the VIVA-1s were created. The subsequent VIVA-2s were created from VIVA-1 cells that had invaded through an invasion chamber assay in 1-week. Both the VIVA-1s and the VIVA-2s were found to have increased invasion at 48hr and 1-week compared to their parental MDA-MB-134VIs. Preliminary characterization of the VIVAs showed that their ILC protein profile remains the same, and there is no significant change in their cell growth over time compared to the parental cell line. Changes in miRNA expression were seen through evaluation of specific miRNA expression and a miRNome analysis. miR-23c and miR-23b-3p were not found to regulate the VIVAs increased invasive capabilities, but other miRNAs were identified, and their expression should be evaluated in future investigations. Changes were also seen in the VIVAs mRNA expression profile, as presented in the Clariom™ Assay results. These changes may identify targets that modulate the increased invasive capabilities of the VIVAs, as well as pathways that may uncover potential diagnostic and therapeutic tools for ILC. By generating an additional model of invasive ILC, we hope to further studies into ILC invasion/metastasis that may continue to uncover new therapies and tools for patients with metastatic ILC.

Two specific miRNA, miR-23c and miR-23b-3p were found to have significantly increased expression in the invasive MDA-MB-330 cell line compared to the minimally invasive ILC cell lines. Through the modulation of their levels within the MDA-MB-330 and MDA-MB-134VI cell lines, miR-23c and miR-23b-3p were found to decrease and increase invasion in the cell lines respectively. Opposite results were seen within the UACC-3133 cell line, where increased miR-23c and miR-23b-3p levels caused a decrease in invasion. miR-23c and miR-23b-3p were found to regulate invasion; however, no changes were seen in the MDA-MB-330s or MDA-MB-134VIs migration or cell viability, as well as the UACC-3133 cell line's cell viability. Due to their roles in regulating ILC cell line invasion, we may speculate that in the context of the MDA-MB-330 and MDA-MB-134VI cell lines, miR-23c and miR-23b-3p act as oncogenes due to their increased expression in the invasive compared to minimally invasive cell lines (Iorio et al., 2005).

To identify possible targets of miR-23c and miR-23b-3p that may be responsible for the changes seen in the invasive capabilities of the MDA-MB-330 and MDA-MB-134VI cell lines with modulated levels of miR-23c and miR-23b-3p, Clariom™ Assays were conducted. None of the selected targets from the MDA-MB-134VI Clariom™ Assays validated, which led to further speculation of the efficiency of the mimics and hairpin inhibitors. Thus, the expression of miR-23c and miR-23b-3p were evaluated within patient ILC FFPE tumours, which discovered that mean miR-23c expression was decreased and mean miR-23b-3p expression was slightly increased in metastatic compared to non-metastatic samples, however these findings were found to be not significant. Therefore, a miRNome analysis of metastatic and non-metastatic ILC identified numerous miRNAs for further investigation. These cohorts are still rather small, therefore additional samples will be needed to uncover novel miRNAs with possible roles in regulating ILC metastasis.

In conclusion, this thesis has identified miRNAs with possible roles in regulating ILC and ILC invasion/metastasis. It is through further investigation into these miRNAs that possible regulators of ILC invasion/metastasis may be found, leading to possible diagnostic and therapeutic targets. It is believed through additional patient ILC FFPE tissue samples that a signature of metastatic potential may be derived, which would aid in the diagnosis and identification of treatment regimens for patients with ILC.

Chapter 5: References

Allinen, M., Beroukhim, R., Cai, L., Brennan, C., Lahti-Domenici, J., Huang, H., Porter, D., Hu, M., Chin, L., Richardson, A., et al. (2004). Molecular characterization of the tumor microenvironment in breast cancer. Cancer Cell *6*, 17–32.

Almeida, M.I., Nicoloso, M.S., Zeng, L., Ivan, C., Spizzo, R., Gafà, R., Xiao, L., Zhang, X., Vannini, I., Fanini, F., et al. (2012). Strand-specific miR-28-5p and miR-28-3p have distinct effects in colorectal cancer cells. Gastroenterology *142*, 886–896.

American Type Culture Collection (2019a). UACC-3133 (ATCC® CRL-2988™). https://www.atcc.org/products/all/CRL-2988.aspx#characteristics

American Type Culture Collection (2019b). MDA-MB-330 (ATCC® HTB-127™). https://www.atcc.org/Products/All/HTB-127.aspx#culturemethod

American Type Culture Collection (2019c). MDA-MB-330 (ATCC® HTB-127™). https://www.atcc.org/Products/All/HTB-127.aspx

American Type Culture Collection (2019d). UACC-3133 (ATCC® CRL-2988™). https://www.atcc.org/products/all/CRL-2988.aspx#generalinformation

Amrhein, V., Greenland, S., and McShane, B. (2019). Retire statistical significance. Nature *567*, 305–307.

An, Y., Zhang, Z., Shang, Y., Jiang, X., Dong, J., Yu, P., Nie, Y., and Zhao, Q. (2015). MiR-23b-3p regulates the chemoresistance of gastric cancer cells by targeting ATG12 and HMGB2. Cell Death Dis. *6*, e1766.

An, Y., Adams, J.R., Hollern, D.P., Zhao, A., Chang, S.G., Gams, M.S., Chung, P.E.D., He, X., Jangra, R., Shah, J.S., et al. (2018). *Cdh1* and *Pik3ca* mutations cooperate to induce immune-related invasive lobular carcinoma of the breast. Cell Rep. *25*, 702-714.

Ananias, H.J.K., van den Heuvel, M.C., Helfrich, W., and de Jong, I.J. (2009). Expression of the gastrin-releasing peptide receptor, the prostate stem cell antigen and the prostate-specific membrane antigen in lymph node and bone metastases of prostate cancer. Prostate *69*, 1101–1108.

Annunziato, S., Kas, S.M., Nethe, M., Yücel, H., Del Bravo, J., Pritchard, C., Ali, R. B, van Gerwen, B., Siteur, B., Drenth, A.P., et al. (2016). Modeling invasive lobular breast carcinoma by CRISPR/Cas9-mediated somatic genome editing of the mammary gland. Genes Dev. *30*, 1470–1480.

appliedbiosystems, and ThermoFisher Scientific (2017). Transcriptome analysis console (TAC) 4.0.1 user guide.

Arpino, G., Bardou, V.J., Clark, G.M., and Elledge, R.M. (2004). Infiltrating lobular carcinoma of the breast: Tumor characteristics and clinical outcome. Breast Cancer Res. *6*, R149-R156.

Bader, A.G., Brown, D., and Winkler, M. (2010). The promise of microRNA replacement therapy. Cancer Res. *70*, 7027–7030.

Begum, S., Hayashi, M., Ogawa, T., Jabboure, F.J., Brait, M., Izumchenko, E., Tabak, S., Ahrendt,

S.A., Westra, W.H., Koch, W., et al. (2015). An integrated genome-wide approach to discover deregulated microRNAs in non-small cell lung cancer: Clinical significance of miR-23b-3p deregulation. Sci. Rep. *5*, 13236.

Bentz, J.S., Yassa, N., and Clayton, F. (1998). Pleomorphic lobular carcinoma of the breast: Clinicopathologic features of 12 cases. Mod. Pathol. *11*, 814–822.

Bignotti, E., Calza, S., Tassi, R.A., Zanotti, L., Bandiera, E., Sartori, E., Odicino, F.E., Ravaggi, A., Todeschini, P., and Romani, C. (2016). Identification of stably expressed reference small non-coding RNAs for microRNA quantification in high-grade serous ovarian carcinoma tissues. J. Cell. Mol. Med. *20*, 2341–2348.

Boelens, M.C., Nethe, M., Klarenbeek, S., de Ruiter, J.R., Schut, E., Bonzanni, N., Zeeman, A.L., Wientjens, E., van der Burg, E., Wessels, L., et al. (2016). PTEN loss in E-cadherin-deficient mouse mammary epithelial cells rescues apoptosis and results in development of classical invasive lobular carcinoma. Cell Rep. *16*, 2087–2101.

Bovell, L., Shanmugam, C., Katkoori, V.R., Zhang, B., Vogtmann, E., Grizzle, W.E., and Manne, U. (2013). MicroRNAs are stable in formalin-fixed paraffin-embedded archival tissue specimens of colorectal cancers stored for up to 28 years. Front. Biosci (Elite Ed). *4*, 1937-1940.

Brennecke, J., Stark, A., Russell, R.B., and Cohen, S.M. (2005). Principles of microRNA-target recognition. PLoS Biol. *3*, e85.

Brinkley, B.R., Beall, P.T., Wible, L.J., Mace, M.L., Turner, D.S., and Cailleau, R.M. (1980). Variations in cell form and cytoskeleton in human-breast carcinoma-cells in vitro. Cancer Res. *40*, 3118–3129.

Cai, S., Zhang, P., Dong, S., Li, L., Cai, J., and Xu, M. (2018). Downregulation of SPINK13 promotes metastasis by regulating uPA in ovarian cancer cells. Cell Physiol. Biochem. *45*, 1061–1071.

Cailleau, R., Young, R., Olivé, M., and Reeves, W.J. (1974). Breast tumor cell lines from pleural effusions. J. Natl. Cancer Inst. *53*, 661–674.

Cailleau, R., Olivé, M., and Cruciger, Q.V.J. (1978). Long-term human breast carcinoma cell lines of metastatic origin: Preliminary characterization. In Vitro *14*, 911–915.

Calin, G.A., Sevignani, C., Dumitru, C.D., Hyslop, T., Noch, E., Yendamuri, S., Shimizu, M., Rattan, S., Bullrich, F., Negrini, M., Croce, C. M. (2004). Human microRNA genes are frequently located at fragile sites and genomic regions involved in cancers. PNAS. *101*, 2999–3004.

Canadian Cancer Society (2019a). Breast cancer statistics. https://www.cancer.ca/en/cancer-information/cancer-type/breast/statistics/?region=on

Canadian Cancer Society (2019b). Breast cancer: Survival statistics for breast cancer. https://www.cancer.ca/en/cancer-information/cancer-type/breast/prognosis-and-survival/survival-statistics/?region=on

Canadian Cancer Society (2019c). Breast Cancer: Treatments for stage 4 breast cancer. https://www.cancer.ca/en/cancer-information/cancer-type/breast/treatment/stage-4/?region=on

Canadian Cancer Statistics Advisory Committee (2018). Canadian Cancer Statistics 2018 (Toronto, Ontario: Canadian Cancer Society).

Chen, X., Ba, Y., Ma, L., Cai, X., Yin, Y., Wang, K., Guo, J., Zhang, Y., Chen, J., Guo, X., et al. (2008). Characterization of microRNAs in serum: A novel class of biomarkers for diagnosis of cancer and other diseases. Cell Res. *18*, 997–1006.

Christgen, M., and Derksen, P.W.B. (2015). Lobular breast cancer: Molecular basis, mouse and cellular models. Breast Cancer Res. *17*, 16.

Christgen, M., Bruchhardt, H., Hadamitzky, C., Rudolph, C., Steinemann, D., Gadzicki, D., Hasemeier, B., Römermann, D., Focken, T., Krech, T., et al. (2009). Comprehensive genetic and functional characterization of IPH-926: A novel CDHI-null tumour cell line from human lobular breast cancer. J. Pathol. *217*, 620–632.

Ciriello, G., Gatza, M.L., Beck, A.H., Wilkerson, M.D., Rhie, S.K., Pastore, A., Zhang, H., McLellan, M., Yau, C., Kandoth, C., et al. (2015). Comprehensive molecular portraits of invasive lobular breast cancer. Cell *163*, 506–519.

Conklin, B., Hanspers, K., Pico, A., Willighagen, E., Salomonis, N., and roudbari, z. (2018). GPCRs, class A rhodopsin-like (Homo sapiens). https://www.wikipathways.org/index.php/Pathway:WP455

Cottu, P., Marangoni, E., Assayag, F., de Cremoux, P., Vincent-Salomon, A., Guyader, C., de Plater, L., Elbaz, C., Karboul, N., Fontaine, J. J., et al. (2012). Modeling of response to endocrine therapy in a panel of human luminal breast cancer xenografts. Breast Cancer Res. Treat. *133*, 595–606.

Cristofanilli, M., Gonzalez-Angulo, A., Sneige, N., Kau, S.W., Broglio, K., Theriault, R.L., Valero, V., Buzdar, A.U., Kuerer, H., Buccholz, T.A., Hortobagyi, G.N. (2005). Invasive lobular carcinoma classic type: Response to primary chemotherapy and survival outcomes. J. Clin. Oncol. *23*, 41–48.

Derksen, P.W.B., Liu, X., Saridin, F., van der Gulden, H., Zevenhoven, J., Evers, B., van Beijnum, J.R., Griffioen, A.W., Vink, J., Krimpenfort, P., et al. (2006). Somatic inactivation of E-cadherin and p53 in mice leads to metastatic lobular mammary carcinoma through induction of anoikis resistance and angiogenesis. Cancer Cell *10*, 437–449.

Derksen, P.W.B., Braumuller, T.M., van der Burg, E., Hornsveld, M., Mesman, E., Wesseling, J., Krimpenfort, P., and Jonkers, J. (2011). Mammary-specific inactivation of E-cadherin and p53 impairs functional gland development and leads to pleomorphic invasive lobular carcinoma in mice. Dis. Model. Mech. *4*, 347–358.

Domann, F.E., Rice, J.C., Hendrix, M.J.C., and Futscher, B.W. (2000). Epigenetic silencing of maspin gene expression in human breast cancers. Int. J. Cancer *85*, 805–810.

Doornebal, C.W., Klarenbeek, S., Braumuller, T.M., Klijn, C.N., Ciampricotti, M., Hau, C.S., Hollmann, M.W., Jonkers, J., and de Visser, K.E. (2012). A preclinical mouse model of invasive lobular breast cancer metastasis. Cancer Res. *73*, 353–363.

Ethier, S.P., Mahacek, M.L., Gullick, W.J., Frank, T.S., and Weber, B.L. (1993). Differential isolation of normal luminal mammary epithelial cells and breast cancer cells from primary and

metastatic sites using selective media. Cancer Res. *53*, 627–635.

Feigin, M.E., Xue, B., Hammell, M.C., and Muthuswamy, S.K. (2014). G-protein-coupled receptor GPR161 is overexpressed in breast cancer and is a promoter of cell proliferation and invasion. PNAS. *111*, 4191–4196.

Fijten, R., Fehrhart, Willighagen, E., Cirillo, E., and Kutmon, M. (2019). Nuclear receptors meta-pathway (Homo sapiens). https://www.wikipathways.org/index.php/Pathway:WP2882

van Gestel, M.A., van Erp, S., Sanders, L.E., Brans, M.A.D., Luijendijk, M.C.M., Merkestein, M., Pasterkamp, R.J., and Adan, R.A.H. (2014). shRNA-induced saturation of the microRNA pathway in the rat brain. Gene Ther. *21*, 205–211.

de Graauw, M., van Miltenburg, M.H., Schmidt, M.K., Pont, C., Lalai, R., Kartopawiro, J., Pardali, E., Le Dévédec, S.E., Smit, V.T., van der Wal, A., et al. (2010). Annexin A1 regulates TGF-β signaling and promotes metastasis formation of basal-like breast cancer cells. PNAS. *107*, 6340–6345.

Granados-López, A.J., Ruiz-Carrillo, J.L., Servín-González, L.S., Martínez-Rodríguez, J.L., Reyes-Estrada, C.A., Gutiérrez-Hernández, R., and López, J.A. (2017). Use of mature miRNA strand selection in miRNAs families in cervical cancer development. Int. J. Mol. Sci. *18*, 407.

GraphPad Software (2009). What is the meaning of * or ** or *** in reports of statistical signifcance from Prism or InStat. https://www.graphpad.com/support/faq/what-is-the-meaning-of--or--or--in-reports-of-statistical-significance-from-prism-or-instat/

Griffiths-Jones, S., Grocok, Russell, J., van Dongen, S., Bateman, A., and Enright, A. J. (2006). miRBase: microRNA sequences, targets and gene nomenclature. Nucleic Acids Res. *34*, D140–D144.

Hanahan, D., and Weinberg, R.A. (2000). The hallmarks of cancer. Cell *100*, 57–70.

Hanahan, D., and Weinberg, R.A. (2011). Hallmarks of cancer: The next generation. Cell *144*, 646–674.

Hancox, R.A., Allen, M.D., Holliday, D.L., Edwards, D.R., Pennington, C.J., Guttery, D.S., Shaw, J.A., Walker, R.A., Pringle, J.H., and Jones, J.L. (2009). Tumour-associated tenascin-C isoforms promote breast cancer cell invasion and growth by matrix metalloproteinase-dependent and independent mechanisms. Breast Cancer Res. *11*, R24.

Hanspers, K., Riutta, A., and Willighagen, E. (2018). PI3K-Akt signaling pathway (Homo sapiens). https://www.wikipathways.org/index.php/Pathway:WP4172

Hollestelle, A., Elstrodt, F., Nagel, J.H.A., Kallemeijn, W.W., and Schutte, M. (2007). Phosphatidylinositol-3-OH kinase or RAS pathway mutations in human breast cancer cell lines. Mol. Cancer Res. *5*, 195–201.

Hollestelle, A., Nagel, J.H.A., Smid, M., Lam, S., Elstrodt, F., Wasielewski, M., Ng, S.S., French, P.J., Peeters, J.K., Rozendaal, M.J., et al. (2010). Distinct gene mutation profiles among luminal-type and basal-type breast cancer cell lines. Breast Cancer Res. Treat. *121*, 53–64.

Howe, G.A., Kazda, K., and Addison, C.L. (2017). MicroRNA-30b controls endothelial cell

capillary morphogenesis through regulation of transforming growth factor beta 2. PLoS ONE *12*, e0185619.

Hwang, H., and Sahoo, S. (2016). Invasive Lobular Carcinoma. In A Comprehensive Guide to Core Needle Biopsies of the Breast, S.J. Shin, ed. (Cham, Switzerland: Springer International Publishing), 595–620.

Iorfida, M., Maiorano, E., Orvieto, E., Maisonneuve, P., Bottiglieri, L., Rotmensz, N., Montagna, E., Dellapasqua, S., Veronesi, P., Galimberti, V., et al. (2012). Invasive lobular breast cancer: Subtypes and outcome. Breast Cancer Res. Treat. *133*, 713–723.

Iorio, M. V., Ferracin, M., Liu, C.G., Veronese, A., Spizzo, R., Sabbioni, S., Magri, E., Pedriali, M., Fabbri, M., Campiglio, M., et al. (2005). MicroRNA gene expression deregulation in human breast cancer. Cancer Res. *65*, 7065–7070.

Jackson ImmunoResearch Laboratories, INC. (2017). Western blot troubleshooting guide! 1–6.

Jacobs, C., Clemons, M., Addison, C., Robertson, S., and Arnaout, A. (2015). Issues affecting the loco-regional and systemic management of patients with invasive lobular carcinoma of the breast. Breast J. *22*, 45–53.

Jambal, P., Badtke, M.M., Harrell, J.C., Borges, V.F., Post, M.D., Sollender, G.E., Spillman, M.A., Horwitz, K.B., and Jacobsen, B.M. (2013). Estrogen switches pure mucinous breast cancer to invasive lobular carcinoma with mucinous features. Breast Cancer Res. Treat. *137*, 431–448.

Jeong, G., Lim, Y.H., Kim, N.J., Wee, G., and Kim, Y.K. (2017). Knockout of miR-221 and miR-222 reveals common and specific targets for paralogous miRNAs. RNA Biol. *14*, 197–205.

Jiang, L., He, D., Yang, D., Chen, Z., Pan, Q., Mao, A., Cai, Y., Li, X., Xing, H., Shi, M., et al. (2014). MiR-489 regulates chemoresistance in breast cancer via epithelial mesenchymal transition pathway. FEBS Lett. *588*, 2009–2015.

Kas, S.M., de Ruiter, J.R., Schipper, K., Annunziato, S., Schut, E., Klarenbeek, S., Drenth, A.P., van der Burg, E., Klijn, C., ten Hoeve, J. J., et al. (2017). Insertional mutagenesis identifies drivers of a novel oncogenic pathway in invasive lobular breast carcinoma. Nat. Genet. *49*, 1219–1230.

Kozomara, A., Birgaoanu, M., and Griffiths-Jones, S. (2019). MiRBase: From microRNA sequences to function. Nucleic Acids Res. *47*, D155–D162.

Kuroda, H., Tamaru, J. I., Takeuchi, I., Ohnisi, K., Sakamoto, G., Adachi, A., Kaneko, K., and Itoyama, S. (2006). Expression of E-cadherin, α-catenin, and β-catenin in tubulolobular carcinoma of the breast. Virchows Arch *448*, 500–505.

Lagos-Quintana, M., Rauhut, R., Yalcin, A., Meyer, J., Lendeckel, W., and Tuschl, T. (2002). Identification of tissue-specific microRNAs from Mouse. Curr. Biol. *12*, 735–739.

Li, J., Smyth, P., Flavin, R., Cahill, S., Denning, K., Aherne, S., Guenther, S.M., O'Leary, J.J., and Sheils, O. (2007). Comparison of miRNA expression patterns using total RNA extracted from matched samples of formalin-fixed paraffin-embedded (FFPE) cells and snap frozen cells. BMC Biotechnol. *7*, 36.

Liang, Z., Yoon, Y., Votaw, J., Goodman, M.M., Williams, L., and Shim, H. (2005). Silencing of

CXCR4 blocks breast cancer metastasis. Cancer Res. *65*, 967–971.

Lin, S., and Gregory, R.I. (2015). MicroRNA biogenesis pathways in cancer. Nat. Rev. Cancer *15*, 321–333.

Lin, M.L., Patel, H., Remenyi, J., Banerji, C.R.S., Lai, C.F., Periyasamy, M., Lombardo, Y., Busonero, C., Ottaviani, S., Passey, A., et al. (2015). Expression profiling of nuclear receptors in breast cancer identifies TLX as a mediator of growth and invasion in triple-negative breast cancer. Oncotarget *6,* 21685-21703.

Liu, W., and Wang, X. (2019). Prediction of functional microRNA targets by integrative modeling of microRNA binding and target expression data. Genome Biol. *20*, 18.

Liu, H., Wei, W., Wang, X., Guan, X., Chen, Q., Pu, Z., Xu, X., and Wei, A. (2018). MiR-23b-3p promotes the apoptosis and inhibits the proliferation and invasion of osteosarcoma cells by targeting SIX1. Mol. Med. Rep. *18*, 5683–5692.

Liu, X.X., Li, X.J., Zhang, B., Liang, Y.J., Zhou, C.X., Cao, D.X., He, M., Chen, G.Q., He, J.R., and Zhao, Q. (2011). MicroRNA-26b is underexpressed in human breast cancer and induces cell apoptosis by targeting SLC7A11. FEBS Lett. *585*, 1363–1367.

Ma, J., Huang, H., Han, Z., Zhu, C., and Yue, B. (2015). RLN2 is a positive regulator of AKT-2-induced gene expression required for osteosarcoma cells invasion and chemoresistance. Biomed Res. Int. *2015,* 147468.

Ma, L., Teruya-Feldstein, J., and Weinberg, R.A. (2007). Tumour invasion and metastasis initiated by microRNA-10b in breast cancer. Nature *449*, 682–688.

Magnon, C., Hall, S.J., Lin, J., Xue, X., Gerber, L., Freedland, S.J., and Frenette, P.S. (2013). Autonomic nerve development contributes to prostate cancer progression. Science. *341*, 1236361.

Mann, M., and Jensen, O.N. (2003). Proteomic analysis of post-translational modifications. Nat. Biotechnol. *21*, 255–261.

Martinez, V., and Azzopardi, J.G. (1979). Invasive lobular carcinoma of the breast: incidence and variants. Histopathology *3*, 467–488.

Matlock, B., and ThermoFisher Scientific. (2015). Assessment of Nucleic Acid Purity. Technical Note 52646.

Mcfall, T., McKnight, B., Rosati, R., Kim, S., Huang, Y., Viola-Villegas, N., and Ratnam, M. (2018). Progesterone receptor A promotes invasiveness and metastasis of luminal breast cancer by suppressing regulation of critical microRNAs by estrogen. J. Biol. Chem. *293*, 1163–1177.

McGuire, A., Brown, J.A.L., and Kerin, M.J. (2015). Metastatic breast cancer: the potential of miRNA for diagnosis and treatment monitoring. Cancer Metastasis Rev. *34*, 145–155.

Merhautova, J., Demlova, R., and Slaby, O. (2016). MicroRNA-based therapy in animal models of selected gastrointestinal cancers. Front. Pharmacol. *7,* 329.

Miao, C., Liang, C., Tian, Y., Xu, A., Zhu, J., Zhao, K., Zhang, J., Hua, Y., Liu, S., Dong, H., et al. (2017). Overexpression of CAPN2 promotes cell metastasis and proliferation via AKT/mTOR signaling in renal cell carcinoma. Oncotarget *8*, 97811–97821.

Michaut, M., Chin, S.F., Majewski, I., Severson, T.M., Bismeijer, T., de Koning, L., Peeters, J.K., Schouten, P.C., Rueda, O.M., Bosma, A.J., et al. (2016). Integration of genomic, transcriptomic and proteomic data identifies two biologically distinct subtypes of invasive lobular breast cancer. Sci. Rep. *6*, 18517.

Moll, R., Mitze, M., Frixen, U.H., and Birchmeier, W. (1993). Differential loss of E-cadherin expression in infiltrating ductal and lobular breast carcinomas. Am. J. Pathol. *143*, 1731–1742.

Moore, C., and AbD Serotec (2009). Introduction to Western Blotting. 1–48.

National Comprehensive Cancer Network (2018a). NCCN guidelines for patients: Breast cancer metastatic. NCCN Guid. Patients. 1-48.

National Comprehensive Cancer Network (2018b). NCCN guidelines for patients: Breast cancer invasive. NCCN Guid. Patients. 1-72.

Navin, N., Kendall, J., Troge, J., Andrews, P., Rodgers, L., McIndoo, J., Cook, K., Stepansky, A., Levy, D., Esposito, D., et al. (2011). Tumour evolution inferred by single-cell sequencing. Nature *472*, 90–94.

Ontario Tumour Bank, and Ontario Institute for Cancer Research (2019). About the Ontario Tumour Bank. https://ontariotumourbank.ca/about

Pal, B., Chen, Y., Bert, A., Hu, Y., Sheridan, J.M., Beck, T., Shi, W., Satterley, K., Jamieson, P., Goodall, G.J., et al. (2015). Integration of microRNA signatures of distinct mammary epithelial cell types with their gene expression and epigenetic portraits. Breast Cancer Res. *17*, 85.

Pestalozzi, B.C., Zahrieh, D., Mallon, E., Gusterson, B.A., Price, K.N., Gelber, R.D., Holmberg, S.B., Lindtner, J., Snyder, R., Thürlimann, B., et al. (2008). Distinct clinical and prognostic features of infiltrating lobular carcinoma of the breast: Combined results of 15 international breast cancer study group clinical trials. J. Clin. Oncol. *26,* 3006-3014.

Provenzano, P.P., Inman, D.R., Eliceiri, K.W., Beggs, H.E., and Keely, P.J. (2008). Mammary epithelial-specific disruption of focal adhesion kinase retards tumor formation and metastasis in a transgenic mouse model of human breast cancer. Am. J. Pathol. *173*, 1551–1565.

QIAGEN (2011). miScript PCR system handbook. *4,* 1-55.

QIAGEN (2012). miScript PreAMP handbook. 1-52.

QIAGEN (2013). Human miRNome miScript miRNA PCR array. Product Sheet. 1-20.

QIAGEN (2015). Guidelines for miRNA mimic and miRNA inhibitor experiments. 1-42.

QIAGEN (2018). miScript miRNA PCR array handbook. 1-63.

Qian, H., Yang, C., and Yang, Y. (2017). MicroRNA-26a inhibits the growth and invasiveness of malignant melanoma and directly targets on *MITF* gene. Cell Death Discov. *3*, 17028.

Rakha, E.A., van Deurzen, C.H.M., Paish, E.C., Macmillan, R.D., Ellis, I.O., and Lee, A.H.S. (2013). Pleomorphic lobular carcinoma of the breast: Is it a prognostically significant pathological subtype independent of histological grade? Mod. Pathol. *26*, 496–501.

Reed, A.E.M., Kutasovic, J.R., Lakhani, S.R., and Simpson, P.T. (2015). Invasive lobular

carcinoma of the breast: Morphology, biomarkers and 'omics. Breast Cancer Res. *17*, 12.

Reis-Filho, J.S., Simpson, P.T., Turner, N.C., Lambros, M.B., Jones, C., Mackay, A., Grigoriadis, A., Sarrio, D., Savage, K., Dexter, T., et al. (2006). FGFR1 emerges as a potential therapeutic target for lobular breast carcinomas. Clin. Cancer Res. *12*, 6652–6662.

Riaz, M., van Jaarsveld, M.T.M., Hollestelle, A., Prager-van der Smissen, W.J.C., Heine, A.A.J., Boersma, A.W.M., Liu, J., Helmijr, J., Ozturk, B., Smid, M., et al. (2013). miRNA expression profiling of 51 human breast cancer cell lines reveals subtype and driver mutation-specific miRNAs. Breast Cancer Res. *15*, R33.

Robertson, B., Dalby, A.B., Karpilow, J., Khvorova, A., Leake, D., and Vermeulen, A. (2010). Specificity and functionality of microRNA inhibitors. Silence *1*, 10.

Rosa-Rosa, J.M., Caniego-Casas, T., Leskela, S., Cristobal, E., González-Martínez, S., Moreno-Moreno, E., López-Miranda, E., Holgado, E., Pérez-Mies, B., Garrido, P., Palacios, J. (2019). High frequency of *ERBB2* activating mutations in invasive lobular breast carcinoma with pleomorphic features. Cancers. *11*, 74.

Santra, M., Santra, S., Roberts, C., Zhang, R.L., and Chopp, M. (2009). Doublecortin induces mitotic microtubule catastrophe and inhibits glioma cell invasion. J. Neurochem. *108*, 231–245.

Sarrió, D., Pérez-Mies, B., Hardisson, D., Moreno-Bueno, G., Suárez, A., Cano, A., Martín-Pérez, J., Gamallo, C., and Palacios, J. (2004). Cytoplasmic localization of p120ctn and E-cadherin loss characterize lobular breast carcinoma from preinvasive to metastatic lesions. Oncogene *23*, 3272–3283.

Schackmann, R.C.J., van Amersfoort, M., Haarhuis, J.H.I., Vlug, E.J., Halim, V.A., Roodhart, J.M.L., Vermaat, J.S., Voest, E.E., van der Groep, P., van Diest, P.J., et al. (2011). Cytosolic p120-catenin regulates growth of metastatic lobular carcinoma through Rock1-mediated anoikis resistance. J. Clin. Invest. *121*, 3176–3188.

Schoolmeesters, A., Eklund, T., Leake, D., Vermeulen, A., Smith, Q., Aldred, S.F., and Fedorov, Y. (2009). Functional profiling reveals critical role for miRNA in differentiation of human mesenchymal stem cells. PLoS One *4*, e5605.

Schrijver, W.A.M.E., van Diest, P.J., Dutch Distant Breast Cancer Metastases Consortium, and Moelans, C.B. (2017). Unravelling site-specific breast cancer metastasis: A microRNA expression profiling study. Oncotarget *8*, 3111–3123.

Scott, M.S., and Ono, M. (2011). From snoRNA to miRNA: Dual function regulatory non-coding RNAs. Biochimie *93*, 1987–1992.

Sflomos, G., Dormoy, V., Metsalu, T., Jeitziner, R., Battista, L., Scabia, V., Raffoul, W., Delaloye, J.F., Treboux, A., Fiche, M., et al. (2016). A preclinical model for ERα-positive breast cancer points to the epithelial microenvironment as determinant of luminal phenotype and hormone response. Cancer Cell *29*, 407–422.

Shi, X., and Teng, F. (2015). Down-regulated miR-28-5p in human hepatocellular carcinoma correlated with tumor proliferation and migration by targeting insulin-like growth factor-1 (IGF-1). Mol. Cell. Biochem. *408*, 283–293.

Shi, W., Gerster, K., Alajez, N.M., Tsang, J., Waldron, L., Pintilie, M., Hui, A.B., Sykes, J., P'ng, C., Miller, N., et al. (2011). MicroRNA-301 mediates proliferation and invasion in human breast cancer. Cancer Res. *71*, 2926–2937.

Sikora, M.J., Cooper, K.L., Bahreini, A., Luthra, S., Wang, G., Chandran, U.R., Davidson, N.E., Dabbs, D.J., Welm, A.L., and Oesterreich, S. (2014). Invasive lobular carcinoma cell lines are characterized by unique estrogen-mediated gene expression patterns and altered tamoxifen response. Cancer Res. *74*, 1463–1474.

Sinn, H.P., and Kreipe, H. (2013). A brief overview of the WHO classification of breast tumors, 4th edition, focusing on issues and updates from the 3rd edition. Breast Care *8*, 149–154.

Slenter, D.N., Kutmon, M., Hanspers, K., Riutta, A., Windsor, J., Nunes, N., Mélius, J., Cirillo, E., Coort, S.L., DIgles, D., et al. (2018). WikiPathways: A multifaceted pathway database bridging metabolomics to other omics research. Nucleic Acids Res. *46*, D661–D667.

Sørlie, T., Perou, C.M., Tibshirani, R., Aas, T., Geisler, S., Johnsen, H., Hastie, T., Eisen, M.B., van de Rijn, M., Jeffrey, S.S., et al. (2001). Gene expression patterns of breast carcinomas distinguish tumor subclasses with clinical implications. PNAS *98*, 10869–10874.

Tasdemir, N., Bossart, E.A., Li, Z., Zhu, L., Sikora, M.J., Levine, K.M., Jacobsen, B.M., Tseng, G.C., Davidson, N.E., and Oesterreich, S. (2018). Comprehensive phenotypic characterization human invasive lobular carcinoma cell lines in 2D and 3D cultures. Cancer Res. *78*, 6209–6222.

Thomson, D.W., Bracken, C.P., Szubert, J.M., and Goodall, G.J. (2013). On measuring miRNAs after transient transfection of mimics or antisense inhibitors. PLoS One *8*, e55214.

Wang, W., and Luo, Y.P. (2015). MicroRNAs in breast cancer: Oncogene and tumor suppressors with clinical potential*. J. Zhejiang Univ-Sci. B. (Biomed & Biotechnol.) *16*, 18–31.

Wei, D.M., Dang, Y.W., Feng, Z.B., Liang, L., Zhang, L., Tang, R.X., Chen, Z.M., Yu, Q., Wei, Y.C., Luo, D.Z., et al. (2018). Biological effect and mechanism of the miR-23b-3p/ANXA2 axis in pancreatic ductal adenocarcinoma. Cell. Physiol. Biochem. *50*, 823–840.

Westbrook, J.A., Cairns, D.A., Peng, J., Speirs, V., Hanby, A.M., Holen, I., Wood, S.L., Ottewell, P.D., Marshall, H., Banks, R.E., et al. (2016). CAPG and Gipc1: Breast cancer biomarkers for bone metastasis development and treatment. J. Natl. Cancer Inst. *108*, djv360.

Wong, N., and Wang, X. (2015). miRDB: An online resource for microRNA target prediction and functional annotations. Nucleic Acids Res. *43*, D146–D152.

Wu, H., Yao, S., Zhang, S., Wang, J.R., Guo, P. D, Li, X.M., Gan, W.J., Mei, L., Gao, T.M., and Li, J.M. (2017). Elevated expression of Erbin destabilizes ERα protein and promotes tumorigenesis in hepatocellular carcinoma. J. Hepatol. *66*, 1193–1204.

Xiao, F., Cheng, Z., Wang, P., Gong, B., Huang, H., Xing, Y., and Liu, F. (2018). MicroRNA-28-5p inhibits the migration and invasion of gastric cancer cells by suppressing AKT phosphorylation. Oncol. Lett. *15*, 9777–9785.

Yao, J., Liang, L.H., Zhang, Y., Ding, J., Tian, Q., Li, J.J., and He, X.H. (2012). GNAI1 suppresses tumor cell migration and invasion and is post-transcriptionally regulated by mir-320a/c/d in hepatocellular carcinoma. Cancer Biol. Med. *9*, 234–241.

Yoder, B.J., Wilkinson, E.J., and Massoll, N.A. (2007). Molecular and morphologic distinctions between infiltrating ductal and lobular carcinoma of the breast. Breast J. *13*, 172–179.

Yoeli-Lerner, M., Yiu, G.K., Rabinovitz, I., Erhardt, P., Jauliac, S., and Toker, A. (2005). Akt blocks breast cancer cell motility and invasion through the transcription factor NFAT. Mol. Cell *20*, 539–550.

Zaman, M.S., Thamminana, S., Shahryari, V., Chiyomaru, T., Deng, G., Saini, S., Majid, S., Fukuhara, S., Chang, I., Arora, S., et al. (2012). Inhibition of PTEN gene expression by oncogenic miR-23b-3p in renal cancer. PLoS One *7*, e50203.

Zhang, L., Wang, Y., Wang, L., Yin, G., Li, W., Xian, Y., Yang, W., and Liu, Q. (2018). miR-23c suppresses tumor growth of human hepatocellular carcinoma by attenuating ERBB2IP. Biomed. Pharmacother. *107*, 424–432.

Chapter 6: Appendix

miRNA	MDA-MB-330 vs. MDA-MB-134VI		VIVA-1 vs. MDA-MB-134VI		VIVA-2 vs. MDA-MB-134VI		Metastatic vs. Non-Metastatic	
	Fold Regulation	p value	Fold Regulation	p value	Fold Regulation	p value	Fold Regulation	p value
miR-642a-5p	3	0.007	2.5	0.005	3.5	0.4	1.2	0.2
miR-3607-3p	-3.4	0.049	-25.5	0.01	-5.8	0.01	-1.2	0.5
miR-199b-5p	-33.1	0.03	-5.1	0.03	-1.7	0.5	-1.1	0.3
miR-3647-3p	-5.9	0.047	-24.6	0.02	-4.1	0.1	-1.1	0.06
miR-199b-3p	-13.4	0.02	-3.4	0.03	-1.0	0.5	1.0	0.2

Supplementary Table 1: miRNA targets identified from matching the miRNome analyses of the cell lines, VIVAs and patient ILC FFPE tissues.

miRNA targets that may regulate ILC invasion were selected from cross referencing of the MDA-MB-330 to the VIVA and patient FFPE miRNomes. The table was created after controlling all the cell line miRNomes to the MDA-MB-134VI cell line, and all the miRNomes to SNORD95. The VIVA-1s were found to have numerous miRNAs that match the MDA-MB-330 dataset; however, only one from the VIVA-2 dataset was found to match with significant differential expression (miR-3607-3p). In relation to the metastatic compared to non-metastatic patient FFPE tissue miRNome, no miRNA with significant differential expression were found to match the MDA-MB-330 dataset. Thus, these miRNAs may be worth investigating in the context of the ILC cell lines and the VIVA sub-populations, and perhaps their targets may identify pathways important to ILC.

A

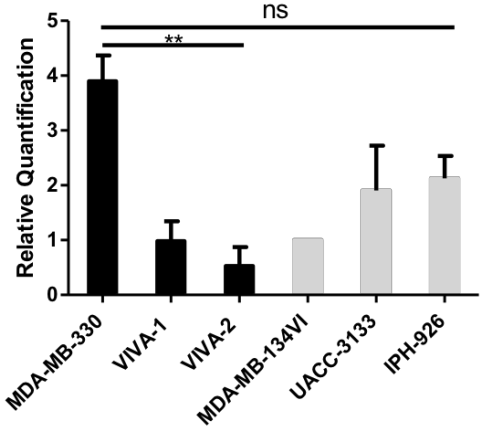
miR-642a-5p
ns
**
Relative Quantification
0
1
2
3
4
5
MDA-MB-330
VIVA-1
VIVA-2
MDA-MB-134VI
UACC-3133
IPH-926

B

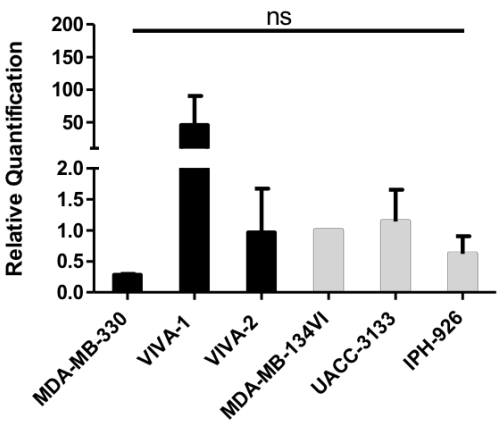
miR-3607-3p
ns
Relative Quantification
0.0
0.5
1.0
1.5
2.0
50
100
150
200
MDA-MB-330
VIVA-1
VIVA-2
MDA-MB-134VI
UACC-3133
IPH-926

C

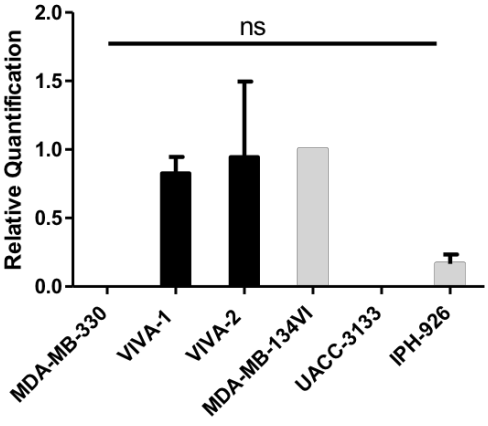
miR-199b-5p
ns
Relative Quantification
0.0
0.5
1.0
1.5
2.0
MDA-MB-330
VIVA-1
VIVA-2
MDA-MB-134VI
UACC-3133
IPH-926

D

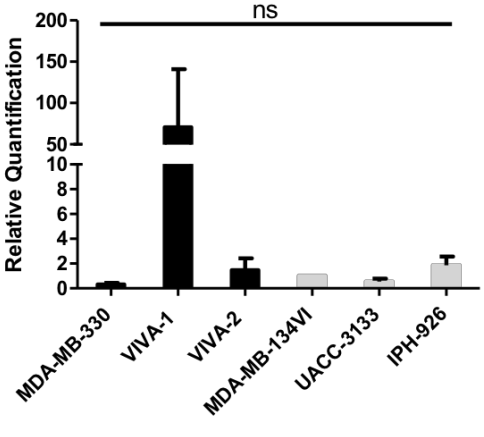
miR-3647-3p
ns
Relative Quantification
0
2
4
6
8
10
50
100
150
200
MDA-MB-330
VIVA-1
VIVA-2
MDA-MB-134VI
UACC-3133
IPH-926

E

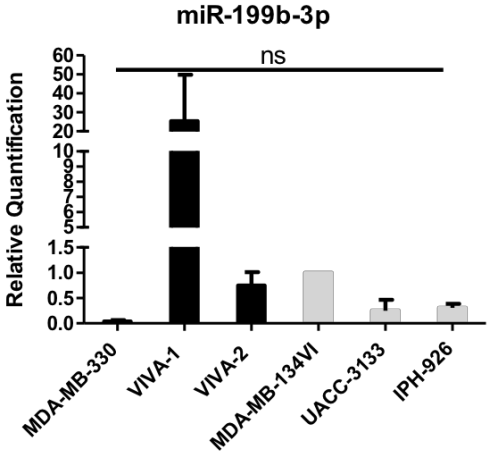
miR-199b-3p
ns
Relative Quantification
0.0
0.5
1.0
1.5
5
6
7
8
9
10
20
30
40
50
60
MDA-MB-330
VIVA-1
VIVA-2
MDA-MB-134VI
UACC-3133
IPH-926

Supplementary Figure 1: Further analysis of the expression of the miRNA identified in supplementary table 1 found that they did not validate in the ILC cell lines or the VIVA sub-populations.

Though the miRNA identified in Supplementary Table 1 may not have translated to the patient dataset, their expression in the ILC cell lines and the VIVA sub-populations was investigated. RNA was isolated from the four ILC cell lines as well as the two VIVA sub-populations and cDNA was made. The expression of the selected miRNA was analyzed by qPCR and normalized to SNORD95 as well as the MDA-MB-134VI cell line. The relative quantification of each miRNA in each cell line was plotted with the SEM. (A) miR-642a-5p was found to have significantly increased expression in the MDA-MB-330 cell line compared to the two VIVA sub-populations (p value 0.0031). The other evaluated miRNA (B) miR-3607-3p, (C) miR-199b-5p (p value 0.0177), (D) miR-3647-3p and (E) miR-199b-3p did not have significant differential expression within any of the ILC cell lines or VIVA sub-populations (n=3 biological replicates, One-way ANOVA with Tukey's multiple comparisons). ns, p value >0.05, ** p value ≤0.01.

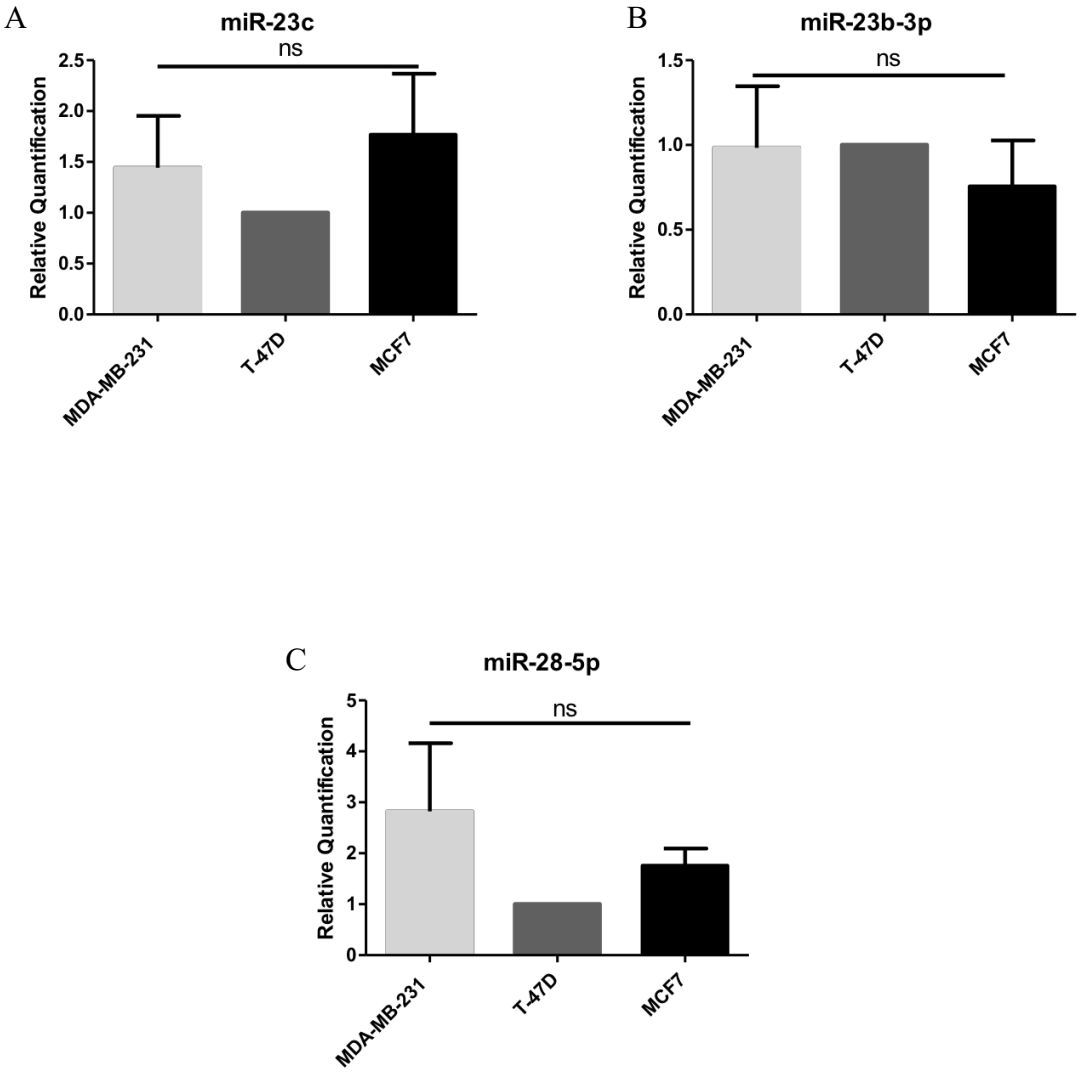
A
miR-23c
ns
Relative Quantification
2.5
2.0
1.5
1.0
0.5
0.0
MDA-MB-231
T-47D
MCF7
B
miR-23b-3p
ns
Relative Quantification
1.5
1.0
0.5
0.0
MDA-MB-231
T-47D
MCF7
C
miR-28-5p
ns
Relative Quantification
5
4
3
2
1
0
MDA-MB-231
T-47D
MCF7

Supplementary Figure 2: Expression of miR-23c, miR-23b-3p and miR-28-5p in three IDC cell lines with different invasive capabilities.

RNA was isolated from plated cells, following which cDNA was made and a qPCR was conducted to observe the expression of miR-23c, miR-23b-3p and miR-28-5p. Relative quantification was calculated and plotted with the SEM. The samples were normalized to SNORD95 and the T-47D cell line. None of (A) miR-23c, (B) miR-23b-3p, and (C) miR-28-5p appear to be associated with regulating IDC cell line invasion, as their expression does not correspond to the invasive capabilities of the cell lines. (n=3 biological replicates, One-way ANOVA with Tukey's multiple comparisons). ns, p value >0.05.

A

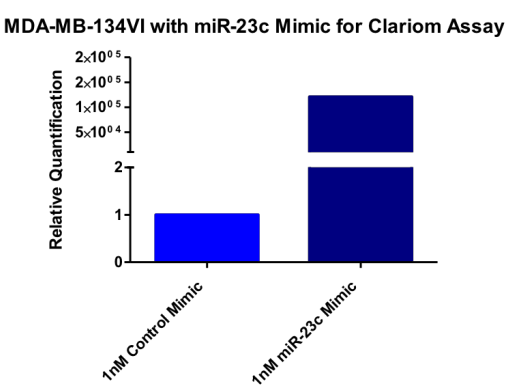
MDA-MB-134VI with miR-23c Mimic for Clariom Assay
Relative Quantification
2x10^05
2x10^05
1x10^05
5x10^04
2
1
0
1nM Control Mimic
1nM miR-23c Mimic

B

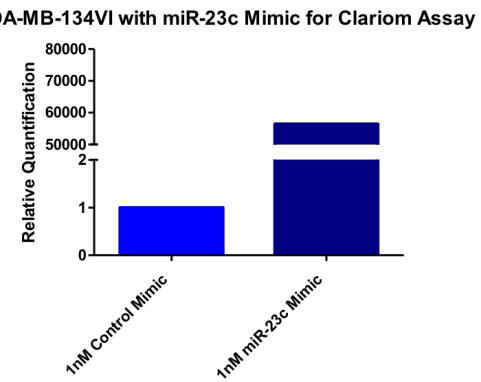
MDA-MB-134VI with miR-23c Mimic for Clariom Assay
Relative Quantification
80000
70000
60000
50000
2
1
0
1nM Control Mimic
1nM miR-23c Mimic

C

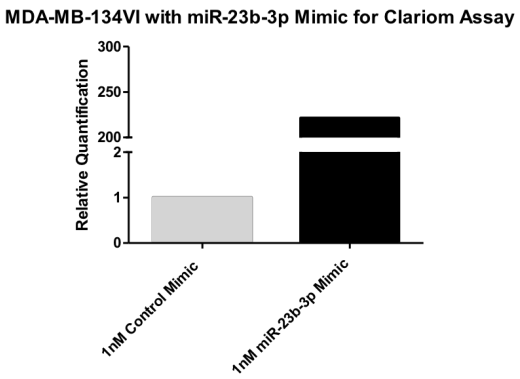
MDA-MB-134VI with miR-23b-3p Mimic for Clariom Assay
Relative Quantification
300
250
200
2
1
0
1nM Control Mimic
1nM miR-23b-3p Mimic

D

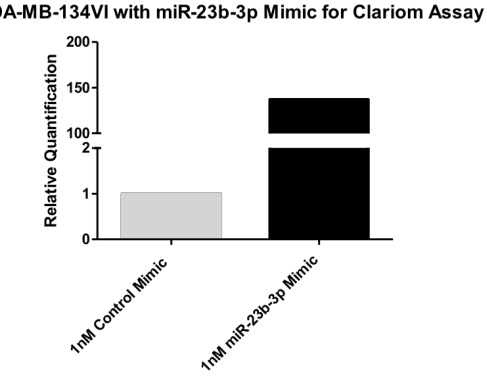
MDA-MB-134VI with miR-23b-3p Mimic for Clariom Assay
Relative Quantification
200
150
100
2
1
0
1nM Control Mimic
1nM miR-23b-3p Mimic

Supplementary Figure 3: Confirmation that miR-23c and miR-23b-3p levels were increased with mimics in the MDA-MB-134VI cell line prior to being sent for Clariom™ Assays.

Two biological replicates of the MDA-MB-134VI cell line were transfected with miR-23c, miR-23b-3p or non-targeting mimic. RNA was then isolated 48hr later and prepared following the guidelines provided by the Génome Québec Innovation Center (McGill University). A proportion of the RNA was used to make cDNA that was then analyzed for the levels of miR-23c and miR-23b-3p by qPCR. Samples were normalized to SNORD95 and the control non-targeting mimic. The relative quantification was then calculated and plotted. The levels of miR-23c were found to be increased in the (A) first and (B) second biological replicate of MDA-MB-134VIs transfected with mimic compared to the non-targeting control. miR-23b-3p levels were found to be higher in the (A) first and (B) second biological replicate of MDA-MB-134VIs transfected with mimic compared to the non-targeting control. Due to the successful increase of the levels of miR-23c and miR-23b-3p by mimic compared to the control, the RNA samples were sent to the Génome Québec Innovation Center at McGill University to conduct Clariom™ S Assays (n=1 biological replicates).

A

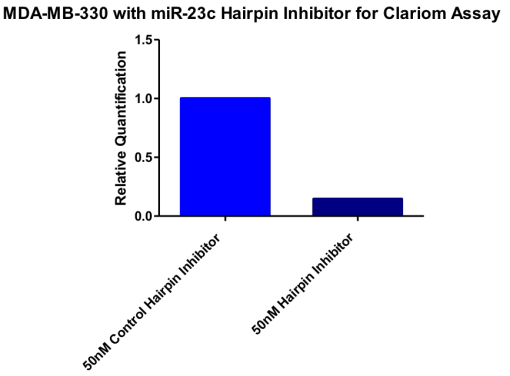
MDA-MB-330 with miR-23c Hairpin Inhibitor for Clariom Assay
Relative Quantification
1.5
1.0
0.5
0.0
50nM Control Hairpin Inhibitor
50nM Hairpin Inhibitor

B

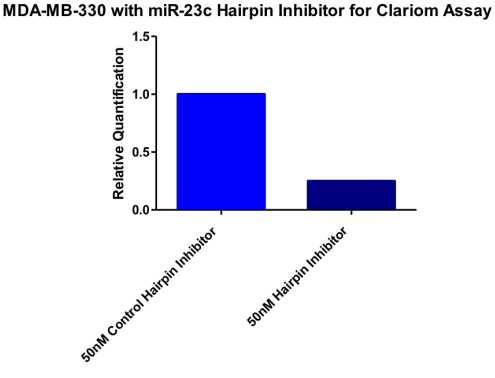
MDA-MB-330 with miR-23c Hairpin Inhibitor for Clariom Assay
Relative Quantification
1.5
1.0
0.5
0.0
50nM Control Hairpin Inhibitor
50nM Hairpin Inhibitor

C

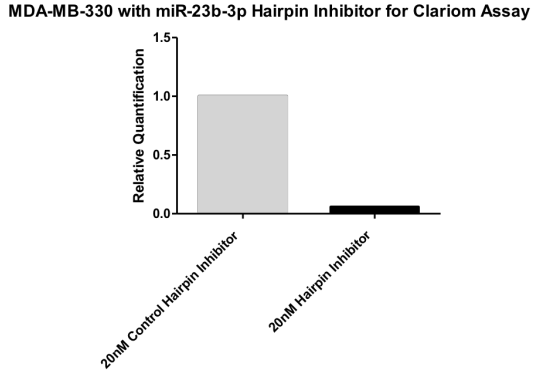
MDA-MB-330 with miR-23b-3p Hairpin Inhibitor for Clariom Assay
Relative Quantification
1.5
1.0
0.5
0.0
20nM Control Hairpin Inhibitor
20nM Hairpin Inhibitor

D

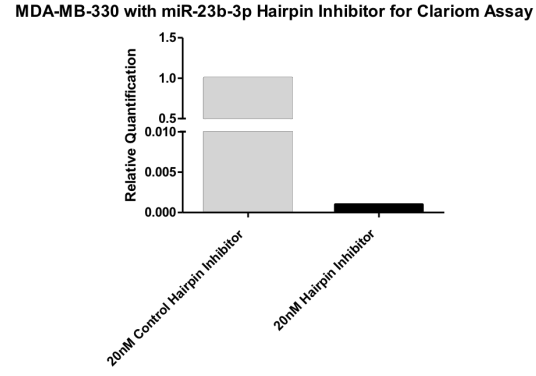
MDA-MB-330 with miR-23b-3p Hairpin Inhibitor for Clariom Assay
Relative Quantification
1.5
1.0
0.5
0.010
0.005
0.000
20nM Control Hairpin Inhibitor
20nM Hairpin Inhibitor

Supplementary Figure 4: Confirmation that miR-23c and miR-23b-3p levels were decreased with hairpin inhibitors in the MDA-MB-330 cell line prior to being sent for Clariom™ Assays.

Two biological replicates of the MDA-MB-330 cell line were transfected with miR-23c, miR-23b-3p or non-targeting hairpin inhibitor. RNA was then isolated 48hr later and prepared following the guidelines provided by the Génome Québec Innovation Center (McGill University). A proportion of the RNA was used to make cDNA that was then analyzed for the levels of miR-23c and miR-23b-3p by qPCR. Samples were normalized to SNORD95 and the control non-targeting hairpin inhibitor. The relative quantification was then calculated and plotted. The levels of miR-23c were found to be decreased in the (A) first and (B) second biological replicate of MDA-MB-330s transfected with hairpin inhibitor compared to the non-targeting control. miR-23b-3p levels were found to be lower in the (A) first and (B) second biological replicate of MDA-MB-330s transfected with hairpin inhibitor compared to the non-targeting control. Due to the successful decrease of the levels of miR-23c and miR-23b-3p by hairpin inhibitor compared to the non-targeting control, the RNA samples were sent to the Génome Québec Innovation Center at McGill University to conduct Clariom™ S Assays (n=1 biological replicates).

SickKids
The Hospital for Sick Children
Senior Scientist
Program in Cell Biology

Sean Egan

University of Toronto
Faculty of Medicine
Professor
Department of Molecular Genetics

May 22, 2019

To whom it may concern,

I give Victoria Allen permission to use our emails conducted on May 21-22, 2019 as a personal communication citation within her thesis. Our communication pertained to a paper from my lab titled *Cdh1* and *Pik3ca* Mutations Cooperate to Induce Immune-related Invasive Lobular Carcinoma of the Breast (2018), and her question regarding our mouse model and whether it generated metastatic lesions. During our investigation we did not see metastatic lesions, and I therefore give her permission to address this within her thesis.

Sincerely;

Sean Egan

Supplementary Figure 5: Letter of permission to cite personal communication with Dr. Sean Egan.

A letter was received from Dr. Sean Egan giving permission to use our email correspondence as a personal communication citation within this thesis. The emails were sent from May 21-22, 2019 and discussed his 2018 paper titled *Cdh1* and *Pik3ca* mutations cooperate to induce immune-related invasive lobular carcinoma of the breast (An et al., 2018). The emails confirmed our question, of whether metastatic lesions were seen in Dr. Sean Egan's generated mouse model.

Chapter 7: Curriculum Vitae

Victoria Allen

Education

Master of Science, Biochemistry 2016-2019

University of Ottawa, Ottawa, ON

- Specialization in Human and Molecular Genetics
- Supervised by Dr. Christina Addison at The Ottawa Hospital Research Institute in association with the University of Ottawa

Thesis title: Uncovering Pathways Regulating ILC Metastasis Through miRNA Expression Analysis and Generation of Novel Invasive ILC Models

Bachelor of Science, Honours Molecular Biology and Genetics 2012-2016

University of Guelph, Guelph, ON

- Honour's research project under the supervision of Dr. T. Ryan Gregory, titled: Evaluating Levels of Endopolyploidy in the Malpighian Tubules of Insects

University of Ottawa, Ottawa, ON

- Transferred to the University of Guelph after completion of first year at the University of Ottawa

Research Experience

Graduate Student 2016-2019

The Ottawa Hospital Research Institute, Ottawa, ON

- Masters student under the supervision of Dr. Christina Addison
- Worked on project evaluating the role of miRNA in Invasive Lobular Carcinoma
- Presented seminars, work in progresses, posters, research days
- Participated in the interview and decision process for CO-OP summer students as well as trained them
- Brainstormed grant ideas with Dr. Addison and contributed to projects within the Addison laboratory
- Analyzed and prepared data for Dr. Addison

Honours Student Jan 2015-Apr 2016

The University of Guelph, Guelph, ON

- Began as a volunteer and obtained field specimens as well as collaborated with a taxonomist
- Conducted an honors project on the levels of endopolyploidy within the Malpighian tubules of insects
- Dissection of tissue from small specimens, prepared and stained microscope slides
- Performed image analysis to estimate nuclear DNA content

Work Experience

Food and Beverage Services July 2016- Aug 2016

City of Brantford, Brantford, ON

- Organized food and beverage for city of Brantford golf course (Smart Serve Certified)

Seasonal Contract Apr 2014-Sep 2015

Lowes, Burlington, ON

Research and Development June 2014-Aug 2014

Valspar (formerly Madison Chemical Industries Inc.), Milton, ON

- Performed administrative functions with research and development lab as well as MSDS administration

Additional Skills

American College of Veterinary Surgeons

- Certified in Animal Care, September 2016
- Specifically trained in mouse care, prepared cells in culture for injections, assisted with injections, drug administration, and follow-up

Conferences and Presentations

Oral Presentations

The Ottawa Hospital Research Day, Ottawa, ON

- Selected for presentation through the submission of an abstract to a panel of evaluators
- Prepared with a panel of professors and administrators to generalize the presentation
- Allen V, Zhao H, Howe G, Addison CL. Towards Diagnostic and Therapeutic Targets of Invasive Lobular Carcinoma. November 8, 2018. St-Elias Banquet Center, Ottawa, Ontario.

The University of Ottawa Department of Medicine Research Day, Ottawa, ON.

- Selected for presentation through the submission of an abstract to a panel of evaluators
- Allen V, Zhao H, Howe G, Addison CL. Towards Diagnostic and Therapeutic Targets of Invasive Lobular Cancer. June 6, 2018. Centurion Conference and Events Centre, Ottawa, Ontario.

The University of Ottawa BMI Seminar Day, Ottawa, ON

- Participated in the presentation competition and awarded third place
- Allen V, Zhao H, Howe G, Addison CL. Towards Diagnostic and Therapeutic Targets of Invasive Lobular Cancer. March 8, 2018. Roger Guindon, University of Ottawa.

Poster Presentations

AACR Special Conference: Advances in Breast Cancer Research, Hollywood, CA

- Second author of poster presented by Dr. Grant Howe
- Howe G, Allen V, Addison CL. Palbociclib treatment activates FAK and use of palbociclib in combination with the FAK inhibitor PF-562,271 enhances antitumour activity in ER-positive breast cancer cells. October 7-10, 2017. Hollywood, California. DOI: 10.1158/1557-3125.ADVBC17-B35.

Scholarships and Awards

BCH M.Sc. Seminar Presentation Award 2018

The University of Ottawa BMI Seminar Day, Ottawa, ON

- Awarded third place in my category

Dr. Syed Sattar MSc Award for Outstanding Contribution to Research 2019

- The University of Ottawa BMI Department, Ottawa, ON

Languages

French - Intermediate proficiency, graduated with a French Immersion certificate from Nelson High School, 2012

German- Basic proficiency, beginners German Classes: Germania Language School, 2009 and University of Ottawa, 2012

Volunteer Activities

Let's Talk Science 2017-2018

- Classroom Volunteer – Liaison with the teacher and organized kits
- CSI Day Organizer – Collaborated with volunteers, team lead, and headed the genetic proportion

Canadian Cancer Society 2009-2016

- Volunteered from 2009-2016 – Specifically team captain from 2009-2015